

ASSESSMENT OF BRIDGE LOAD CARRYING CAPACITY UNDER STATIC AND DYNAMIC LOAD TESTING

**A Dissertation Submitted
In Partial Fulfillment of the Requirements for the
Degree of**

MASTER OF TECHNOLOGY

**in
Structural Engineering
by**

**BIMAL SHARMA
(2K22/STE/19)**

Under the supervision of

CO-SUPERVISOR

**Dr. NAVEET KAUR
Senior Scientist
CSIR-CRRI**

SUPERVISOR

**Dr. SHILPA PAL
Associate Professor
Delhi Technological University**



**Department of Civil Engineering
DELHI TECHNOLOGICAL UNIVERSITY
(Formerly Delhi College of Engineering)
Shahbad Daultpur, Main Bawana Road, Delhi-110042**

May, 2024

ASSESSMENT OF BRIDGE LOAD CARRYING CAPACITY UNDER STATIC AND DYNAMIC LOAD TESTING

A Dissertation Submitted
In Partial Fulfillment of the Requirements for the
Degree of

MASTER OF TECHNOLOGY

in
Structural Engineering
by

**BIMAL SHARMA
(2K22/STE/19)**

Under the supervision of

CO-SUPERVISOR

**Dr. NAVEET KAUR
Senior Scientist
CSIR-CRRI**

SUPERVISOR

**Dr. SHILPA PAL
Associate Professor
Delhi Technological University**



**Department of Civil Engineering
DELHI TECHNOLOGICAL UNIVERSITY
(Formerly Delhi College of Engineering)
Shahbad Daultpur, Main Bawana Road, Delhi-110042**

May, 2024

**©DELHI TECHNOLOGICAL UNIVERSITY, SHAHBAD
DAULATPUR, MAIN BAWANA ROAD, DELHI-110042**

ALL RIGHT RESERVED

Dedicated
To
My Parents
And
Brother

“If there had a mathematical equation of life, I would integrate with respect to ‘happiness’ and differentiate with respect to ‘burden and pain’.”

-----Bimal Sharma



DELHI TECHNOLOGICAL UNIVERSITY

(Formerly Delhi College of Engineering)

Shahbad Daulatpur, Main Bawana Road, Delhi-110042


CANDIDATE'S DECLARATION

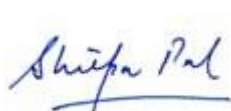
I, **Bimal Sharma**, M. Tech (Structural Engineering) student, having **Roll no: 2K22/STE/19**, hereby certify that the work which is being presented in the dissertation entitled “**Assessment of Bridge Load Carrying Capacity Under Static and Dynamic Load Testing**” in the partial fulfilment of the requirements of the award of the Degree **Master of Technology in Structural Engineering**, submitted in the **Department of Civil Engineering, Delhi Technological University** is an authentic record of my work carried out under the supervision of **Dr. Shilpa Pal**, Associate Professor, Department of Civil Engineering, Delhi Technological University, Delhi and **Dr. Naveet Kaur**, Senior Scientist, Bridge Engineering and Structures Division, CSIR- CRRI, New Delhi.

The matter present in this dissertation has not been submitted by me for the award of any other degree of this or any other institute.


(**Bimal Sharma**)

This is to certify that the student has incorporated all the corrections suggested by the examiners in the thesis and the statement made by the candidate is correct to the best of our knowledge.


Dr. Naveet kaur
(Co-Supervisor)


Dr. Shilpa Pal
(Supervisor)

Place: Delhi, Date:

The Viva-Voce of Mr. Bimal Sharma has been held on.....
(Signature of External Examiner)



DELHI TECHNOLOGICAL UNIVERSITY

(Formerly Delhi College of Engineering)

Shahbad Daulatpur, Main Bawana Road, Delhi-110042

CERTIFICATE BY THE SUPERVISOR(s)

Certified that **Bimal Sharma (2K22/STE/19)** has carried out his research work presented in this thesis entitled “**Assessment of Bridge Load Carrying Capacity Under Static and Dynamic Load Testing**” for the award of **Master of Technology in Structural Engineering** from the Department of Civil Engineering, Delhi Technological University, Delhi, under our supervision. The thesis embodies the results of original work and studies are carried out by the student himself. The contents of the thesis do not form the basis for the award of any degree to the candidate or to anybody else from this or any other University/Institution.

A handwritten signature in blue ink, reading 'Naveet kaur'.

Dr. Naveet kaur
(Co-Supervisor)
Senior Scientist
CSIR-CRRI

A handwritten signature in blue ink, reading 'Shilpa Pal'.

Dr. Shilpa Pal
(Supervisor)
Associate Professor
Delhi Technological University

Place: Delhi

Date:

ABSTRACT

Bridges are important structures in the field of civil engineering, failure of which can result the massive loss of life and the economy of the nation. With proper Structural Health Monitoring (SHM) and timely assessment of the bridges, failure of bridges can be reduced. The assessment of bridge load carrying capacity can be done using Static Load Testing (SLT) and Dynamic Load Testing (DLT). The primary purpose of this study is to explore the feasibility of DLT for the assessment of load carrying capacity of the bridge. The SLT entails the gradual application of load to a bridge, in contrast to DLT where moving load is applied on the bridge. This approach is not only expensive and time-intensive but also causes traffic disruptions during testing. The logistics of managing instruments and heavy equipment for SLT, particularly, in remote areas, present considerable challenges. However, dynamic load testing load overcomes the drawbacks of static load testing providing quick assessment of load carrying capacity of the bridge.

To relate the static and dynamic parameters of the bridge, a numerical study has been conducted in MIDAS Civil 2024 V 1.1. With the help of the numerical model and the experimental static load testing data, the static parameter and the dynamic parameter of the bridge are used for the calculation of the Dynamic Load Carrying Capacity (DLCC) of the bridge. The dynamic load carrying capacity ($DLCC_1$) has been calculated using a deflection value (d_e) of 23.06 mm from the experimental load testing and frequency value (f_n) of 4.145 Hz from the numerical model and found as 170.49 tons, which was not similar to the static load carrying capacity (SLCC) equivalent to the 70R wheeled vehicle including the impact factor (113.15 tons corresponding to bending moment of 4232 KNm) as reported by the CRRI. This is because the numerical model was not in onsite condition but in ideal condition. With the period of time and usage, the structural integrity of the bridge changes as parameters namely, material property (E), boundary condition (B) and moment of inertial (I) affecting the structural properties of the bridge changes. Then, to tune the numerical model with the onsite condition of the bridge, a parametric study has been carried out based on the

parameters: material property (E), boundary condition (B) and moment of inertia (I) and an updated model which resembles with the bridge onsite condition was generated.

The target frequency (f_n') of 3.376 Hz has been observed for the numerical model with modulus of elasticity (E) of M30, moment of inertia (I) of 65.1% and boundary condition as simply supported. Then, the dynamic load carrying capacity (DLCC₁) was again calculated using a deflection value (d_e) of 23.06 mm and frequency value (f_n') of 3.376 Hz and found as 113.05 tons, which is now similar to the static load carrying capacity (SLCC) equivalent to the 70R wheeled vehicle including the impact factor (113.15 tons) as reported by the CRRI.

Therefore, it can be concluded that the flexural load carrying capacity of the bridge determined using dynamic parameter is 4232 KNm which is similar to the flexural load carrying capacity of 4232 KNm determined experimentally.

The study shows static and dynamic parameters bridge can be used to find the dynamic load carrying capacity; which is proposed be equal to static load carrying capacity. In this study, static parameter from the experimental static load testing have been used to calculate the Dynamic Load Carrying Capacity (DLCC₁) of the bridge. In future, the dynamic load parameters from the experimental dynamic load test is proposed to be used to calculate the Dynamic Load Carrying Capacity (DLCC₂) of the bridge.

ACKNOWLEDGEMENT

I, **BIMAL SHARMA**, would like to express my deepest gratitude to all those who have given unforgettable contributions to the successful contribution of this thesis.

I would like to express my immense gratitude to my supervisor **Dr. Shilpa Pal**, Associate Professor, at Delhi Technological University, for providing me an opportunity to work in my field of interest. Her invaluable guidance, and support, insightful suggestions, constructive feedback, and unwavering encouragement throughout the entire research journey have been instrumental in shaping this thesis.

I would also like to extend my sincere gratitude to **Dr. Naveet Kaur**, Senior scientist, at CSIR-CRRI, for allowing me to work with her. She introduced the world of research to me. Her encouragement, motivation and loving nature to the students impressed me in each movement of the research work. Her expertise, guidance, support, astute recommendations, helpful feedback, and steadfast motivation were evident throughout the entirety of the research expedition.

I would like to express my deepest gratitude to **Dr. Pardeep Kumar**, Senior Technical Officer, CSIR-CRRI, for his invaluable support in every technical problem I encountered.

I am thankful to all faculty, staff and PhD scholars of Delhi Technological University [DTU], especially, the Department of Civil Engineering, for helping me whenever needed.

I would also like to thank **Subodh Bende**, **Dipesh Tharu** and all my friends who helped me directly or indirectly throughout the entire research period.

I would like to give a huge token of gratitude to my parents and all family members for their unwavering support and understanding throughout this journey. Their encouragement, motivation, and belief in my abilities have been a constant source of strength.

I am grateful to the Indian Council for Cultural Relations (ICCR) and the Embassy of India, Kathmandu, Nepal for providing a scholarship to pursue my M.Tech at DTU.

Last, but not least, I would like to express my immense gratitude towards god. I don't think I would have been what I am today if it was not his/her blessing. Please god, always keep me on the list of your much-loved children.



Bimal Sharma
(2K22/STE/19)

TABLE OF CONTENTS

CANDIDATE’S DECLARATION	i
CERTIFICATE BY THE SUPERVISOR(s)	ii
ABSTRACT	iii
ACKNOWLEDGEMENT	v
TABLE OF CONTENTS.....	vi
LIST OF TABLES	ix
LIST OF FIGURES	x
LIST OF SYMBOLS AND ABBREVIATIONS	xiv
CHAPTER 1	
INTRODUCTION.....	1-10
1.1 GENERAL	1
1.2 MOTIVATION	2
1.3 STATIC LOAD TESTING	3
1.3.1 Instrumentations.....	3
1.3.2 Acceptance criteria as per IRC.....	4
1.4 DYNAMIC LOAD TESTING	5
1.4.1 Methods of Dynamic Load Testing.....	5
1.4.2 Instrumentation	6
1.5 RESEARCH OBJECTIVE AND SCOPE	9
1.6 ORGANIZATION OF THESIS.....	9
CHAPTER 2	
LITERATURE REVIEW.....	11-20
2.1 INTRODUCTION	11
2.2 LITERATURE REVIEW ON STATIC LOAD TESTING	12
2.3 LITERATURE REVIEW ON DYNAMIC LOAD TESTING	13
2.4 LITERATURE REVIEW ON TOGETHER USE OF BOTH STATIC LOAD TESTING AND DYNAMIC LOAD TESTING.....	15
2.5 GAP OF THE STUDY	19
CHAPTER 3	
NUMERICAL STUDY TO ANALYZE THE EFFECT OF ECCENTRICITY OF THE MOVING VEHICLE FROM THE KERB OF THE BRIDGE	21-32
3.1 INTRODUCTION	21

3.2 VALIDATION OF NUMERICAL MODEL.....	21
3.4 NUMERICAL MODEL FOR STUDY IN ANSYS WORKBENCH.....	22
3.4.1 Bridge and Loading Details	22
3.4.2 Modelling Details.....	22
3.4.3 Transient/Moving Loading	25
3.5 RESULTS AND DISCUSSIONS	28
3.6 CONCLUDING REMARK	32
CHAPTER 4	
NUMERICAL STUDY TO INVESTIGATE THE DEFLECTION BEHAVIOR IN A CONCRETE BRIDGE UNDER IRC RECOMMENDED LOADING SCENARIOS	33-47
4.1 GENERAL	33
4.2 BRIDGE DETAILS	33
4.4 CONSIDERED IRC LOADINGS	38
4.5 NUMERICAL MODELLING AND VALIDATION.....	40
4.6 DEFLECTION UNDER DIFFERENT IRC RECOMMENDED LOAD SCENARIOS	43
4.7 CONCLUDING REMARK	47
CHAPTER 5	
PROPOSED METHODOLOGY FOR DYNAMIC LOAD TEST	48-70
5.1 GENERAL	48
5.2 STATIC LOAD TEST	49
5.2.1 Loading Scheme for Static Load Test	49
5.2.2 Experimental Static Load Test	50
5.2.3 Discussion of Results	51
5.3 NUMERICAL MODELLING OF THE BRIDGE IN MIDAS CIVIL	52
5.3.1 Validation of The Model	55
5.4 DYNAMIC LOAD TEST	64
5.4.1 Proposed Methodology for Determining Load Carrying Capacity of Bridge Using Static and Dynamic Parameters	64
5.4.2 Dynamic Load Carrying Capacity (DLCC) for the Bridge.....	67
5.4.3 Numerical Model Updating.....	68
5.5 CONCLUSION	70
CHAPTER 6	
CONCLUSION AND FUTURE WORK	71-74
6.1 GENERAL	71

6.2 CONCLUSION	71
6.3 FUTURE WORK.....	74
REFERENCES.....	75
APPENDIX A	78
PUBLICATIONS	80

LIST OF TABLES

Table	Caption	Page no.
1.1	Percentage recovery of deflections after retention for various types of bridges (IRC:6-2017).....	5
3.1	Results for different moving paths.....	31-32
4.1	Details of the span P3-P4 (Source: CRRRI Report, 2019).....	34
4.2	Details of tapering of girder (Source: CRRRI Report, 2019).....	35
4.3	Vehicle position for maximum deflection for different load cases.....	46
5.1	Weight of Loaded Trucks for Load Testing of Span P3-P4.....	50
5.2	Deflection Data during load test of Span P3-P4.....	52
5.3	Section Properties of left end girder (G2).....	54
5.4	Eccentricity values calculated to define the moving load path concerning the reference line.....	55
5.5	Maximum Bending moment and Maximum deflection in RM bridge and MIDAS CIVIL under various load cases considered...	63
5.6	Calculation for the dynamic load carrying capacity (DLCC ₁) of the bridge before model updating.....	67
5.7	Frequency of the bridge for varying E & I.....	69
6.1	Different Formulae to calculate DLCC for different boundary conditions (Islam et al., 2015).....	72

LIST OF FIGURES

Figure	Caption	Page no.
1.1	Static loads over bridges (a) by the close-up of loads (Lantsoght et.al, 2017) (b) by placing vehicle (internet).....	3
1.2	Instruments used for measurement in static load testing.....	4
1.3	Various types of dynamic loads used for load testing : (a) Moving vehicle passed over the bridge as a dynamic load (Baishrhakur and Chakraborty, 2021), (b) Impact load applied over the bridge as a dynamic load (Gatti, 2019) and (c) Hydraulic actuator as a dynamic load over the bridge (Laure et.al, 2016).....	6
1.4	Showing monitoring scheme for dynamic load test and typical instrumentations (a) Scheme of monitoring system (Magalhães et al., 2008) and (b) Lasevibrometer (Abedin et al., 2021) and (d) Inductive Displacement Transducer, Accelerometer set up, Strain Sensor and Installation of the accelerometer (Benčat and Kohár, 2018).....	8
3.1	T-Beam and Slab Bridge-Deck for 15m of span used for validation (Gupta et al., 2023) (a) Cross-section of and (b) Plan of Bridge-Deck.....	22
3.2	Deflected bridge model in ANSYS used for validation.....	23
3.3	Deflection for different mesh sizes in CSiBridge (Gupta et al., 2023).....	23
3.4	T-beam and Slab Bridge Deck used in the study (Gupta et al., 2023) (a) Cross-section of and (b) Plan of Bridge-Deck.....	24
3.5	IRC Class AA tracked vehicle load (IRC:6-2017).....	24
3.6	Cross-sectional and 3D view of the bridge in ANSYS.....	25
3.7	Showing boundary conditions and loadings.....	26
3.8	Showing meshing in the model.....	26
3.9	Maximum deflection vs Mesh size.....	26
3.10	(a) Analysis setting, (b) Vehicle's first position at 0.2 sec., (c) Vehicle's second position at 0.6 sec., (d) Vehicle's third position at 0.8 sec., (e) Vehicle's fourth position at 1.0 sec. and (f) Vehicle's fifth position at 1.2 sec.....	27
3.11	Maximum total deformation, maximum equivalent stress and maximum equivalent strain for an eccentricity of 1200mm for the moving vehicle (a) Maximum total deformation, (b) Maximum equivalent stress and (c) Maximum equivalent strain.....	29
3.12	Representation of the position of the vehicle for maximum values of studied parameters.....	30

Figure	Caption	Page no.
3.11	Maximum total deformation, maximum equivalent stress and maximum equivalent strain for an eccentricity of 1200mm for the moving vehicle (a) Maximum total deformation, (b) Maximum equivalent stress and (c) Maximum equivalent strain.....	29
3.12	Representation of the position of the vehicle for maximum values of studied parameters.....	30
3.13	Maximum total deformation with respect to the eccentric distance of the moving vehicle from the kerb of the bridge.....	30
3.14	Maximum equivalent stress with respect to the eccentric distance of the moving vehicle from the kerb of the bridge.....	31
3.15	Maximum equivalent strain with respect to the eccentric distance of the moving vehicle from the kerb of the bridge.....	31
4.1	3D view of Span P3-P4 (Source: CRRRI Report, 2019).....	34
4.2	Cross section at ends of span.....	35
4.3	Cross section at the middle of the span.....	35
4.4	Left girder cross section at end span.....	36
4.5	Left girder cross section at mid-span.....	36
4.6	Profile of cross-girder.....	36
4.7	Simplified geometry for numerical modelling:(a) section at intermediate portion, (b) section at end portion. (c) 3D view	37
4.8	IRC Class AA tracked and wheeled Vehicle (IRC:6-2017).....	38
4.9	IRC 2-Lanes Class A vehicle (IRC:6-2017).....	39
4.10	IRC 70R Wheeled Loading (IRC:6-2017).....	39
4.11	Pictorial representation of Class AA wheeled load applied in the model using DLOAD Subroutine.....	40
4.12	3D view of the bridge with boundary conditions in ABAQUS.....	41
4.13	Finite element model with meshing.....	41
4.14	Finite element model showing various parts.....	41
4.15	Surface selection to apply moving load.....	42
4.16	Application of typical moving load using DLOAD Subroutine.....	42
4.17	Maximum Vertical deflection under self-weight in RM-bridge.....	42
4.18	Maximum Vertical deflection under self-weight in ABAQUS.....	43
4.19	Typical figure representing the position of a vehicle on the bridge...	43
4.20	(a)Analysis for Class AA tracked vehicle for eccentric condition and (b) Maximum deflection under Class AA tracked vehicle for eccentric condition.....	44
4.21	(a)Analysis for Class AA tracked vehicle for eccentric condition and (b) Maximum deflection under Class AA tracked vehicle load for eccentric condition.....	44

Figure	Caption	Page no.
4.22	(a) Analysis for 2-lane Class A vehicle for eccentric condition and (b) Maximum deflection under 2-lane Class A vehicle for eccentric condition.....	44
4.23	(a) Analysis for 2-lane Class A vehicle for symmetric condition and (b) Maximum deflection under 2-lane Class A vehicle for symmetric condition.....	45
4.24	(a) Analysis for 70R wheeled vehicle for eccentric condition and (b) Maximum deflection under 70R wheeled vehicle for eccentric condition.....	45
4.25	(a) Analysis for 70R wheeled vehicle for symmetric condition and (b) Maximum deflection under 70R wheeled vehicle for symmetric condition.....	45
4.26	Maximum deflections under various load cases.....	46
5.1	Showing the bridge on which the static load test was performed (Source: CRRI Report, 2019).....	48
5.2	Load Testing Scheme for span P3-P4 (Source: CRRI Report, 2019).....	50
5.3	3D view of Bridge in Midas Civil 2024 V1.1.....	53
5.4	Material properties chosen in Midas Civil 2024 V1.1.....	54
5.5	Moving load path for the 70R eccentric loading condition.....	56
5.6	Deflected shape of the bridge in 3D under self-weight.....	57
5.7	Bending moment diagram of girders under self-weight.....	57
5.8	Deflected shape of the bridge in 3D under Class A wheeled 2-lane eccentric loading.....	57
5.9	Bending moment diagram of girders under Class A wheeled 2-lane eccentric loading.....	58
5.10	Deflected shape of the bridge in 3D under Class A wheeled 2-lane symmetric loading.....	58
5.11	Bending moment diagram of girders under Class A wheeled 2-lane symmetric loading.....	58
5.12	Deflected shape of the bridge in 3D under 70R 1-lane eccentric loading.....	59
5.12	Deflected shape of the bridge in 3D under 70R 1-lane eccentric loading.....	59
5.13	Bending moment diagram of girders under 70R 1-lane eccentric loading.....	59
5.14	Deflected shape of the bridge in 3D under 70R 1-lane symmetric loading.....	59

Figure	Caption	Page no.
5.15	Bending moment diagram of girders under 70R 1-lane symmetric loading.....	60
5.16	Deflected shape of the bridge in 3D under Class AA wheeled eccentric loading.....	60
5.17	Bending moment diagram of girders under Class AA wheeled eccentric loading.....	61
5.18	Deflected shape of the bridge in 3D under Class AA tracked eccentric loading.....	61
5.19	Bending moment diagram of girders under Class AA wheeled eccentric loading.....	61
5.20	Deflected shape of the bridge in 3D under Stage -1 (42T) loading....	62
5.21	Bending moment diagram of girders under Stage -1 (42T) loading...	62
5.22	Deflected shape of the bridge in 3D under Stage -2 (42T+62T) loading.....	62
5.23	Bending moment diagram of girders under Stage -2 (42T+62T) loading.....	62
5.24	Load Scheme for 42T+62T loading in MIDAS CIVIL.....	63
5.25	Mode shape of the bridge span P3-P4 in 1 st mode of vibration.....	64
5.26	Scheme for the comparative study of Static Load Test and Dynamic Load Test.....	66
5.27	Graph Showing frequency (f_n) for varying I&E.....	69
6.1	Summary of the layout of the thesis.....	72

LIST OF SYMBOLS AND ABBREVIATIONS

IRC	Indian Road Congress
SP	Special Publication
LVDT	Linear Variable Displacement Transducer
IDT	Inductive Displacement Transducer
SLT	Static Load Testing
DLT	Dynamic Load Testing
AVTs	Ambient Vibration Tests
AVS	Audio visual set-up
PSSB	Prestressed Box Beam
WSN	Wireless Sensor Network
PSC	Prestressed Concrete
AASHTO	American Association of State Highway and Transportation Officials
OMA	Operational Modal Analysis
EMA	Experimental Modal Analysis
SHM	Structural Health Monitoring
HFT	Harmonically Forced Test
HMC	Hamilton Montle Carto
DASP	Data Acquisition and Signal Processing
RCC	Reinforced Cement Concrete
FE/FEM	Finite Element/Finite Element Modelling
CSIR	Council of Scientific and Industrial Research
CRRI	Central Road Research Institute
DLCC	Dynamic Load Carrying Capacity
SLCC	Static Load Carrying Capacity
B	Boundary Condition
I	Moment of Inertia
Δ or d	Deflection
f	Frequency
m_t	Total Mass of Bridge
L	Length of the Bridge
D	Density
V	Volume
K	Stiffness of the Bridge
f_e	Experimental frequency
f_n	Numerical model frequency
d_e	Experimental deflection

CHAPTER 1

INTRODUCTION

1.1 GENERAL

Assessment of bridge load-carrying capacity is a part of the bridge evaluation which quantitatively evaluates the live-load resistance that the bridge can safely withstand; and provides the basic data that can be used for future planning regarding traffic volume and heavier loads as well as maintenance of repair and reinforcement work, thus ensuring the public safety (Ko and Kim, 2023).

A bridge is a structure built to span a physical obstacle such as a river, valley, road, or railroad to provide passage over it, serving as a critical link in the transportation networks, enabling connectivity between different areas and facilitating the movement of people, goods, and services. It is considered one of the important structures in the field of civil engineering, failure of which can result in the massive loss of life and the economy of the nation (Cook, 2014).

Although bridge load-carrying capacity assessment can be performed throughout a bridge's lifecycle, two key stages are particularly important –Stage I: During the design and construction, and Stage II: During the operation and maintenance. Stage I is the initial stage where the bridge load-carrying capacity is first determined in the newest condition and also verify the design with the codal compliance, to ensure safety. Once the bridge is operational, with age, the bridge load-carrying capacity reduces as it deteriorates due to weather, traffic, and other factors. So, Stage II assessments are crucial to monitor its condition and ensure it continues to meet its load-carrying capacity. In addition to that, two main stages where Stage II assessments need to be carried out are: after the major event like an earthquake, flood, or other significant event, and before rehabilitation and strengthening.

The study on the cause of failure of bridges in India from 1997 to 2017 showed that 80.30% of bridge failures are due to natural disasters, 10.10% by the deterioration of the material, 4.13% by design and construction, 3.28% by overloading

and 2.19% of the failure by Human-Made disaster (Garg et al., 2023). With proper Structural Health Monitoring (SHM) and timely assessment of the load-carrying capacity of bridges, failure of the bridge can be reduced.

Dissanayake and Bandara (2016) performed static load testing and dynamic load testing for the rehabilitation of a wrought iron bridge. Beginning with a condition assessment survey, finite element analysis of the bridge was done to validate the results of field load testing. A locomotive having the number of axles six each of 13.16 tons was used for both static load test and dynamic load test. For different loading conditions, displacement, strain, and acceleration at critical members of the bridge were measured. Then bridge damage due to past loading histories and future fatigue life of the bridge were estimated. Moreover, the bridge's ability for higher loading conditions was confirmed with the help of the validated model. The result showed that the estimated cost for constructing a new abutment and retrofitting work was much less than that for constructing the new bridge.

The study of Padgett et al. (2010) emphasized that the bridge's maintenance and repair increase the bridge's life-cycle cost but also noted the serious effects of extreme events on a structure's life-cycle cost.

1.2 MOTIVATION

In static-load testing where the static load is applied over the bridge gradually. The static load testing is not only time-consuming and expensive but also disturbing to the traffic during the whole testing period. Instruments and heavy equipment management for the static load testing of the bridges in the remotely situated location is problematic and a big challenge. However, dynamic load testing of the bridges mitigates the limitations of static load testing and provides a tool to quickly access the load carrying capacity of bridges.

Bridges are vital, but their ability to handle weight can weaken. To ensure public safety and optimize bridge use, we need a better understanding of how well static load testing of bridges and the dynamic load testing of bridges can complement each other. By comparing these methods, we can refine bridge capacity assessments,

improve maintenance strategies, and potentially develop more advanced testing techniques – all crucial steps for keeping our bridges safe and reliable.

1.3 STATIC LOAD TESTING

In India, static load testing is performed as per the guidelines of the Indian Road Congress, IRC SP 51: 2015. For static load testing, the static load can be applied by placing a close-up of loads as shown in Fig. 1.1 (a), or by placing the vehicle over the bridge as shown in Fig.1.1(b). As per the Indian Road Congress (IRC), for load testing, the loads are placed over the bridge carriageway in such a way that it produces the maximum bending moment in any longitudinal member of the bridge, simulating the specific IRC vehicle for which the design is done. The measurements for the static load testing are the deflections, strains, and crack width.



Fig. 1.1 Static loads over bridges (a) by the close-up of loads (IRC:6-2017) (b) by placing vehicle (Source:Internet)

1.3.1 Instrumentations

The correct type, number, and location of the instrumentation used on the structure during the load test is crucial for achieving a satisfactory outcome. The devices used for measuring the parameters namely, deflections, strain, and inclination are; (a) Linear Variable Displacement Transducer (LVDT) system, least count 0.01mm, (b) Dial gauges, least count 0.01mm, (c) Strain gauges, least count 1 micro-strain, (d) Inclinomometer, least count 0.1° , (e) Digital levelling instrument, least count 0.1mm, (f) Total station, least count 0.1mm, (f) Data acquisition system, and (g) Thermometer least count 0.5°C . Fig. 1.2 shows the instruments used for the measurement of the parameters during the static load testing of the bridges.



Fig. 1.2 Instruments used for measurement in static load testing (IRC:6-2017)

1.3.2 Acceptance criteria as per IRC

For the load test, the acceptance criteria shall be as under:

- At any critical location of a particular structural member, the measured deflections and strains shall be equal to or less than the theoretical deflections and strains obtained from respective designs.
- The theoretical deflection obtained shall be in between (**span/1500**)—as per IRC Special Publication-37 and (**span/1000**)—as per IRC:6-2017: 2017.
- The structure shall not show any cracks more than 0.30 mm for (normal) moderate exposure and 0.20mm for severe conditions of exposure.
- For various types of bridges, the percentage recovery of deflections after retention of the load test for 24 hrs. are mentioned in Table 1.1.

Table 1.1 Percentage recovery of deflections after retention for various types of bridges (IRC:6-2017)

Types of Bridges	The minimum percentage recovery of Deflection at 24 hrs after removal of the test load
1. Reinforced Concrete	75
2. Prestressed Concrete	85
3. Steel	85
4. Composite	75

1.4 DYNAMIC LOAD TESTING

Dynamic load testing of bridges is a crucial test used to assess the structural integrity to evaluate the dynamic behaviour of the bridge under dynamic load, providing real-world simulation. In addition to the resultant parameters of static load testing, dynamic load testing involves the measurement of the dynamic parameters namely: amplitude, frequency, impact coefficients, mode shapes, etc. Dynamic loads are applied to the bridge using specialized equipment such as hydraulic actuators or trucks equipped with heavy weights. Fig. 1.3 (a) shows the moving vehicle passed over the bridge as a dynamic load, Fig. 1.3 (b) shows the impact load applied over the bridge as a dynamic load, Fig. 1.3 (c) shows the hydraulic actuator is applied over the bridge as a dynamic load and Fig.1.3 (d) shows the exciter model hammer used to excite the bridge during dynamic load testing of light wooden bridges. In India, although the IRC: SP:51-2015 acknowledges dynamic load testing for accessing the bridge behaviour under dynamic loading, there are no specific guidelines and provisions for dynamic load testing of bridges.

1.4.1 Methods of Dynamic Load Testing

There are various methods of applying dynamic loads during the load testing over the bridge. Among them, the most used methods are namely: (a) Instrumented Vehicle Testing– in which a heavily loaded truck with instrumented axles crosses the bridge at various speeds, (b) Impact Testing–in which a controlled weight is dropped on the bridge deck to simulate a sudden dynamic load, (c) Ambient Vibration Testing–in which measurements are taken while the bridge is exposed to

everyday traffic, providing bridge's natural frequency (Laura et al., 2020; Gatti, 2019; Samali et al., 2007 and Baisthakur and Chakraborty, 2021)

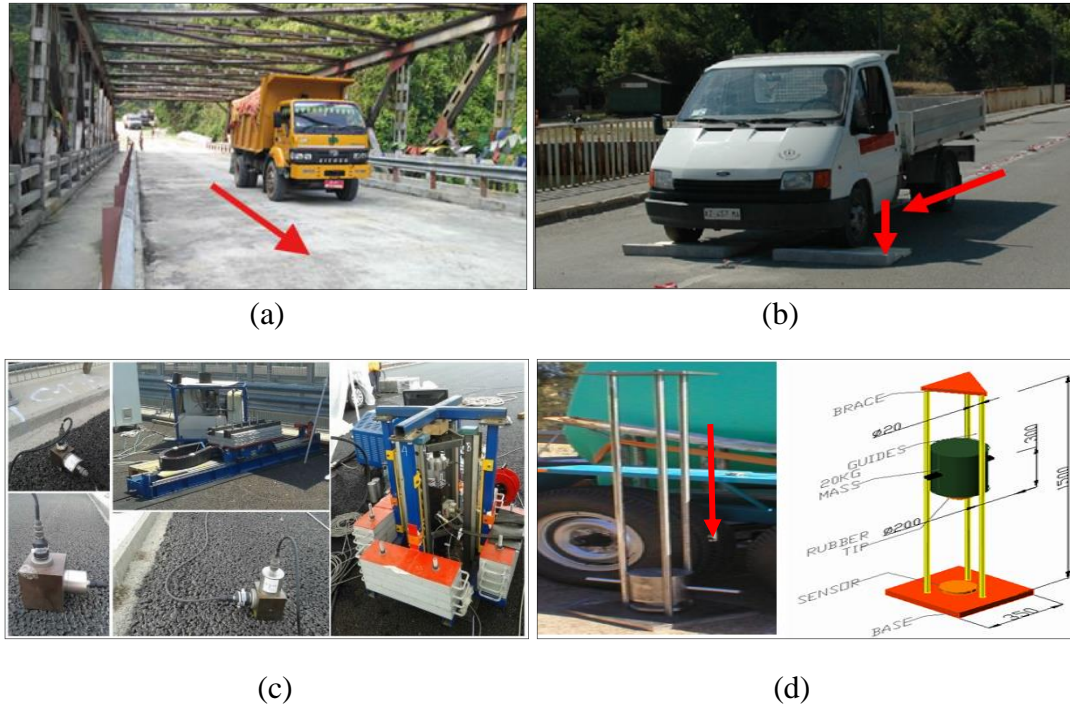


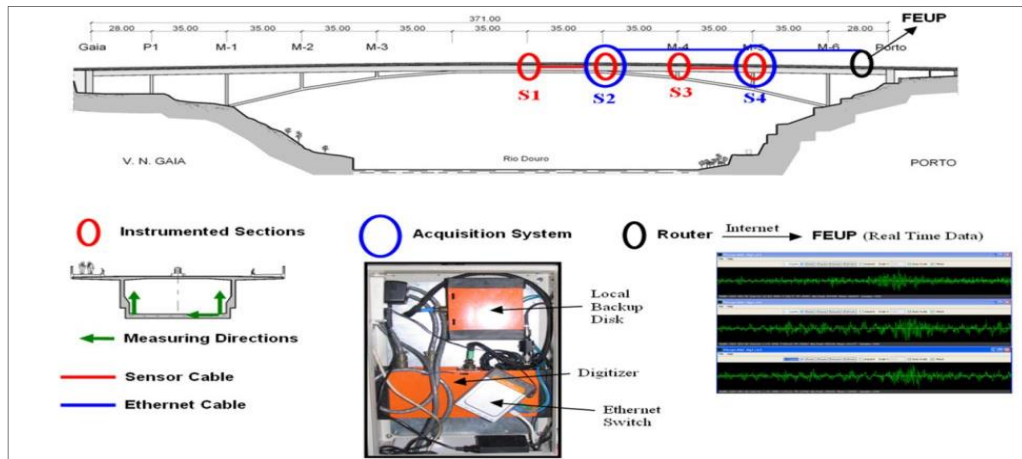
Fig. 1.3 Various types of dynamic loads used for load testing : (a) Moving vehicle passed over the bridge as a dynamic load (Baishrhakur and Chakraborty, 2021), (b) Impact load applied over the bridge as a dynamic load (Gatti, 2019) and (c) Hydraulic actuator as a dynamic load over the bridge (Laura et al., 2020) (d) Exciter model hammer (Samali et al., 2007)

1.4.2 Instrumentation

To conduct dynamic load testing, proper management of the instrumentation is essential. Fig. 1.4 (a) shows a scheme dynamic monitoring system installed along a span concrete arch bridge crossing the Douro River in the city of Proto, Portugal where sensors (accelerometers) are placed at locations S1, S2, S3 and S4. The data acquisition systems are placed at S2 and S4. Sensors are connected to the data acquisition system by sensor cable and information from the sensor are transferred through an ethernet cable to the router and then finally to FEUP (Faculty of Engineering of the University of Porto) through the internet. Fig. 1.4 (b) shows the laser vibrometer used for recording bridge vibration during the dynamic load test. Fig.1.4 (c) shows some instruments used in dynamic load testing namely, Inductive Displacement Transducer (IDT), Accelerometer set up, Strain Sensor and the process

of installation of the accelerometer at the bottom of the bridge. The instruments, generally used for the dynamic load testing of the bridges are pointed out below,

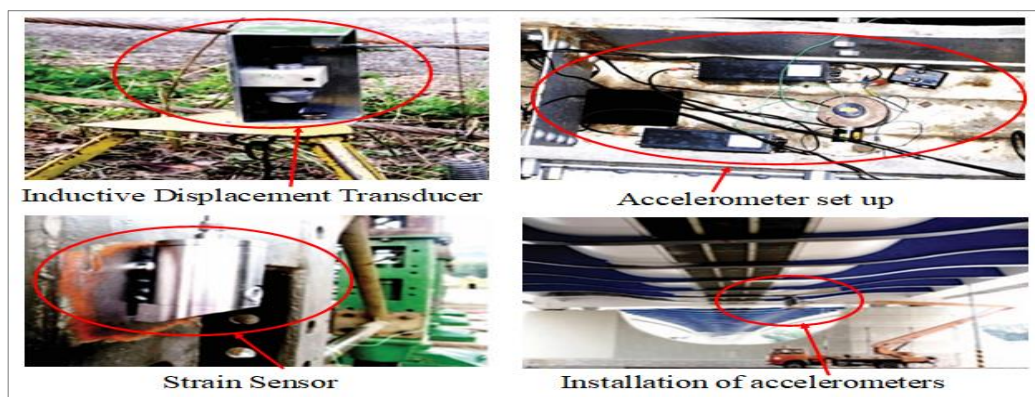
- **Accelerometers:** Accelerometers measure the acceleration of the bridge structure in response to dynamic loads. They are used to assess the bridge's dynamic response and vibrations.
- **Strain Gauges:** Strain gauges are used to measure strains or deformation in the bridge's structural components. They provide valuable information about the distribution of stress under dynamic loading conditions.
- **Displacement sensor:** Displacement sensors, such as LVTDs (Linear Variable Differential Transducer) or potentiometers, measure the displacement or movement of specific points on the bridge structure. They are essential for assessing deflections and deformations during dynamic load testing.
- **Inductive Displacement Transducers (IDT):** Inductive Displacement Transducers (IDT) are mounted at the bridge parapet or bottom of the bridge structure to monitor the amplitude time histories. Its application enables the extraction of the static component from displacement time histories by using filtering techniques.
- **Data Acquisition Systems:** Data acquisition systems are used to collect, store, and analyze data from various sensors during dynamic load testing. These systems typically include hardware for signal conditioning and amplification, as well as software for data visualization and analysis.
- **Environmental Sensors:** Environmental sensors such as anemometer (for wind speed measurements) and seismometers (for seismic activity measurement) may also be used to assess the influence of environmental factors on the bridge's dynamic behaviour.
- **High-Speed Cameras:** High-speed cameras may be employed to capture visual data of the bridge's response to dynamic loads. This visual information can complement the data obtained from other instrumentation.
- **GPS Receivers:** GPS receivers can be used to monitor the movement and displacement of the bridge structure during dynamic load testing, providing spatial data for analysis.



(a) Scheme of monitoring system (Magalhães et al., 2008)



(b) Laser vibrometer (Abedin et al., 2021)



(c) Inductive Displacement Transducer, Accelerometer set up, Strain Sensor and Installation of the accelerometer (Benčát and Kohár, 2018)

Fig. 1.4 Showing monitoring scheme for dynamic load test and typical instrumentations

1.5 RESEARCH OBJECTIVE AND SCOPE

As per the above study, there are two methods used for the assessment of bridge load-carrying capacity namely, static load testing and dynamic load testing. This study gives a comparative study of these two methods of load testing. The objectives of this study involve,

- i) To explore the feasibility of using the Dynamic Load Test (DLT) as an alternative to the conventional Static Load Testing (SLT) for evaluating the load-carrying capacity of bridges.
- ii) To develop a comprehensive numerical model utilizing advanced structural analysis techniques to simulate the response of bridge structures under both static and dynamic loading conditions, enabling the quantitative evaluation of their performance.
- iii) Use the existing available literature data for the static load test to determine the dynamic parameters of the bridge.
- iv) To analyze the obtained data from the numerical simulations for establishing a methodology for determining the load carrying capacity using the dynamic parameter of the bridge.

1.6 ORGANIZATION OF THESIS

The thesis is structured into six chapters, with one serving as the present introduction. In cases where appropriate, important figures and tables have been included. A summary of each chapter's content is provided below.

Chapter 1: Introduction

This chapter gives the general study on the assessment of bridge load carrying capacity using the static load testing and dynamic load testing of the bridge along with the motivation behind the selection of this topic for the dissertation followed by the objectives and scope of the work.

Chapter 2: Literature Review

^ This Chapter provides brief introduction of bridge with some literature work followed by literature review on the static load testing, literature review on dynamic load testing and discusses the gap of the study.

Chapter 3: Numerical Study to Analyze the Effect of Eccentricity of the Moving Vehicle from the Kerb of the Bridge

This chapter provides a finite element analysis of a reinforced concrete bridge by applying IRC Class AA-tracked moving load in longitudinal and transverse directions of the bridge. It includes the study of variation in resultant parameters namely, total deformation, equivalent stress, and equivalent strain produced in the bridge for different eccentric paths of moving load from the kerb of the bridge.

Chapter 4: Numerical Study to Investigate the Deflection Behavior in a Concrete Bridge Under IRC Recommended Loading Scenarios

This chapter provides a numerical study to for the deflection behavior of a concrete bridge under IRC:6-2017 recommended loading scenarios. It includes introduction of the bridge data to be used in the upcoming chapter and builds up the understanding of the nuances of the static load test where different loading conditions.

Chapter 5: Proposed Methodology for Dynamic Load Test

This chapter provides the proposed methodologies to find the Dynamic Load Carrying Capacity (DLCC) of the bridge using parameters from static load test and that from dynamic load test.

Chapter 6 : Conclusion and Future Work

This chapter provides the conclusion of the dissertation and the proposed future work.

Moreover, at the end of this dissertation, references, publications, appendix and curriculum vitae are provided.

CHAPTER 2

LITERATURE REVIEW

2.1 INTRODUCTION

A bridge is an engineered construction meticulously planned to extend across a natural hindrance, such as a river or thoroughfare, establishing a route to streamline transportation and forge a link between two points that would otherwise be distant from each other. Based on the material used, simply, the bridges found are concrete, steel bridges, wooden bridges, and composite bridges (Lin and Yoda, 2017). Literatures have studied different parameters under finite element analysis using different finite element analysis softwares. Song et al. (2002) performed the finite element failure analysis of in-situ deteriorated reinforced concrete T-girder bridges subjected to cyclic loading and studied the deflection at the centre under applied load. Shaikh et al. (2022) performed the static analysis of a reinforced concrete box-girder bridge with a ballastless sub-track system using the finite element method (ANSYS software) to evaluate the deflection and stresses in the bridge when loaded according to Indian Railways Standards. Sasidharan and Johny (2015) performed the finite element analysis using ABAQUS software for the parametric study of curved concrete box girders by varying the span and radius of curvature keeping the span-to-depth ratio constant and studied the variation of parameters like reaction forces, bending stresses, shear stresses, mid-span deflection under different combination of dead load, superimposed load, and live load.

In the realm of civil engineering, the structural integrity and performance bridges stand as critical components of transportation infrastructure (Omar and Nehdi, 2018 and Ryan et al., 2023). One of the fundamental aspects of this evaluation is the analysis of deflection, which serves as a key indicator of a structure's ability to withstand dynamic loads such as moving vehicles (Liu et al., 2019). Understanding the deflection patterns under different loading scenarios is crucial for designing bridges that not only meet regulatory standards but also optimize material usage (Chen et al., 2014). Some literatures related to the measurement of the vertical deflection of

the bridge are Zhou et al. (2012), and Islam et al. (2015). Zhou et al. (2012) developed the FE model in *Strand7* Software and applied the static load over the bridge to find out the static deflection of the bridge. Islam et al. (2015) developed the FE model in ABAQUS software and applied a pressure load over the bridge to find out the static deflection.

Modern infrastructure is not complete without bridges, which act as important arteries for the effective transportation of people and products. For bridges to operate safely and sustainably, their structural soundness and load-bearing capacity must be guaranteed. A difficult and multidimensional task, determining a bridge's load-carrying capacity entails evaluating multiple structural components under various loading scenarios. In this context, static load testing and dynamic load testing have become the two widely used procedures for evaluating bridge load-carrying capacity. This chapter provides a brief overview of the previous research work on the assessment of bridge load-carrying capacity using both static load testing and dynamic load testing and focusing on the dynamic load testing of the bridge.

2.2 LITERATURE REVIEW ON STATIC LOAD TESTING

As per IRC: SP 51-2015 (2015)—guidelines for load testing of bridges, before commencing the load test, theoretical deflection at the critical location of the span to be tested shall be worked out with the design load; all the visual defects in the bridge shall be measured, mapped, and plotted; bearing shall be ensured for their functional condition; expansion joints, gaps shall be ensured for their functional condition; all the instrumentation should be done at a desired location and in a good way. The loading operation stages from 0%, 50%, 75%, 90%, and 100% of the test load placement, which shall be completed in 4 hours. The increment of loading should be done at an interval of 1 hour and during the same time temperature and deflections are recorded for each stage of loading. After completion of 100% loading, it is retained for 24 hours. Again, temperature and the deflection due to this loading are noted. Immediately, after 24 hours of 100% loading, offloading is started as 100% loading to 90% loading, 90% loading to 75% loading, 75% loading to 50% loading, and 50% loading to 0% loading in the reverse way of the loading. The unloading stages are completed within 4 hours as the loading stages at an interval of 1 hour, noting

deflection and temperature during each stage of unloading. After 24 hours of removal of the test load, deflection and temperature are again noted. Then temperature corrections, bearing displacement corrections, and rotation corrections are applied to the deflection and the results are analyzed. The percentage recovery for the deflection values can be calculated as,

$$\text{Percentage recovery} = \frac{R3-R5}{R3-R1} * 100 \% \quad (1.1)$$

Where, R1 is the deflection with no load (initial reading), R2 is the deflection one hour after applying full test load, R3 is the deflection 24 hours after applying full test load, R4 is the deflection immediately after removing the test load and R5 is the deflection 24 hours after removing the test load. The acceptance criteria for the percentage recovery of deflection for various types of bridges are mentioned in Table 1.1.

2.3 LITERATURE REVIEW ON DYNAMIC LOAD TESTING

Samali et al. (2007) conducted the load rating of impaired bridge using a dynamic method. The dynamic assessment procedure involved the measurement of the vibration response of the bridge superstructure using the accelerometer. The excitation was generated by a modal impact hammer. The two frequencies of the bridge were noted: at unloaded condition and loaded (such as truck, concrete block, water tanker, etc, of known weight) at midspan. From these frequencies in-service stiffness of the bridge was estimated and using this stiffness the load carrying capacity of the bridge was estimated following a statistically based analysis.

$$k = \frac{(2\pi)^2 * f_1^2 * f_2^2}{f_1^2 - f_2^2} * \Delta \hat{m}_i \quad (1.2)$$

This equation can predict the flexural stiffness with the added mass, compensated with the modal mass $\Delta \hat{m}_i$. Where, f_1 and f_2 are, respectively, the natural frequencies of the bridge before and after adding mass but expressed in Hertz.

Magalhães et al. (2008) performed the dynamic monitoring of a recently installed long-span concrete arch bridge crossing the Douro River in the city of Porto, Portugal: the “Infante D. Henrique” bridge. They described the experimental and numerical studies developed before equipment installation, characterized the

monitoring system used, and presented the results achieved with MATLAB routines developed to process the data received through the Internet. To estimate the modal parameters experimentally, they used Ambient Vibration Tests (AVTs). Furthermore, the data collected during these tests were of the same type as the data recorded by the dynamic monitoring system so that the same identification could be used. The routines implemented include the online automatic identification of natural frequencies of the bridge with the Frequency Domain Decomposition method, enabling the track of the bridge's first 12 natural frequencies. This unique feature is only possible due to the combination of high-quality acquisition equipment with state of art processing algorithms.

Islam et al. (2015) proposed a method for load load-carrying capacity of the 25-year-old prestressed box beam (PSBB) bridge based on dynamic response collected using a wireless sensor network (WSN). They have taken two bridges namely: Ashtabula Bridge and Trumbull Bridge. They proposed the method based on the data collected using the Ashtabula Bridge and the proposed method was deployed on Trumbull Bridge. The Finite Element (FE) model, in ideal conditions, for the Ashtabula Bridge, was validated using two methods: (1) experimental validation by using frequency analysis and (2) theoretical validation by using static analysis. The FE model was created in the ABAQUS software. For the experimental validation, the fundamental frequency bridge was determined using the FE model and the field acceleration data. The theoretical validation was done using analytical analysis and FE model numerical analysis for maximum stress, maximum deflection and total mass of the bridge under the same loading. The load rating of the bridge was estimated herein from the vibration signatures of the bridge under loads collected using two WSNs each having one monitor and four sensors. The service stiffness of the bridge was calculated to determine the load rating. The application software developed from this research can instantly determine the load rating of a PSSB bridge by collecting its real-time dynamic response.

Sun et al. (2021) introduced an efficient approach to access the load-carrying of girder bridges based on the displacement caused by moving vehicles. The method encompasses three primary steps: dynamic displacement measurement using

radar during a truck pass-by test, extracting the influence line diagram, and estimating displacement under static load conditions. Based on these steps, load-carrying capacity evaluation follows the AASHTO manual guidelines. The validity of this method was confirmed through numerical simulation employing a three three-dimensional finite element method of a typical girder bridge subjected to vehicle loads. The simulations investigated the impact of vehicle weight, speed, and road surface quality on displacement accuracy. Furthermore, a real-world test was conducted on a simply supported pre-stressed concrete girder bridge to assess the practical feasibility and cost-effectiveness of the proposed approach. The results demonstrate the reliable evaluation of girder load ratings, with the added benefit of being more efficient and economical than traditional.

2.4 LITERATURE REVIEW ON TOGETHER USE OF BOTH STATIC LOAD TESTING AND DYNAMIC LOAD TESTING

Zhang et al. (2012) conducted a case study of a single-tower composite girder cable-stayed bridge to assess the load-bearing capacity and performance under designed loads. This evaluation was carried out through both static and dynamic load tests. The dynamic load test focused on measuring the bridge's dynamic attributes, such as vibration frequency, damping, forced vibration amplitude, and impact coefficient. Meanwhile, the static load test examined static properties, including static strain and static deflection. The findings reveal that the bridge exhibits favourable characteristics in terms of rigidity, strength, integrity, and dynamic behaviour. Moreover, the bridge's load-bearing capacity is deemed satisfactory based on the test results.

Caglayan et al. (2012) assessed a concrete bridge located in an earthquake-prone region, in the southern part of Turkey. Based on the structural parameters obtained from the dynamic test and static tests, the FE model of the bridge was generated in COMSOL/S and this model was used for the calculation regarding the structural assessment of the bridge. For the static load test, two diesel locomotives of DE24000 type were used. As per the site condition, the measurement of the parameter of the static load test was done using the tiltmeter. It was then converted into the deflection value after applying the required correction. For

the dynamic load test, the Turkish train was run over the bridge and the dynamic parameters were recorded using the accelerometer.

Laura et al. (2016) published a paper giving best practice examples of highway bridges on which static and dynamic testing procedures are applied. They evaluated and compared structural responses and performances of a multi-span bridge, inaugurated in 2014, along a new highway link, in northern Italy. They analyzed the main steps and results of the bridge passing the Adda River. Loading and unloading sessions were carried out with different configurations of trucks each having a total weight of 420 KN for the static load test to measure the deflections of the viaduct. To qualify the bridge's dynamic behaviour of the bridge AVS was first used for dynamic load analysis with ambient vibrations only, like wind, background noise, etc. Then Operational Modal Analysis (OMA) was utilized to obtain the main frequencies, the corresponding modal shapes, and the damping ratios. Also, Experimental Modal Analysis (EMA) was done using Ambient Vibration Tests (AVTs) and Harmonically Forced Tests (HFTs). The OMA and EMA are equated to twin with the numerical model. The comparison revealed that the dynamic load test can supplement the static load test for the structural evaluation of new viaducts and monitoring of operational viaducts.

Gatti (2019) performed a case study on structural monitoring of an operational bridge. The author examined the structural reactions, performances, and costs of simultaneously conducting static and dynamic load tests while evaluating the structural reliability of a prestressed reinforced concrete bridge constructed in the late 1960s. The test was performed based on the American Association of State Highway and Transportation Officials (AASHTO) requirements. The precision spirit levelling method was employed in the static load test to determine the deflections of the deck brought on by four trucks, each weighing roughly 36 tonnes. Accelerometers mounted on the main beam were utilized in the dynamic load test to measure the vibration frequencies that followed an impulse generated by a 2-ton truck. An improved finite element model of the bridge was produced as a consequence of the dynamic load test. The comparison revealed that the dynamic load test can complement the static load

test for the structural evaluation of new bridges or can take the place of it for the maintenance of existing bridges.

Abedin et al. (2021) conducted a series of static and dynamic load tests, on a precast-prestressed box-beam bridge that had been in service for more than 50 years, to better understand the current behaviour of the bridge and to assess the possible damage to the longitudinal joint. During the static load test, three different types of instruments: dial gauges, linear variable displacement transducer, and total stations were used to record the vertical deflections of the first three precast concrete units that were the closest to the bridge's southern edge. To record bridge vibration accelerometers and a laser vibrometer were used at midspan and the natural frequencies were extracted. A detailed FE model was created with the intent to aid in the analysis of the result of the experiment and investigate the behaviour of the panel joint. The measured panel deflection from the static load test was much more than that from the FE model analysis. Among the three mode shapes of the bridge, the second mode shape corresponding to the torsional mode of structure is sensitive to damage and was found less in the dynamic test than FE modal analysis. Moreover, when actual bridge response and reflective cracking and leaking in the deck's surface at longitudinal joints were compared to the results of the FE model without taking damage into account (bridge deflection and frequency), it was found that the joints were damaged. The results showed that joint damage affects the bridge integrity, alters the live load distribution, and can potentially reduce the bridge load-carrying capacity.

Baishrhakur and Chakraborty (2021) performed an experimental verification for load rating of a steel truss bridge using an improved Hamiltonian Monte Carlo (HMC)-based Bayesian model updating. The early element model was sequentially updated to equate the static and dynamic characteristics of the bridge. The static test was performed as per Indian Road Congress (IRC) guidelines. For the dynamic test, the 22T vehicle was passed, at a speed of 20 kmph, over the bridge and responses were recorded using the wireless accelerometer to identify modal characteristics. The updated modal works as a digital twin of the original structure to predict its load-carrying capacity and performance under proof or design load.

Wang et al. (2022) Performed a moving load test-based repaid bridge capacity evaluation through an actual influence line. In this work, a moving load test method based on influence lines was suggested for a quick assessment of bridge capability. Initially, the moving load test was used to extract the bridge's influence line. The capacity evaluation indices for the bridge were established as the maximum amplitude and total area ratios between the actual and theoretical effect lines. The proposed evaluation indices were shown to be equivalent to the traditional static evaluation index based on numerical validations of three typical deterioration conditions (local damage, change of the boundary condition, and prestress loss). In-situ static load (6 trucks each of 350KN) and moving load tests were also carried out to confirm the efficacy of the suggested methodology. The findings demonstrate that the proposed indices have a maximum difference from the static evaluation index of 1.5% in the numerical validations and 2.2% in the in-situ tests, demonstrating that the proposed method is more precise and efficient for future short/medium-span bridge capacity evaluation.

Lu et al. (2022) proposed a method based on the combined bridge dynamic load test results and the Kriging model to realize the accurate prediction of the bridge static load test results. A three-span continuous inclined leg rigid frame bridge was utilised as an example to forecast the static behaviour of the bridge in order to confirm the accuracy and efficacy of the suggested method. ANSYS software was used to create the bridge's complete finite element analysis model. Five automobiles, each weighing around thirty tonnes, were employed for the static field load test. The weight was added step-by-step to the maximum load level and then gradually unloaded to the zero load level. In a static load test, it was discovered that the measured deflection value and the theoretical deflection value did not match. Data acquisition and signal processing were used in the experiment to conduct the dynamic field load test (DASP). The observed frequency of the bridge and the theoretical computation frequency were found to be inaccurate. The Kriging model's anticipated parameters were used to update the finite element model. It was discovered that following the model update, the frequency value had improved and was becoming closer to the measured value. Additionally, the kriging model's accuracy and adaptability in the infinite element

update and bridge static behaviour prediction were confirmed. This approach can significantly lower the cost and duration of the bridge's static load test, lessen its negative effects on traffic, and prevent needless structural and human damage to the bridge's structure as a result of static load. Additionally, it can be applied to the upkeep and technical state evaluation of already-existing bridge constructions.

De Angelis and Pecce (2023) emphasized the importance of considering both load and dynamic tests in the structural assessment of bridges, a departure from their conventional separate application with distinctive objectives. They employed these two testing methods on a bridge designed by Ricardo Morandi in the early 1950s, in Benevento; the bridge had challenges in terms of its static design, deck and pier sections, and deviation from the boundary condition. The FE model was updated according to the comparison between the experimental and numerical results of the initial FE model to reduce differences. The study highlighted the synergy between dynamic tests, which elucidate linear behaviour and seismic readiness, and load tests, providing insight into nonlinear serviceability responses. Vertical constraints, stiffness, and the impact of structural interventions were also crucial considerations. The study confirmed the bridge's linearity in both static and dynamic tests, emphasizing their complementarity. It advocated the combined use of both tests for robust bridge assessment, emphasizing an engineering approach and precise surveying for precise structural insights.

2.5 GAP OF THE STUDY

The dynamic load test, implemented as an alternative to the static load test in various countries, presents an innovative approach to access structural integrity; nevertheless, within the Indian context, research on this methodology remains scarce. Dynamic load testing offers potential advantages over static counterparts, such as reduced testing time, its application and efficacy within the unique environmental, infrastructural, and regulatory landscape of India necessitate further investigation. Therefore, there is a pressing need to explore the feasibility and effectiveness of substituting the conventional Static Load Test (SLT) with the Dynamic Load Test (DLT) for evaluating the load-carrying capacity of bridges in India. Addressing this research gap is crucial for comprehensively evaluating the feasibility and reliability of

dynamic load testing within the Indian construction industry, thereby facilitating informed decision-making, and ensuring the safety and longevity of infrastructure projects across the nation.

CHAPTER 3

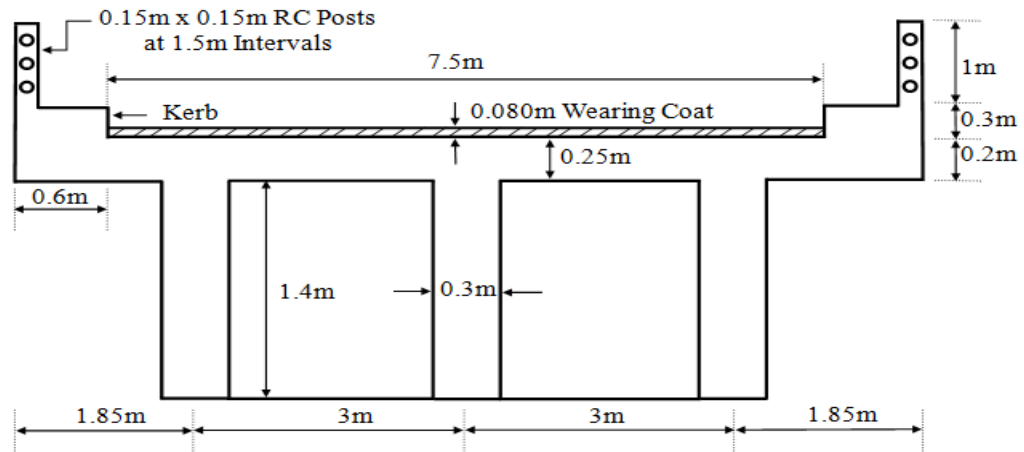
NUMERICAL STUDY TO ANALYZE THE EFFECT OF ECCENTRICITY OF THE MOVING VEHICLE FROM THE KERB OF THE BRIDGE

3.1 INTRODUCTION

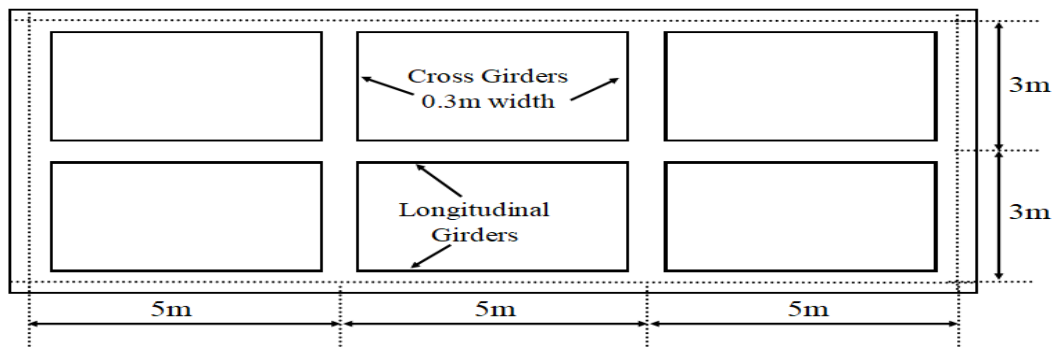
In this chapter, an attempt is made to analyze the reinforced concrete bridge by applying IRC Class AA-tracked moving load in longitudinal and transverse directions of the bridge. The Finite element model is formulated in ANSYS software. The variation in resultant parameters namely, total deformation, equivalent stress, and equivalent strain produced in the bridge are analyzed for moving load passing from different positions across the cross-section of the bridge. Also, for each case, the position of the moving load at which it gives the maximum values for the resultant parameters in the bridge is determined.

3.2 VALIDATION OF NUMERICAL MODEL

The validation of the numerical model has been carried out with respect to the literature (Gupta et al., 2023), taking a 15m span bridge as shown in Fig.3.1. For the validation model, the properties taken for the reinforced concrete of M25 were Young's modulus = 2.5×10^{10} N/m², Density = 2500 kg/m³, Poission's ratio = 0.18 and the live load taken for the analysis was the IRC class AA tracked vehicle as taken in literature (Gupta et al., 2023). In the literature, the analysis of this bridge was done in CSiBridge software. The validation model, showing the path of moving load as per literature (Gupta et al., 2023) is as shown in Fig.3.2. As shown in Fig.3.3, for a mesh size of 20cm in CSiBridge, maximum deflection (deformation) in the bridge was 7.28 mm. For the same mesh size, in ANSYS software, the maximum deformation in the bridge has been observed as 7.56mm, as shown in Fig.3.2. The difference in these two deformations found is 0.28mm and the percentage of error obtained is 3.84%. Since the percentage error is within an acceptable limit, hence the numerical model has been validated in ANSYS software based on the deformation from both the literature and the ANSYS software.



(a) Cross-section of Bridge-Deck



(b) Plan of Bridge-Deck

Fig.3.1 T-Beam and Slab Bridge-Deck for 15m of span used for validation
(Gupta et al., 2023)

3.4 NUMERICAL MODEL FOR STUDY IN ANSYS WORKBENCH

3.4.1 Bridge and Loading Details

Fig.3.4 shows the data for the geometry of the bridge used in this study. The total span length is 16.3m and the boundary condition has been considered as the simply supported condition. For modelling in ANSYS Workbench, properties taken for the reinforced concrete were Young's modulus= 3.162×10^{10} N/m², Density=2500kg/m³, and Poisson's ratio=0.18. The live load taken for the analysis was the IRC class AA tracked vehicle load which is shown in Fig.3.5.

3.4.2 Modelling Details

Modelling of the T-beam girder bridge as shown in Fig.3.4 has been carried out in AutoCAD and imported in the ANSYS Workbench under the transient structural

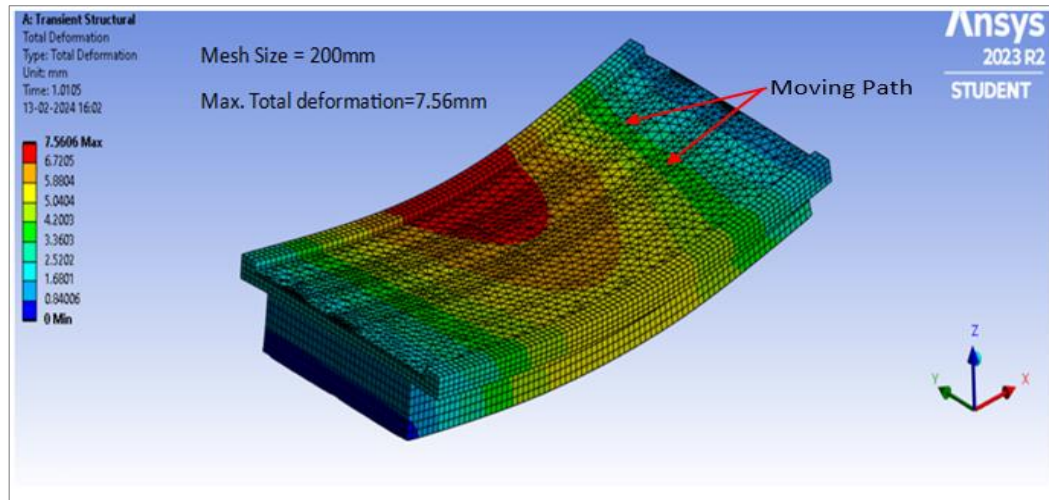


Fig.3.2 Deflected bridge model in ANSYS used for validation

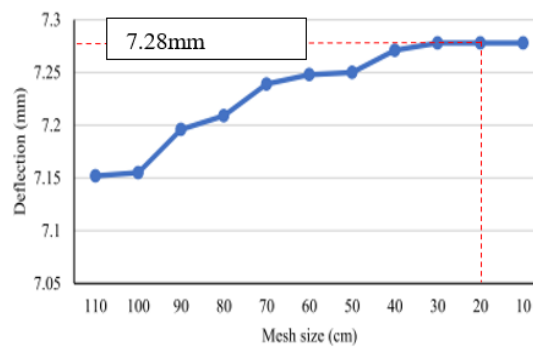
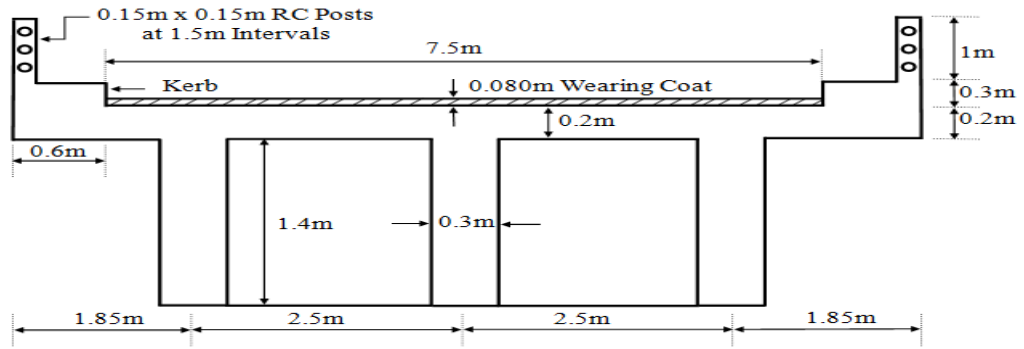
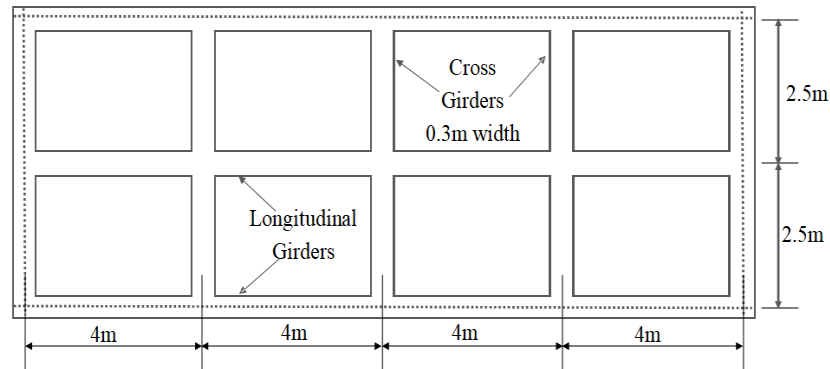


Fig.3.3 Deflection for different mesh sizes in CSiBridge (Gupta et al.,2023)

analysis system. The modelling of the bridge in ANSYS consists of 3D solid elements; precisely, SOLID65 elements for reinforced concrete structures. The cross-sectional and 3D view of the bridge is shown in Fig.3.6. The crash barrier of the bridge shown in Fig.3.4 was not modelled for simplicity, however, the crash barrier load has been applied as the line load of 0.7 N/mm (Raju, 2010). The numerical model showing all boundary conditions and loading is shown in Fig.3.7. In this model, at the left end, hinge support and roller support at the right end were provided as the simply supported boundary condition, the dead load was applied as the standard earth gravity of 9.81 m/s^2 and the live load was applied as the Class AA tracked vehicle load. The meshing of the geometry has been carried out as shown in Fig.3.8, where the wearing coat portion consists of triangular (tetrahedral in 3D) meshing and the cross girders deck and longitudinal girders consist of rectangular (hexahedral in 3D) meshing.



(a) Cross-section of Bridge-Deck



(b) Plan of Bridge-Deck

Fig.3.4 T-beam and Slab Bridge Deck used in the study (Gupta et al., 2023)

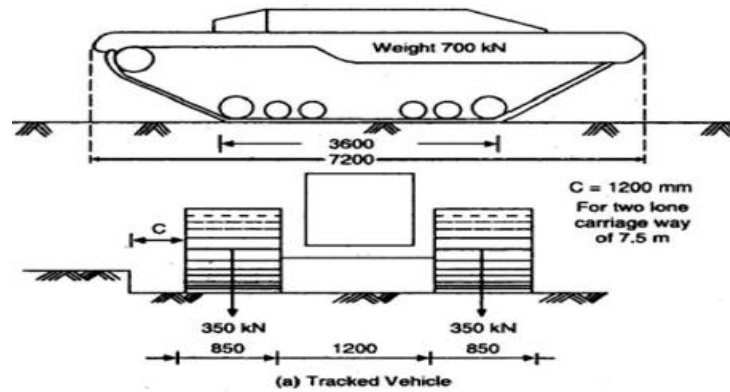


Fig.3.5 IRC Class AA tracked vehicle load (IRC:6-2017)

For the mesh convergence study, the moving load was applied on the bridge at the distance of 1200mm from the kerb and the maximum deformation of the bridge for mesh sizes 500mm, 400mm, 300mm and 200mm were studied. The results were converging for a mesh size of 200mm as shown in Fig.3.9 which shows the variation

of maximum total deformation with respect to mesh size. Based on the convergence study the mesh size adopted for modelling has been taken as 200mm and the model consisted of 81892 nodes and 19188 elements.

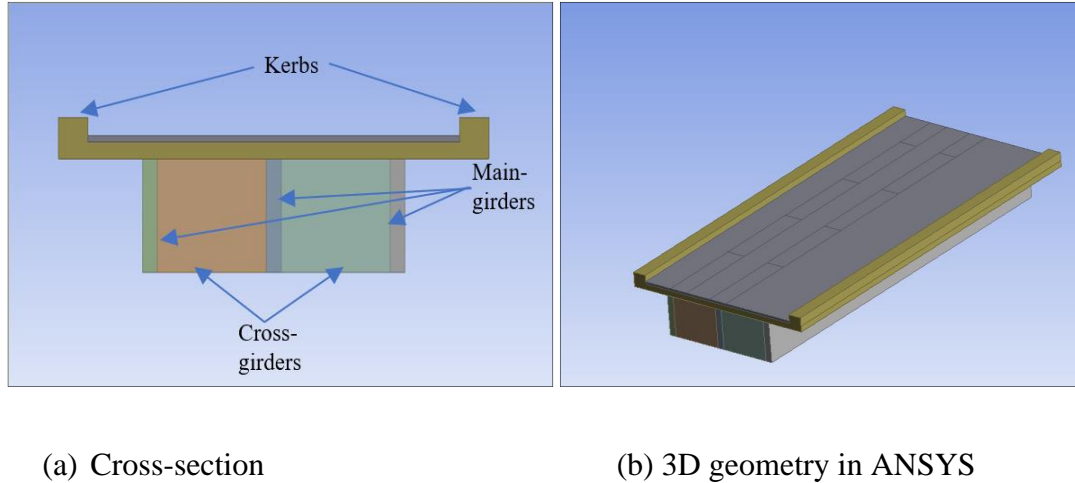


Fig.3.6 Cross-sectional and 3D view of the bridge in ANSYS

3.4.3 Transient/Moving Loading

For the transient analysis, the analysis setting has been chosen as shown in Fig.3.10 (a) where the number of steps taken is 1, the step end time is 1.2 seconds, the time step is 0.2 seconds and the solver type chosen as program controlled. The moving load has been applied over the bridge was IRC Class AA tracked vehicle load shown in Fig.3.5. The loads have been passed from various positions along the cross-section of the bridge. At first, the load was passed at a position 1200mm from the kerb of the bridge. The transient loadings for this condition are shown in Fig.3.10 (b) to Fig.3.10 (f). Fig.3.10 (b) shows the vehicle's first position at 0.2 seconds, Fig.3.10 (c) shows the vehicle's second position at 0.6 seconds, Fig.3.10 (d) shows the vehicle's third position at 0.8 seconds, Fig.3.10 (e) shows the vehicle's fourth position at 1.0 second, Fig.3.10 (f) shows the vehicle's fifth position at 1.2 seconds. Correspondingly, the loadings have been applied on other different eccentric paths at positions of 1300mm, 1400mm, 1500mm, 1600mm, 1700mm, 1800mm, 1900mm, 2000mm, 2100mm, 2200mm, and 2300mm from the kerb to study the variation of parameter namely, maximum total deformation, maximum equivalent stress and maximum equivalent strain.

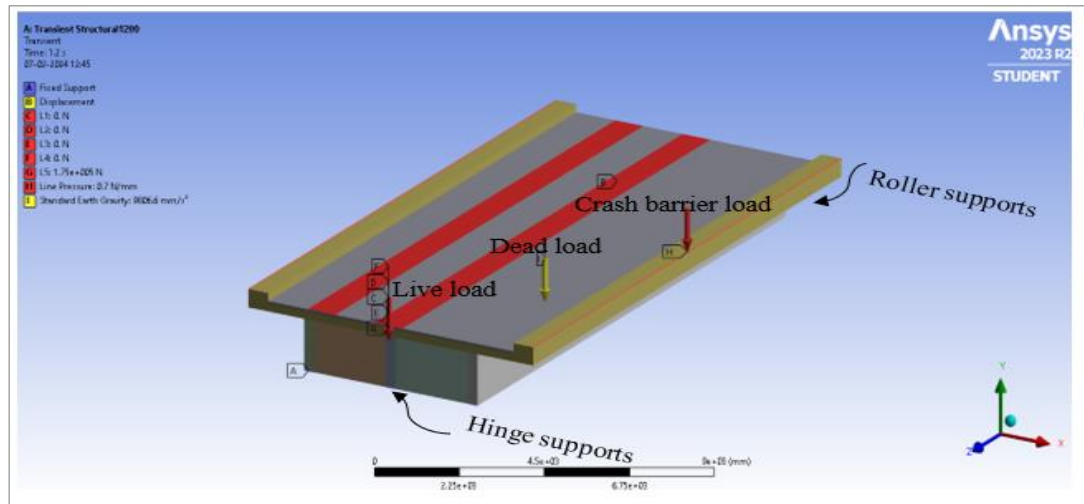


Fig.3.7 Showing boundary conditions and loadings

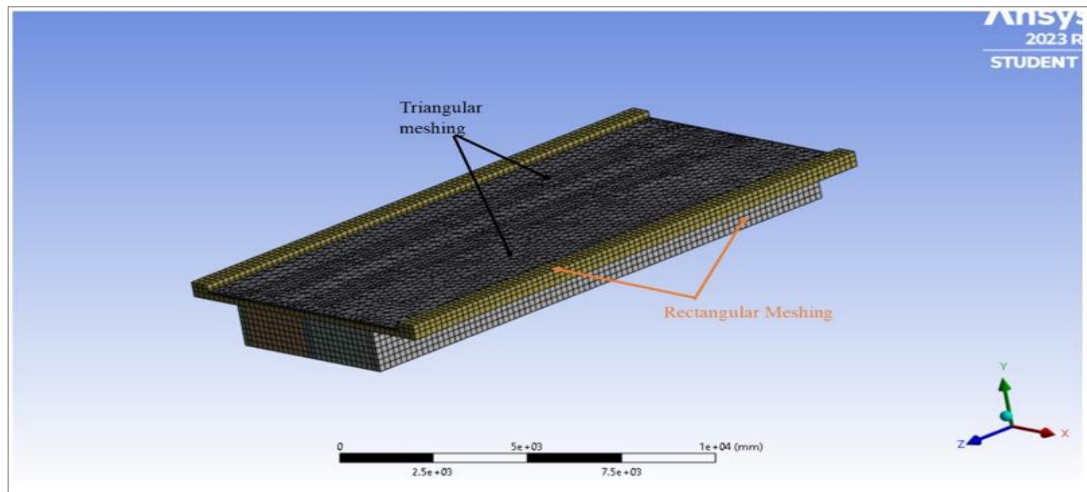


Fig.3.8 Showing meshing in the model

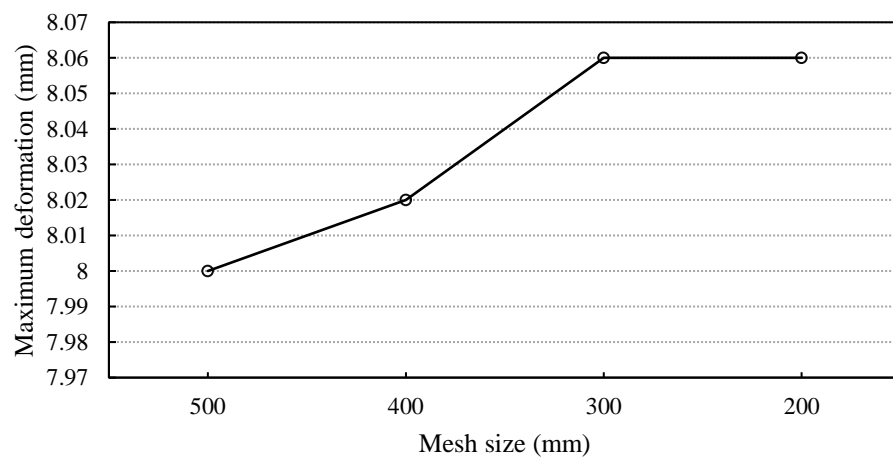
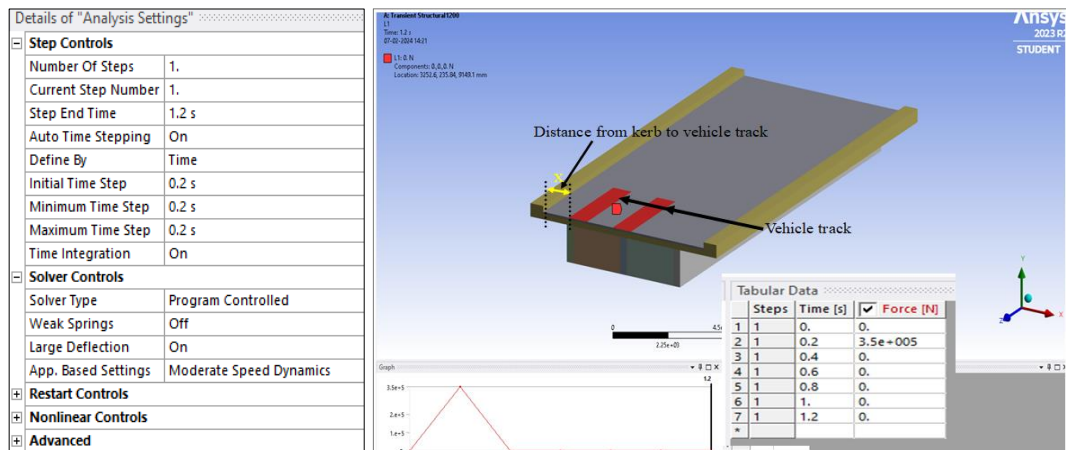
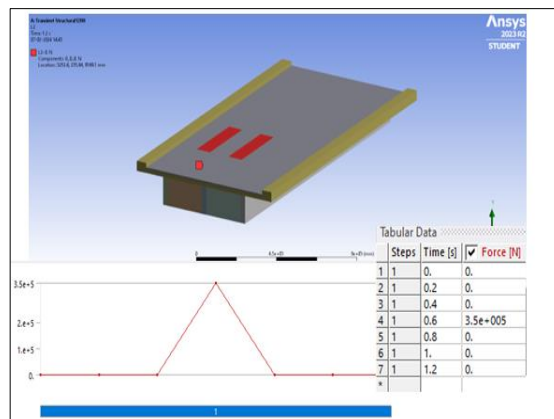


Fig.3.9 Maximum deflection vs Mesh size

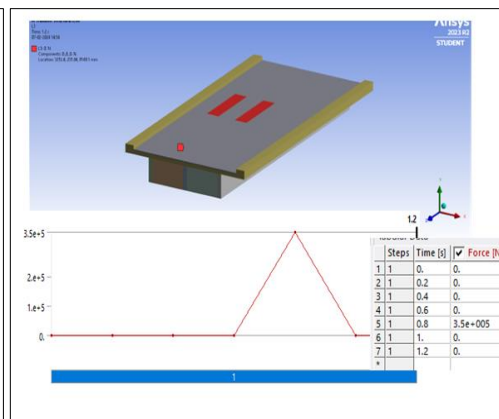


(a)

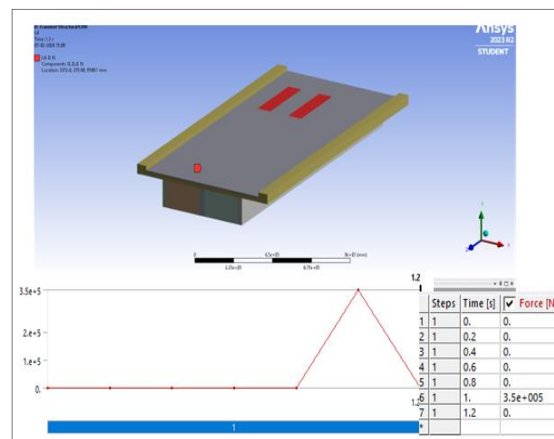
(b)



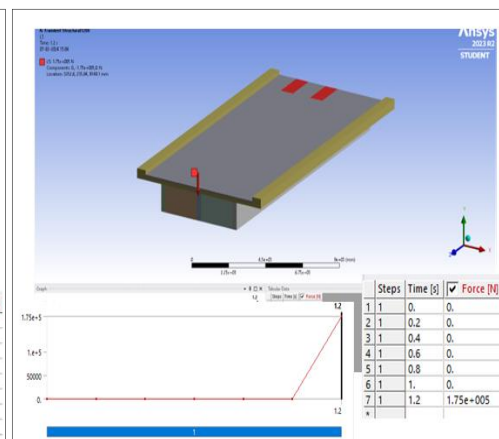
(c)



(d)



(e)



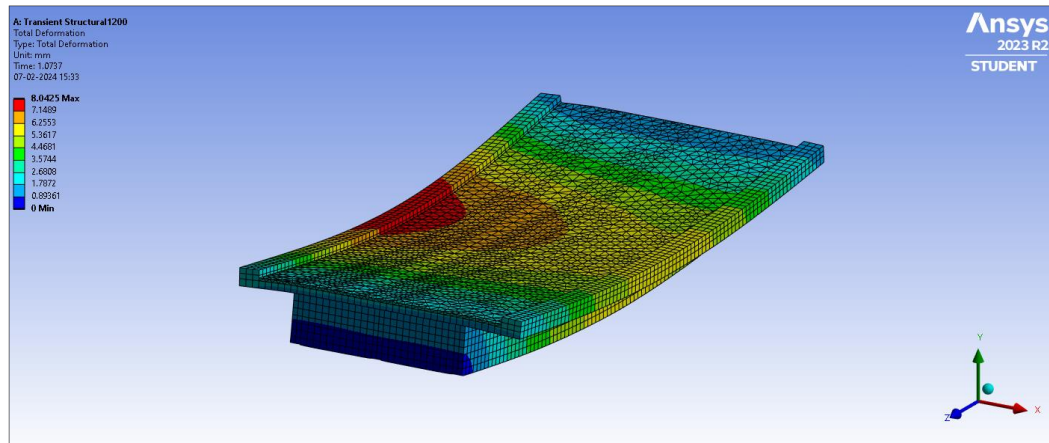
(f)

Fig.3.10 (a) Analysis setting, (b) Vehicle's first position at 0.2 sec., (c) Vehicle's second position at 0.6 sec., (d) Vehicle's third position at 0.8 sec., (e) Vehicle's fourth position at 1.0 sec. and (f) Vehicle's fifth position at 1.2 sec.

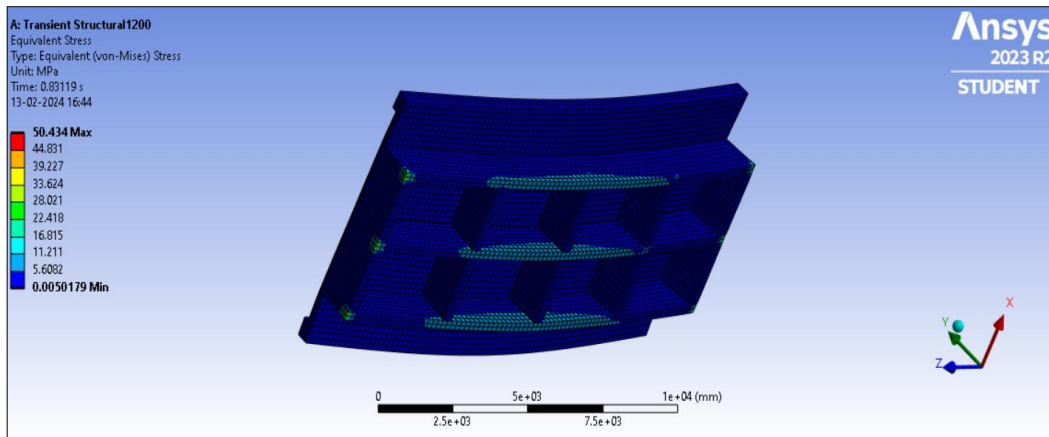
3.5 RESULTS AND DISCUSSIONS

For various moving load positions, the maximum total deformation, maximum equivalent stress, and maximum equivalent strain in the bridge are studied. Fig.3.11 shows the maximum total deformation, maximum equivalent stress and maximum equivalent strain when the moving vehicle is at an eccentricity of 1200mm from the kerb. Fig.3.11(a) shows that the maximum total deformation found in the bridge is 8.0636mm, Fig.3.11(b) shows that the maximum equivalent stress found in the bridge is 51.633MPa and Fig.3.11(c) shows that the maximum equivalent strain found in the bridge is 0.00163, for the 1200mm eccentric loading position. Fig.3.12 shows the position of the moving vehicle for a specific time of 0.8 seconds. Similarly, the positions of the moving vehicle for maximum values of the parameters namely total deformation, equivalent stress and equivalent strain at any specific time were noted. The results for the variation of the maximum total deformation, maximum equivalent stress, and maximum equivalent strain with increasing eccentricity distance of the moving vehicle from the eccentric path at 1200mm position from the kerb to that at 2300mm from the kerb are shown in Fig.3.13 to 3.15 respectively. Fig.3.13 to Fig.3.15 shows that the parameters namely maximum total deformation, maximum equivalent stress and maximum equivalent strain are decreasing with increasing eccentricity of the load path from the kerb. The time and position of the vehicle in the longitudinal direction corresponding to the maximum values of the parameters namely total deformation, equivalent stress and equivalent strain for all the eccentric paths from 1200mm position to 2300mm position from the kerb are listed in Table 3.1. Table 3.1 shows that among all load paths, the maximum total deformation of 8.06mm, maximum equivalent stress of 51.63 MPa and maximum equivalent strain of 0.00163 have been observed for the load path at 1200mm position from the kerb. For this load path, the vehicle position for maximum total deformation is (1200, 10800)mm and that for maximum equivalent stress and maximum equivalent strain is (1200, 7200)mm.

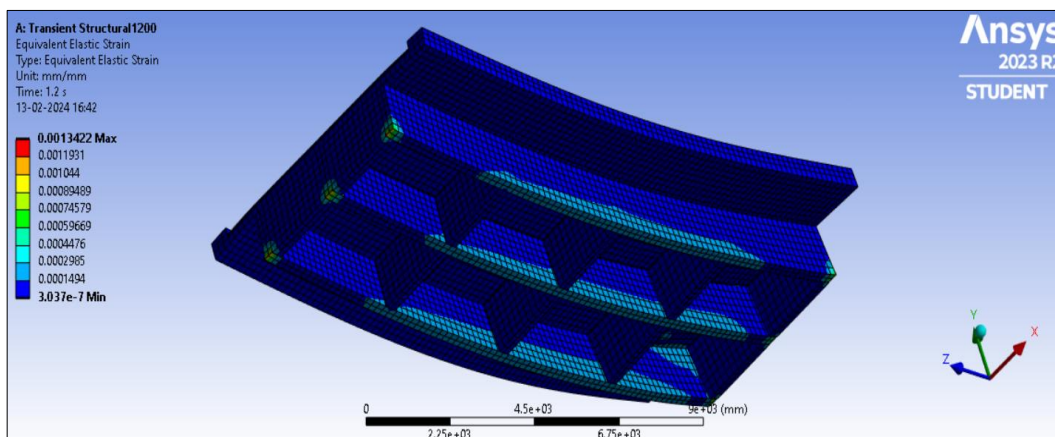
The results show that the percentage decrease in maximum total deformation from a path at 1200mm position to the path at 2300mm position from the kerb is 13.76%, maximum equivalent stress from a path at 1200mm position to the path at 2300mm position from the kerb is 9.48% and maximum equivalent strain from a path at 1200mm position to the path at 2300mm position from the kerb is 9.48%.



(a) Maximum total deformation



(b) Maximum equivalent stress



(c) Maximum equivalent strain

Fig.3.11 Maximum total deformation, maximum equivalent stress and maximum equivalent strain for an eccentricity of 1200mm for the moving vehicle

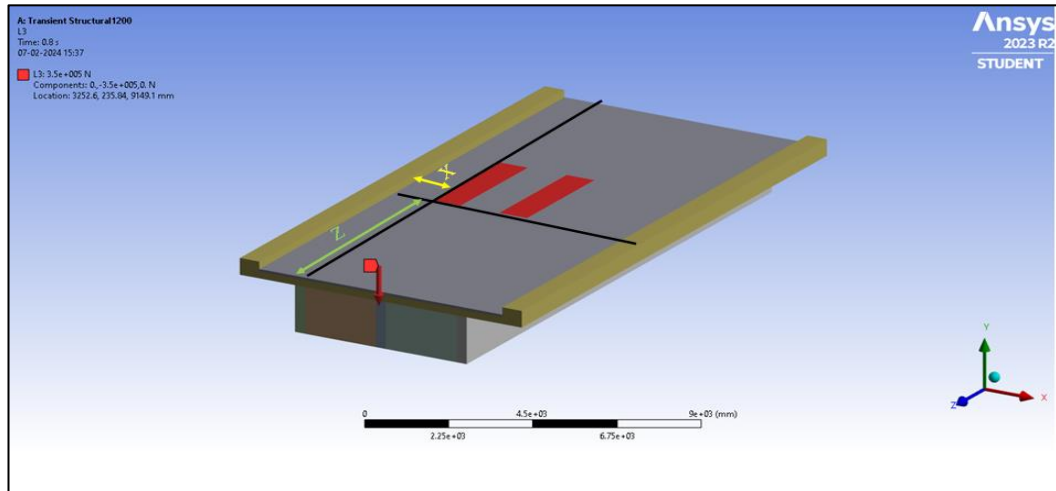


Fig.3.12 Representation of the position of the vehicle for maximum values of studied parameters

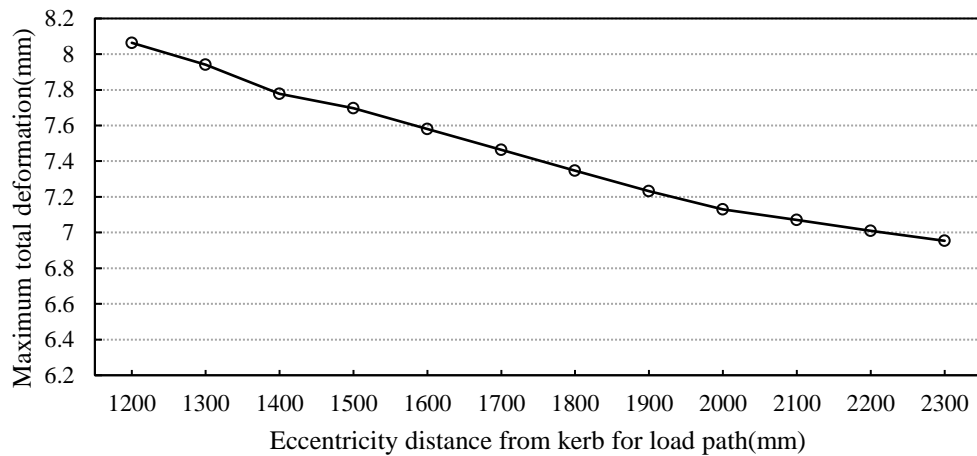


Fig.3.13 Maximum total deformation with respect to the eccentric distance of the moving vehicle from the kerb of the bridge

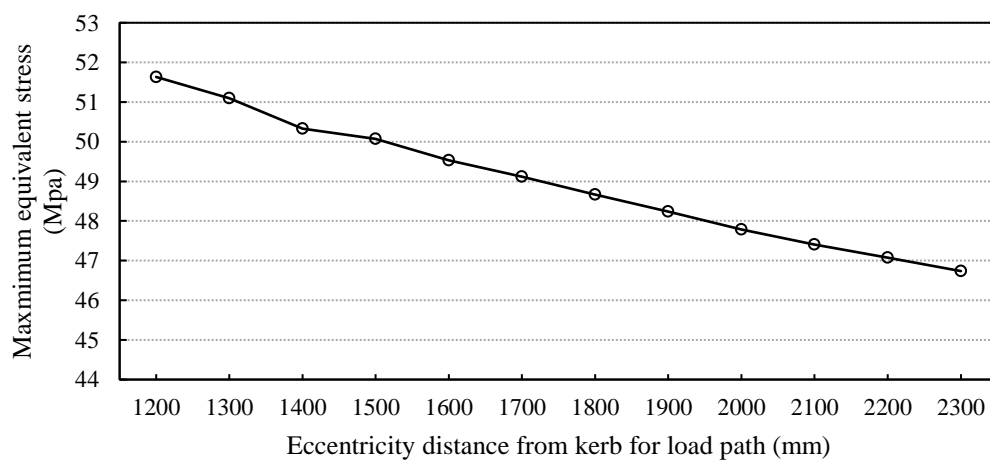


Fig.3.14 Maximum equivalent stress with respect to the eccentric distance of the moving vehicle from the kerb of the bridge

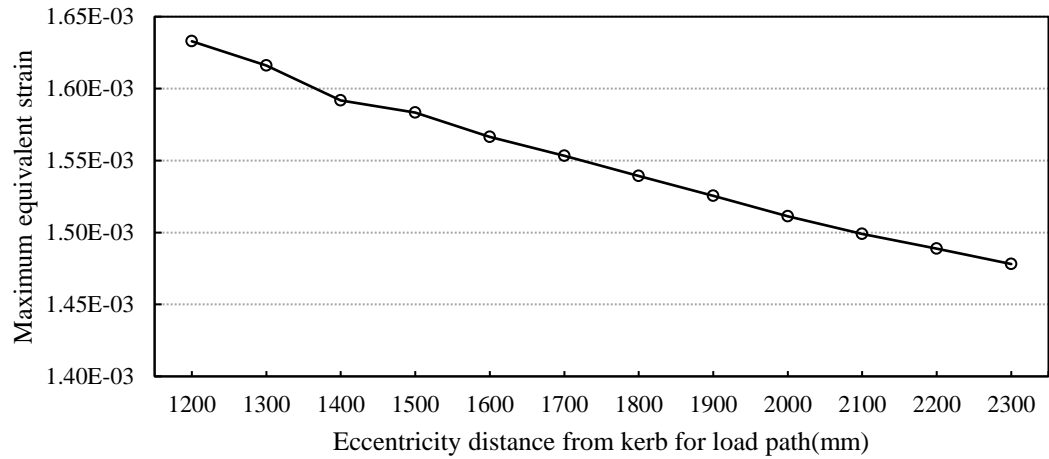


Fig.3.15 Maximum equivalent strain with respect to the eccentric distance of the moving vehicle from the kerb of the bridge

Table 3.1 Results for different moving paths

Eccentricity from kerb [X, mm]	Resultant Parameters	Maximum value	Time (sec.)	Position [Z, mm]
1200	Total deformation	8.063 mm	1.0	10800
	Equivalent stress	51.63 MPa	0.8	7200
	Equivalent strain	0.00163	0.8	7200
1300	Total deformation	7.94 mm	1.0	10800
	Equivalent stress	51.09 MPa	0.8	7200
	Equivalent strain	0.00162	0.8	7200
1400	Total deformation	7.77 mm	1.0	10800
	Equivalent stress	50.33 MPa	0.8	7200
	Equivalent strain	0.00159	0.8	7200
1500	Total deformation	7.69 mm	1.0	10800
	Equivalent stress	50.06 MPa	0.8	7200
	Equivalent strain	0.00158	0.8	7200
1600	Total deformation	7.58 mm	1.0	10800
	Equivalent stress	49.52 MPa	0.8	7200
	Equivalent strain	0.00157	0.8	7200
1700	Total deformation	7.46 mm	1.0	10800
	Equivalent stress	49.11 MPa	0.8	7200
	Equivalent strain	0.00155	0.8	7200
1800	Total deformation	7.34 mm	1.0	10800
	Equivalent stress	48.66 MPa	0.8	7200
	Equivalent strain	0.00154	0.8	7200

(continued on page no.32)

Table 3.1 (continued)

1900	Total deformation	7.23 mm	1.0	10800
	Equivalent stress	48.23 MPa	0.8	7200
	Equivalent strain	0.00153	0.8	7200
2000	Total deformation	7.13 mm	0.8	7200
	Equivalent stress	47.78 MPa	0.8	7200
	Equivalent strain	0.00151	0.8	7200
2100	Total deformation	7.07 mm	0.8	7200
	Equivalent stress	47.40 MPa	0.8	7200
	Equivalent strain	0.00150	0.8	7200
2200	Total deformation	7.01 mm	0.8	7200
	Equivalent stress	47.07 MPa	0.8	7200
	Equivalent strain	0.00149	0.8	7200
2300	Total deformation	6.95 mm	0.8	7200
	Equivalent stress	46.73 MPa	0.8	7200
	Equivalent strain	7.07 mm	0.8	7200

3.6 CONCLUDING REMARK

This chapter provided a study of the effect of the eccentricity of moving load IRC Class AA tracked vehicle from the kerb of a concrete bridge. From Fig.3.13, Fig. 3.14 and 3.15, it is concluded that the values for total deformation, equivalent stress, and equivalent strain in the bridge decrease with increasing eccentricity of the load from the kerb. The next chapter provides the deflection behaviour of a bridge under different moving load scenarios recommended by the Indian Road Congress (IRC).

CHAPTER 4

NUMERICAL STUDY TO INVESTIGATE THE DEFLECTION BEHAVIOR IN A CONCRETE BRIDGE UNDER IRC RECOMMENDED LOADING SCENARIOS

4.1 GENERAL

This chapter provides the numerical investigation of the deflection behaviour in a concrete bridge subjected to various Indian Road Congress (IRC:6-2017) moving load scenarios. A Prestressed Concrete (PSC) bridge is subjected to various Indian Road Congress (IRC) loadings; Class AA tracked load, Class AA wheeled load, Class A wheeled load, and 70R wheeled load, considering both symmetric and eccentric loading conditions to study the deflections of the bridge girders. Through systematic evaluation, the research determines the particular load and loading condition that results in the highest deflection along the girder. This investigation provides insight into the structural response of the bridge under various moving loads, aiding in the design of more resilient and efficient bridge structures.

4.2 BRIDGE DETAILS

The bridge taken for the study was the Prestressed Concrete (PSC) bridge which is located in Mirzapur, India. The data for the bridge has been provided by the CSIR-CRRI. The details of only one span which has been considered for study are mentioned in this chapter. The considered bridge span was named as span P3-P4 and had an effective span of 28.2m. The 3D view of the considered bridge span is shown in Fig.4.1. The details of the bridge span P3-P4 are mentioned in Table 4.1. The bridge has varying geometric details of its girder along its span which can be depicted in Fig.4.1. The details of the tapering of the girder is shown in Table 4.2. Table 4.2 shows the girders have a constant thickness of 0.77m from 0m to 0.9m span, from 0.9m to 1.8m a variable thickness from 0.77m to 0.15m, from 26.4m to 27.3m a variable thickness of 0.15m to 0.77m and from 27.3m to 28.2m a constant thickness of 0.77m. Fig.4.2 shows the cross-section details of the bridge at the ends of the span and Fig.4.3 shows the cross-section details of the bridge at the middle of the span. The bridge has

symmetrical left and right sections. Fig.4.4 shows the left girder cross-section details at the ends span, Fig.4.5 shows the left girder cross-section details of the bridge at the middle of the span and Fig.4.6 shows the details of the profile of the cross girders.

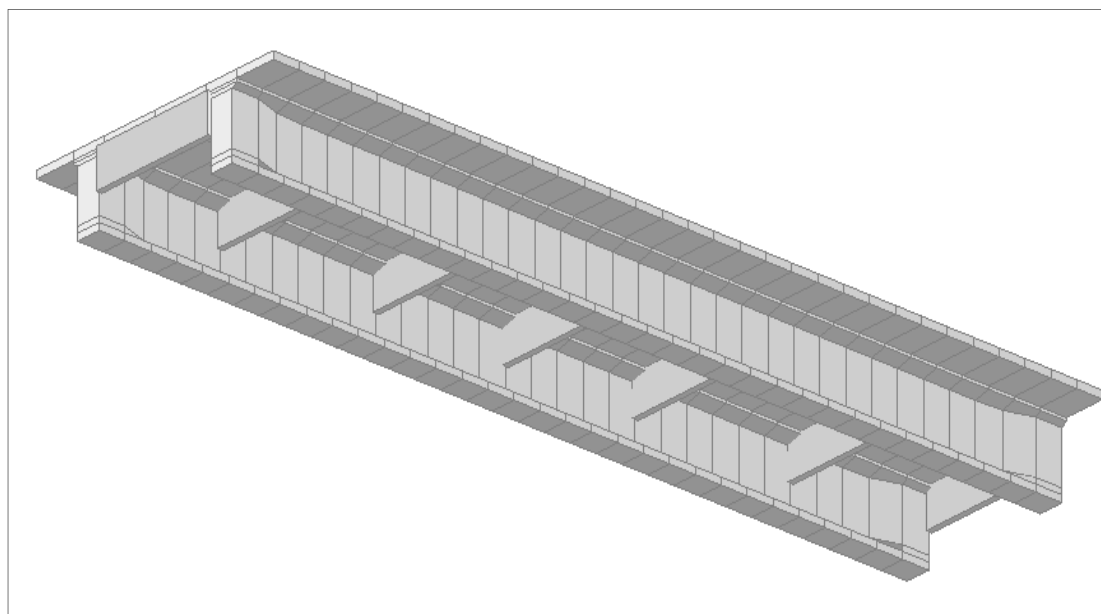


Fig. 4.1 3D view of Span P3-P4 (Source: CRRI Report, 2019)

Table 4.1 Details of the span P3-P4
(Source: CRRI Report, 2019)

Geometry Name	Dimension (m)
Effective span	28.2
Slab Depth	0.2
Slab width	8.45
Girder spacing	4.76
Girder bottom flange width	0.770
Girder bottom flange depth	0.180
Girder bottom honge depth	0.150
Girder depth	1.850
Girder top honge depth	0.075
Girder top flange depth	0.100
Diaphragm width	0.18
Diaphragm depth	0.1
Diaphragm c/c spacing	4.67

Table 4.2 Details of tapering of girder
(Source: CRRI Report, 2019)

Variable A (m)	Variable B (m)	Interpolation
0	0.770	Linear
0.9	0.770	Linear
1.8	0.150	Linear
26.4	0.150	Linear
27.3	0.770	Linear
28.2	0.770	Linear

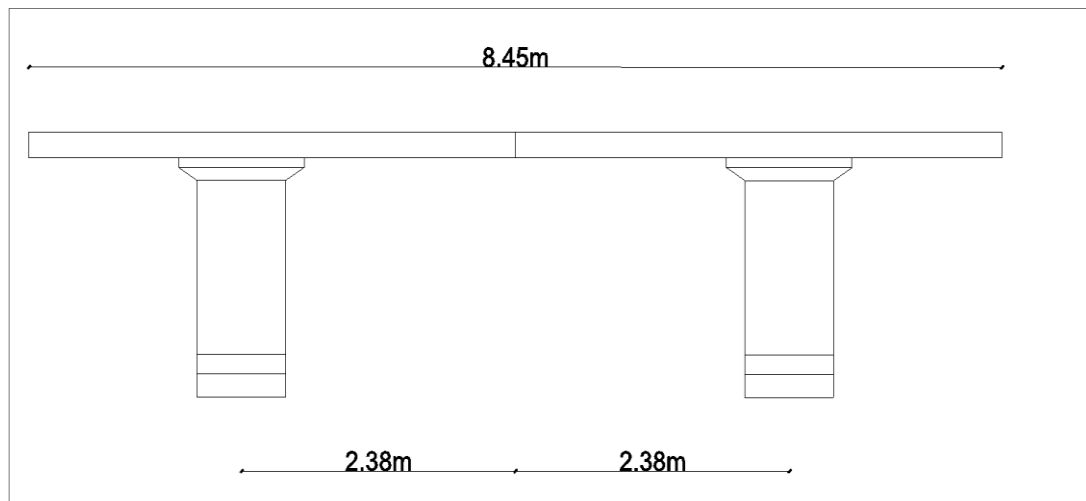


Fig. 4.2 Cross section at ends of span

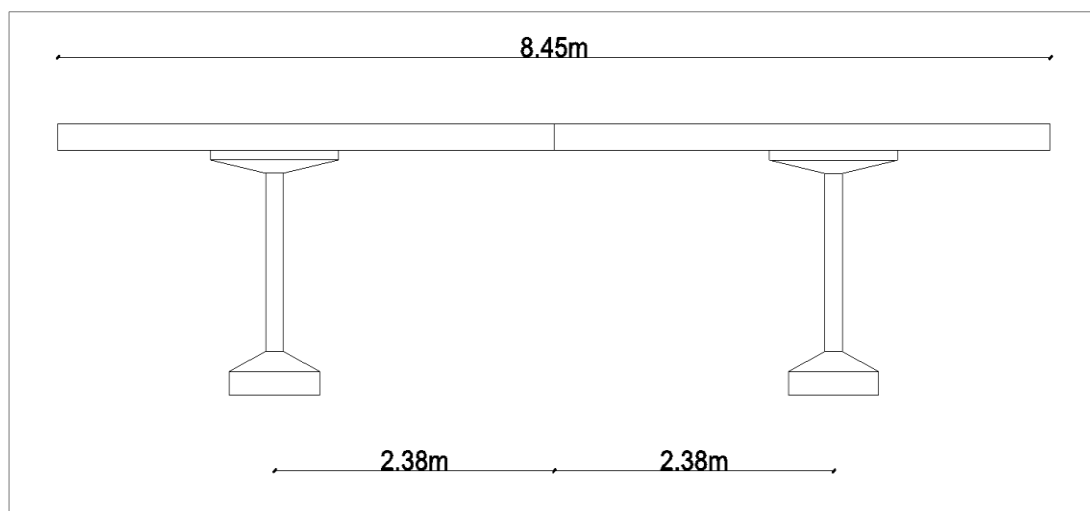


Fig. 4.3 Cross section at the middle of the span

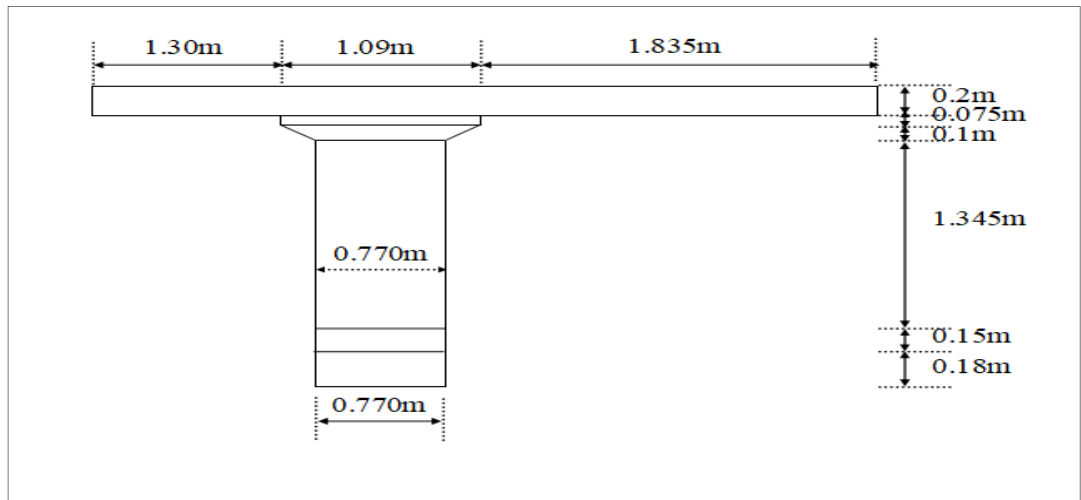


Fig. 4.4 Left girder cross section at end span

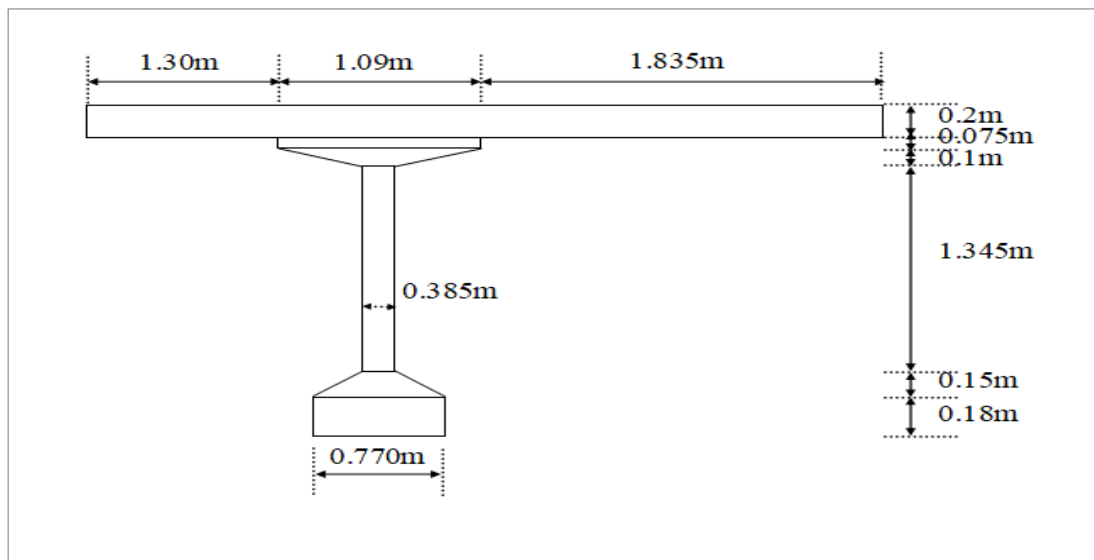


Fig. 4.5 Left girder cross section at mid-span

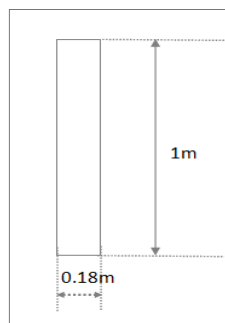


Fig. 4.6 Profile of cross-girder

All the details of the bridge are mentioned in this section as the bridge details, but the study in this chapter 4 includes the analysis of the bridge in ABAQUS software ignoring the prestressing effect in the bridge and using the simplified geometry of the bridge as shown in Fig.4.7, keeping other details as above. The parameters considered for the study in ABAQUS are; density of concrete as $2500 \times 10^6 \text{ ton/mm}^3$, modulus of elasticity as 27386 N/mm^2 and Poisson's ratio as 0.2.

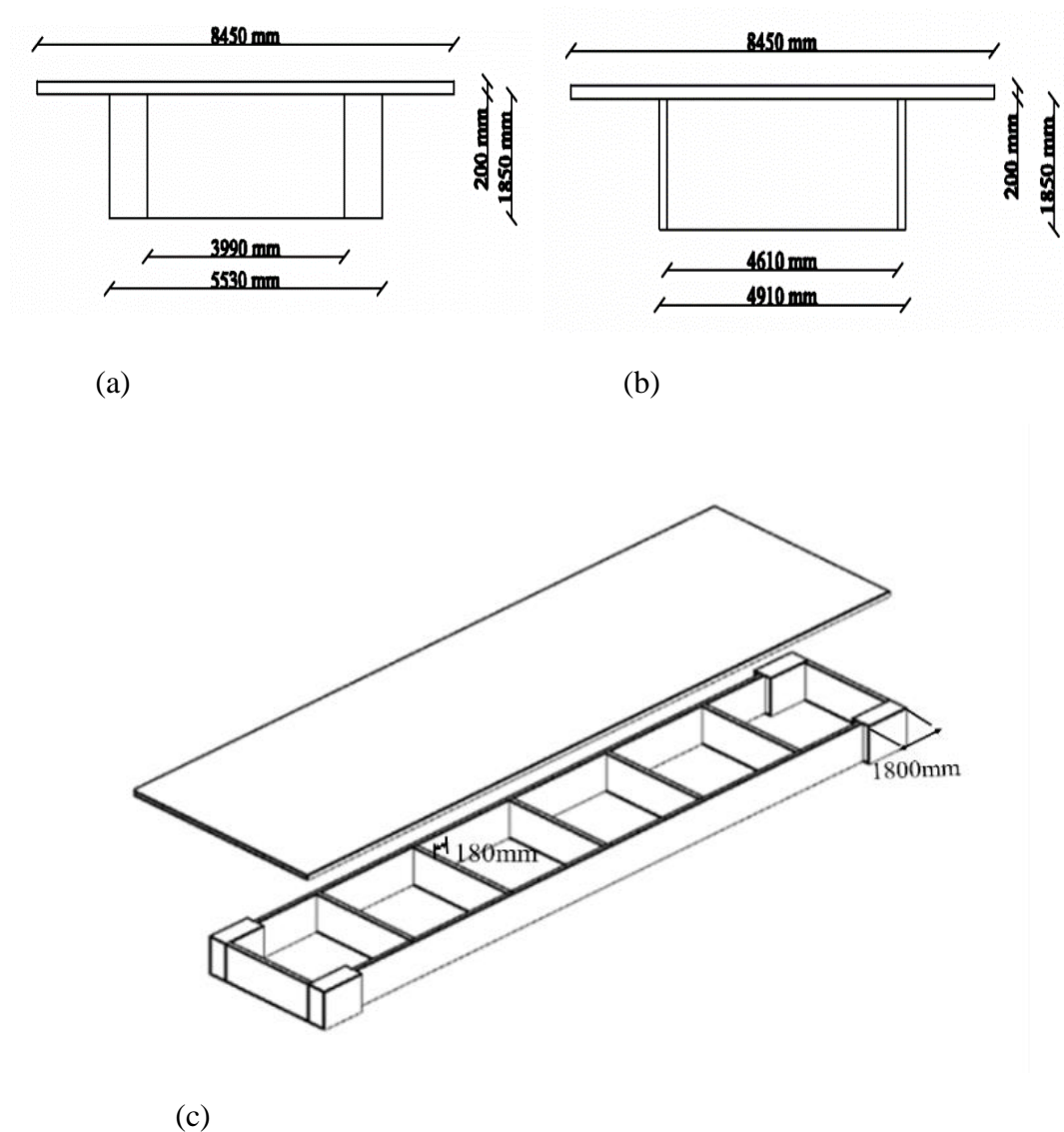


Fig. 4.7 Simplified geomerty for numerical modelling:(a) section at intermediate portion, (b) section at end portion. (c) 3D view

4.4 CONSIDERED IRC LOADINGS

The moving loads, as per the IRC:6-2017, used in this study were Class AA tracked load, Class AA wheeled load, Class A wheeled load, and 70R wheeled load. The DLOAD subroutines have been written in the FORTRAN to define the moving vehicle on the bridge. Fig.4.11 shows the pictorial representation of the Class AA wheeled load applied in the model using the DLOAD Subroutine. The DLOAD Subroutine for this loading is given in APPENDIX A as a sample code for all loadings. During developing the codes, the loads were applied in the form of pressure and the velocity was set as 28.2m/s for all load cases. The subroutine code for Class AA wheeled load and Class AA tracked load was developed as a single lane, for the most eccentric condition, as per the IRC:6-2017. Similarly, for 70R wheeled load the code was developed, but for both eccentric and symmetric loading conditions. Similarly, for Class A wheeled load, a 2-lane Class A wheeled load code was developed for both eccentric and symmetric loading conditions. Fig.4.8 shows the IRC Class AA tracked and wheeled vehicle loads, Fig.4.9 shows the IRC 2-lane class A vehicle load and Fig.4.10 shows the IRC 70R loading.

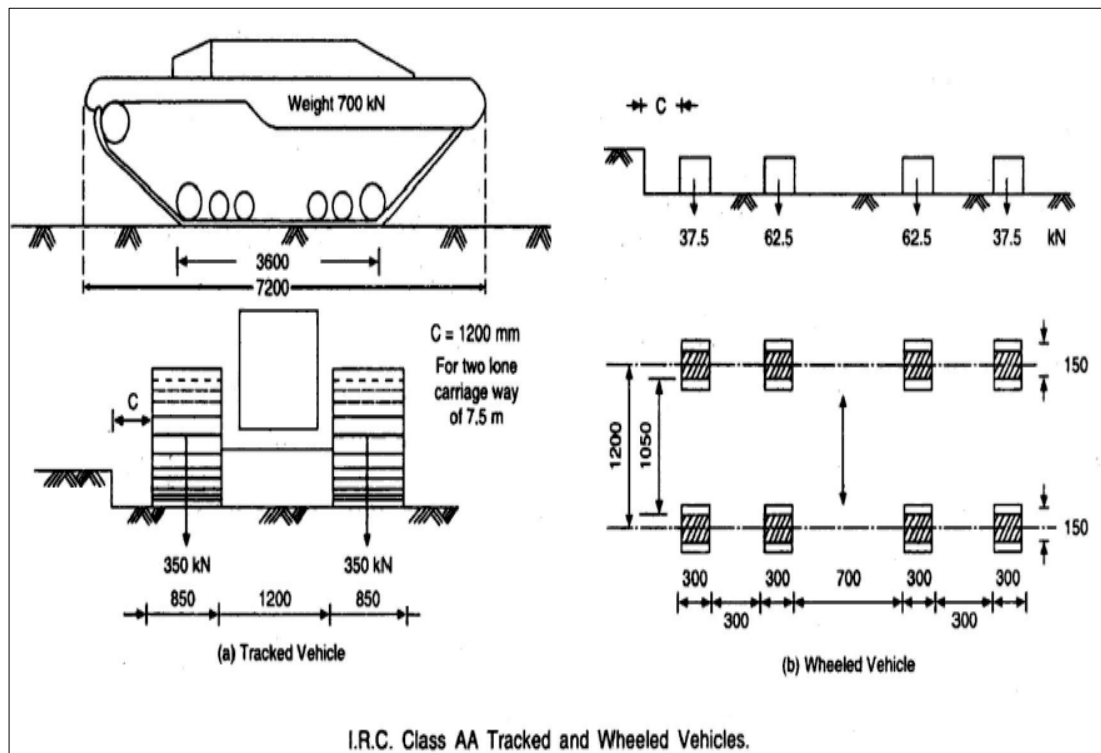


Fig.4.8 IRC Class AA tracked and wheeled Vehicle (IRC:6-2017)

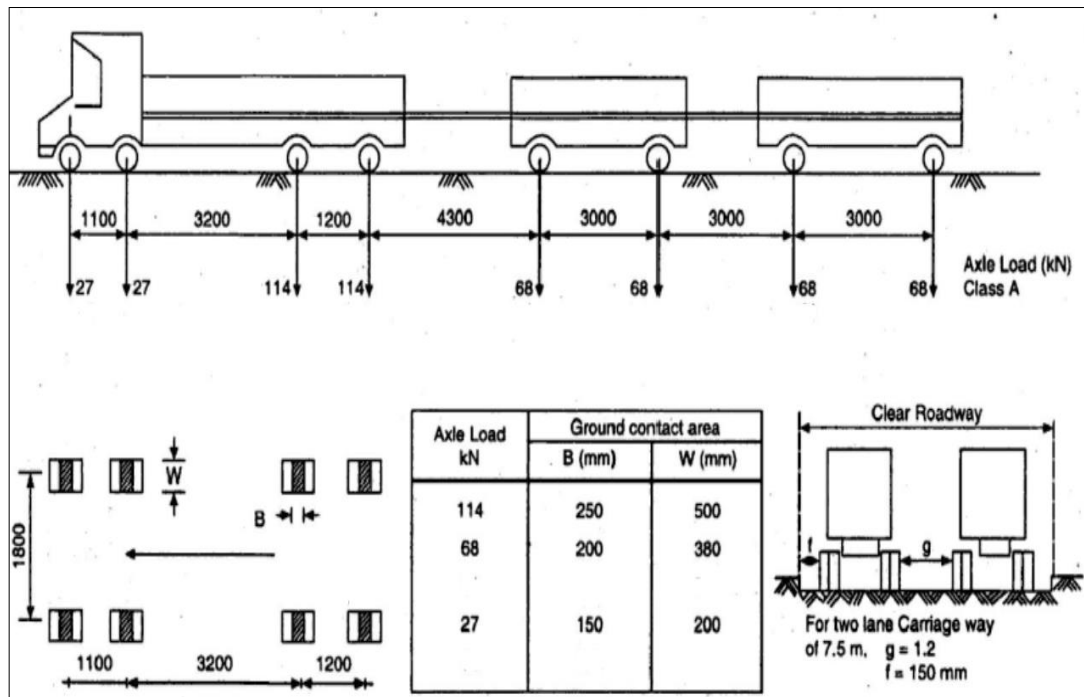


Fig.4.9 IRC 2-Lanes Class A vehicle (IRC:6-2017)

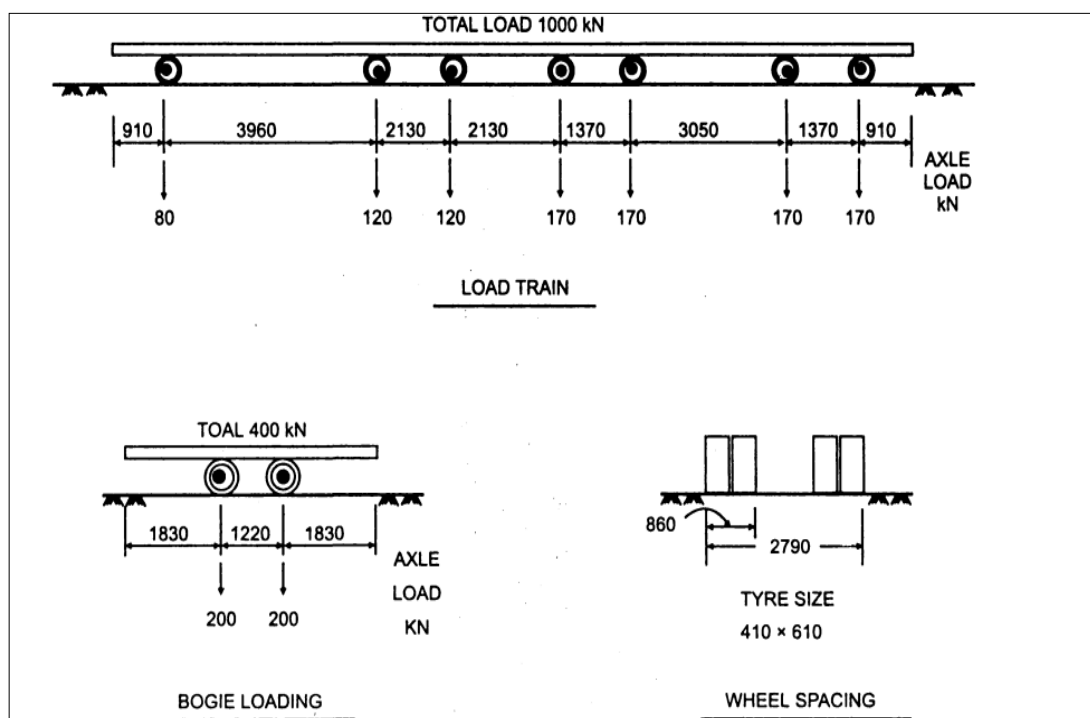


Fig.4.10 IRC 70R Wheeled Loading (IRC:6-2017)

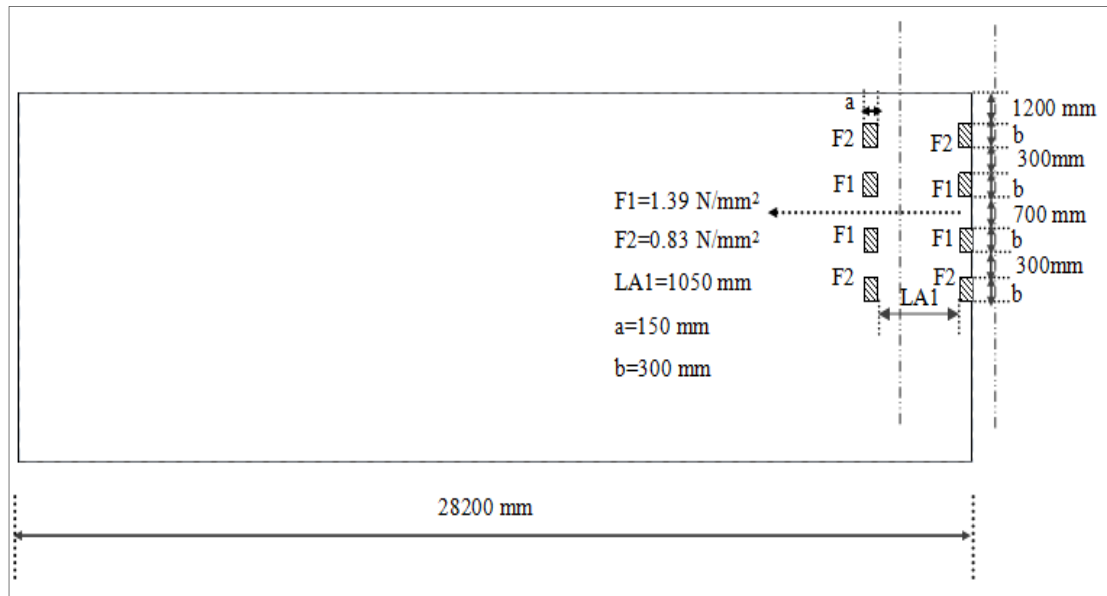


Fig.4.11 Pictorial representation of Class AA wheeled load applied in the model using DLOAD Subroutine

4.5 NUMERICAL MODELLING AND VALIDATION

In this chapter, the numerical modelling has been carried out in the ABAQUS software. Fig.4.12 shows the 3D view of the bridge with boundary conditions. Fig.4.13 shows the finite element model (FEM) with meshing which consists of 5618 nodes and 2445 elements. The element has been taken of type C3D8R having a hexahedral element shape with linear geometric order. The global mesh size taken for the deck part was 400mm, that for cross girders was 200mm and the same for longitudinal girder was 600 mm. Fig.4.14 shows the finite element model showing various parts, Fig.4.15 shows Surface selection to apply moving load and Fig.4.16 shows the application of typical moving load using DLOAD Subroutine.

For the validation of the numerical model in the ABAQUS software, the available results in a study previously done by CRRI was used. Validation of the model was done based on the self-weight of the structure. The vertical maximum deflection of the bridge under self-weight is determined. The vertical maximum deflection in the CRRI study was -16.35 mm as shown in Fig.4.17 and the same found in the ABAQUS software was -16.39 mm as shown in Fig.4.18. The percentage of difference in the result from both software is found to as 0.29% and the model is validated.

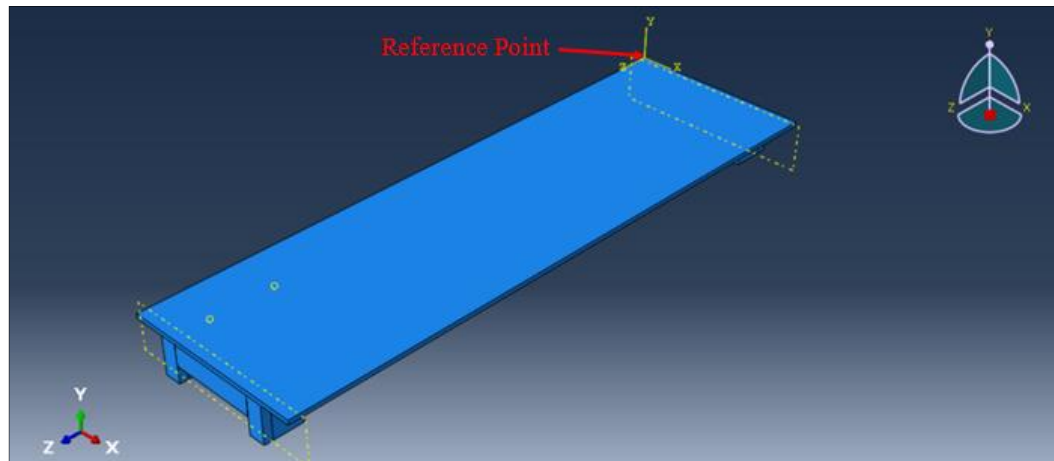


Fig.4.12 3D view of the bridge with boundary conditions in ABAQUS

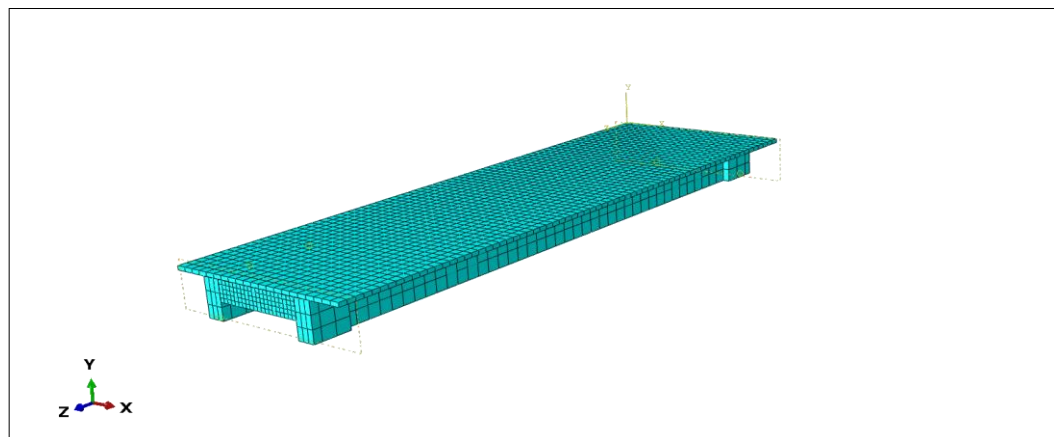


Fig.4.13 Finite element model with meshing

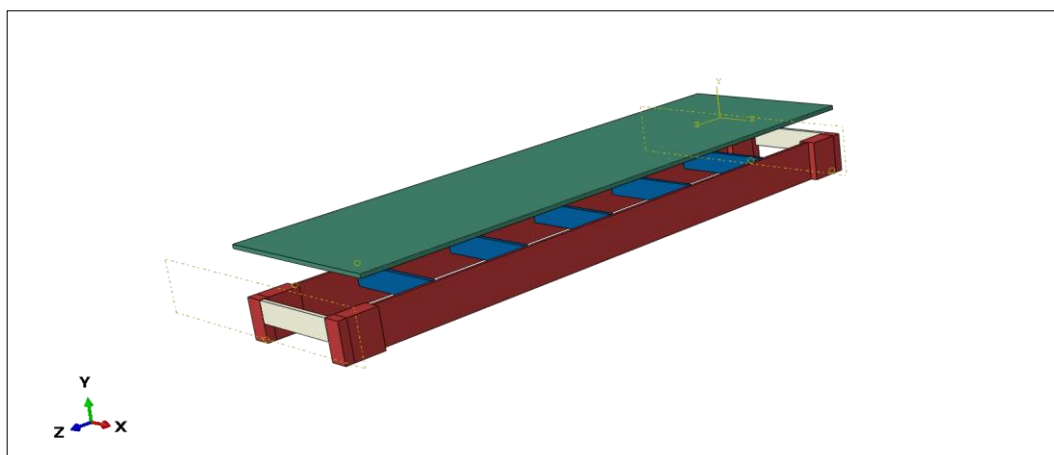


Fig.4.14 Finite element model showing various parts

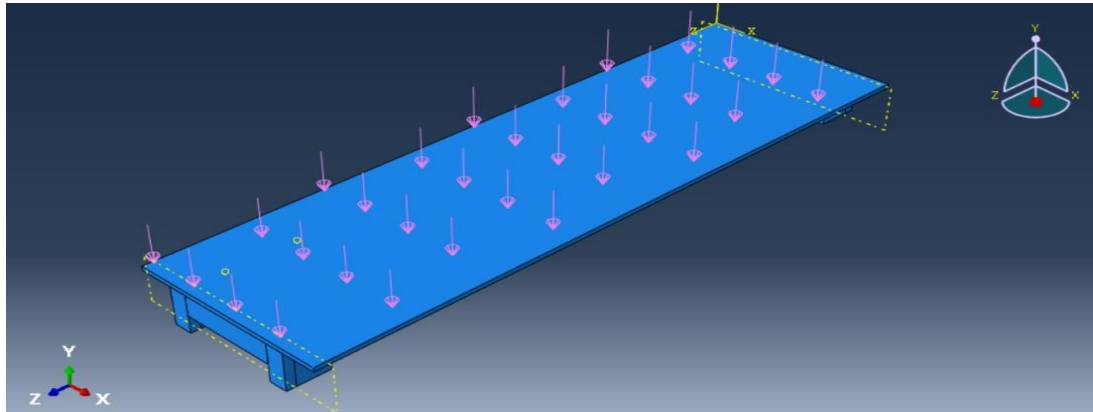


Fig.4.15 Surface selection to apply moving load

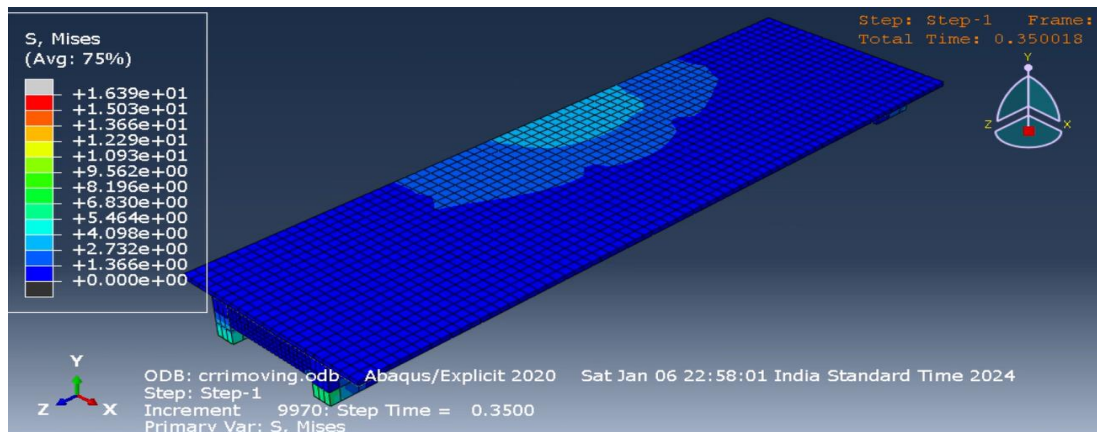


Fig.4.16 Application of typical moving load using DLOAD Subroutine

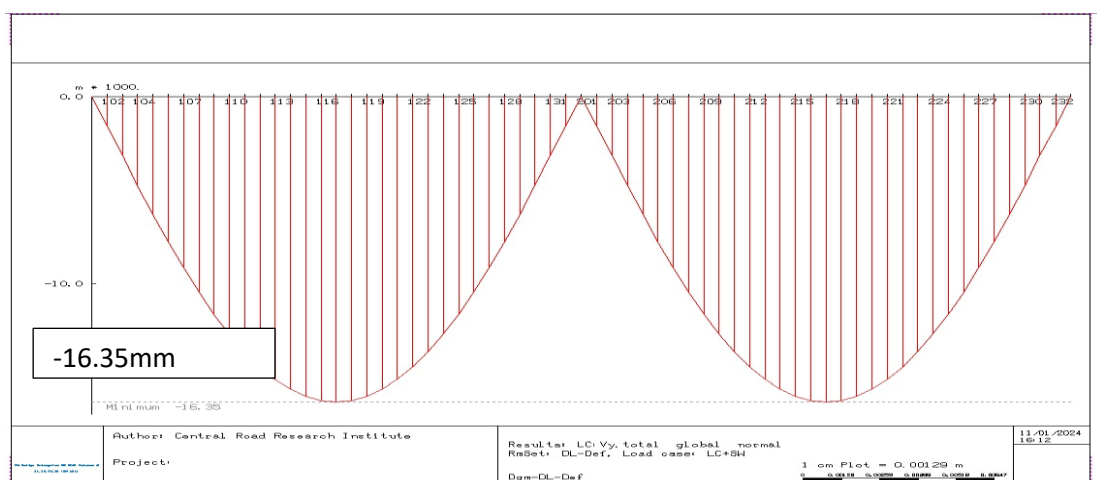


Fig. 4.17 Maximum Vertical deflection under self-weight in RM-bridge

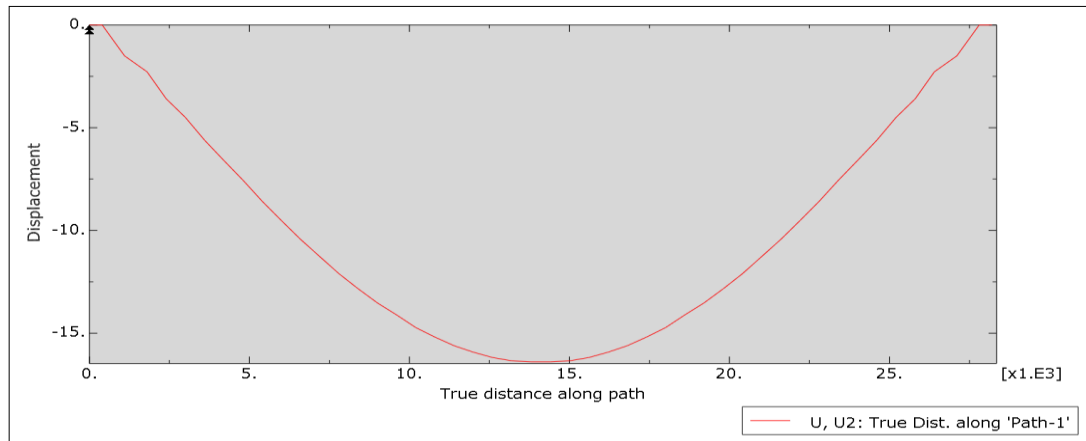


Fig. 4.18 Maximum Vertical deflection under self-weight in ABAQUS

4.6 DEFLECTION UNDER DIFFERENT IRC RECOMMENDED LOAD SCENARIOS

The moving vehicles were passed over the bridge and the time was noted at which the specific load was giving the maximum deflection in the bridge. The velocity of the moving load was set as 28.2m/sec and the time of travel of the vehicle over the bridge was set 1 sec. For the noted time at which the load case was giving maximum vertical deflection in the bridge, the position of the vehicle was calculated using equation $Z_p = Vt$, where, Z_p = position of vehicle at time 't', V = velocity of the vehicle, t = time in seconds. The distance Z_p represents the position of the vehicle as shown typically in Fig. 4.18. For different load cases, the time, position of vehicle and the maximum deflection obtained are shown in Fig.4.20 to Fig.4.25. Fig.4.26 shows the maximum deflections under all cases considered. The vehicle position, with its eccentricity from reference point shown in Fig.4.12, at which the maximum deflection was obtained in the bridge is tabulated in Table 1.

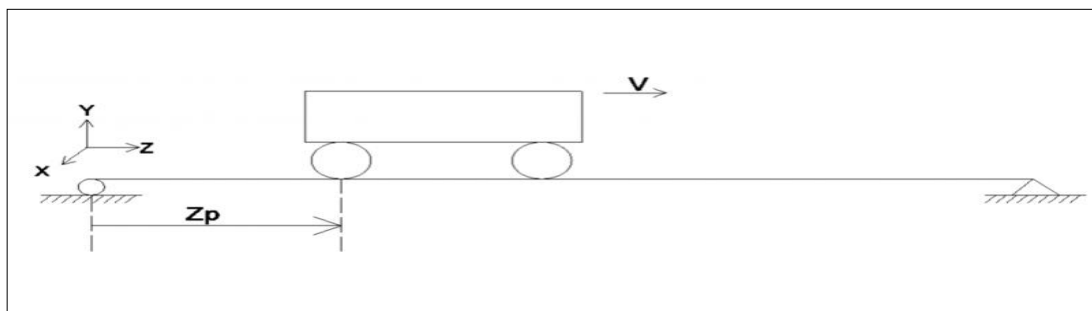
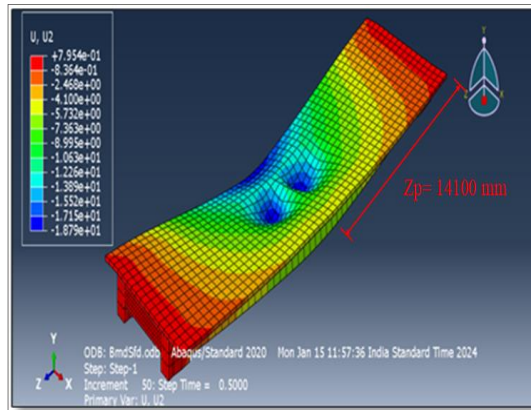
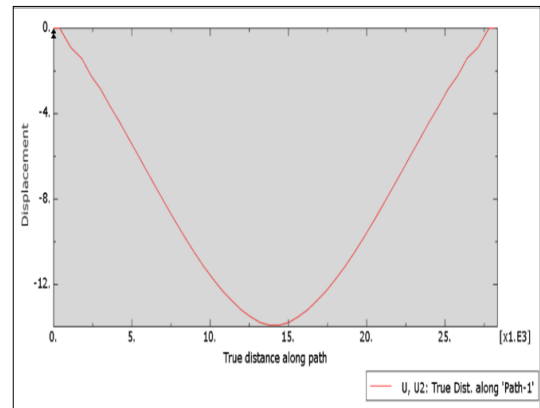


Fig.4.19 Typical figure representing the position of a vehicle on the bridge

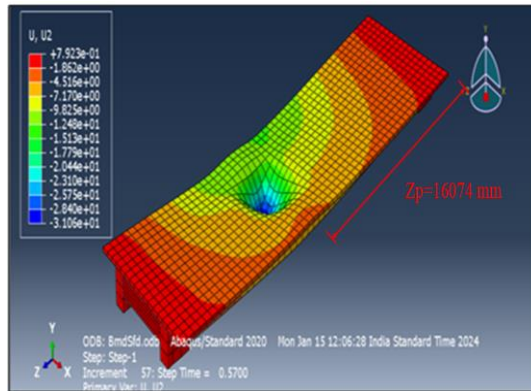


(a)

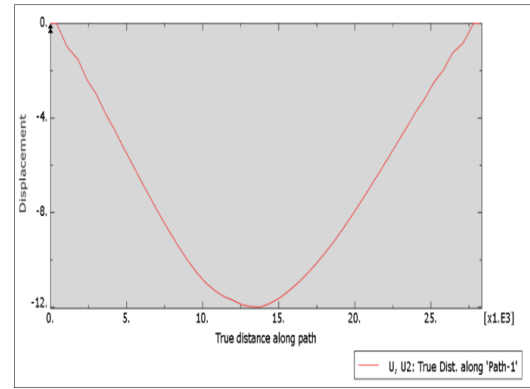


(b)

Fig. 4.20 (a)Analysis for Class AA tracked vehicle for eccentric condition and (b) Maximum deflection under Class AA tracked vehicle for eccentric condition

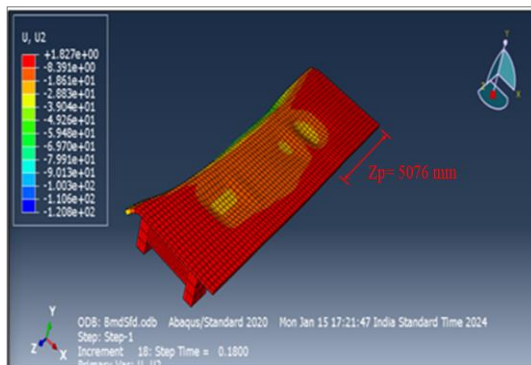


(a)

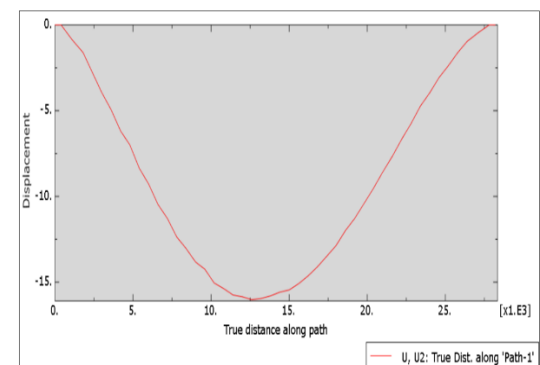


(b)

Fig. 4.21 (a)Analysis for Class AA Wheeled vehicle for eccentric condition and (b) Maximum deflection under Class AA wheeled vehicle load for eccentric condition

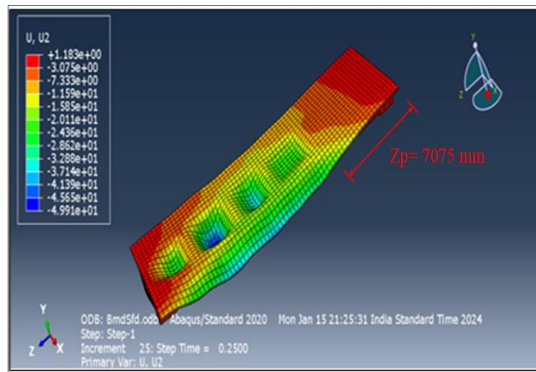


(a)

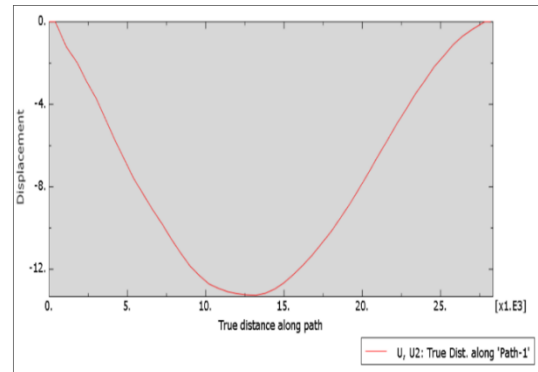


(b)

Fig. 4.22 (a) Analysis for 2-lane Class A vehicle for eccentric condition and (b) Maximum deflection under 2-lane Class A vehicle for eccentric condition

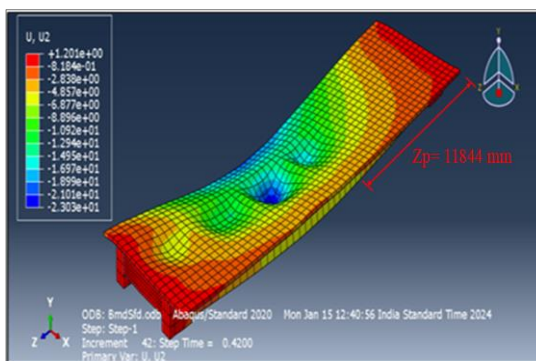


(a)

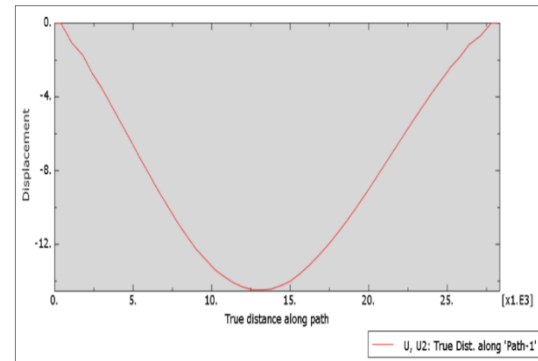


(b)

Fig. 4.23 (a) Analysis for 2-lane Class A vehicle for symmetric condition and (b) Maximum deflection under 2-lane Class A vehicle for symmetric condition

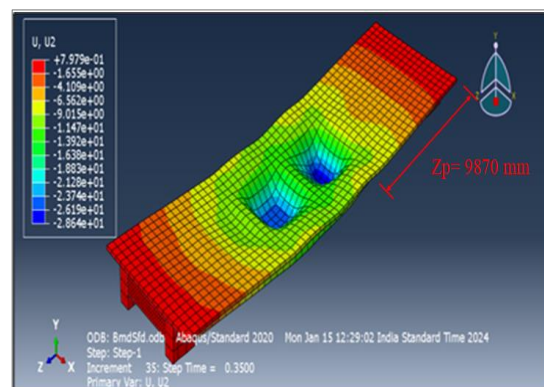


(a)

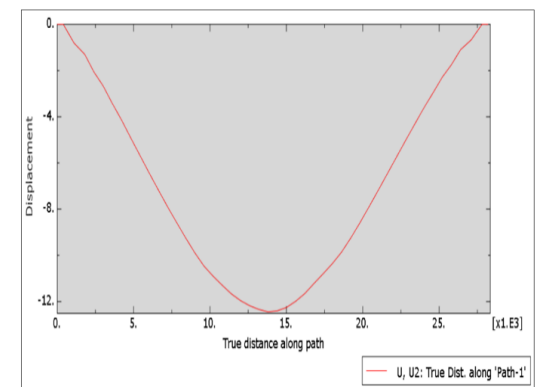


(b)

Fig. 4.24 (a) Analysis for 70R wheeled vehicle for eccentric condition and (b) Maximum deflection under 70R wheeled vehicle for eccentric condition



(a)



(b)

Fig. 4.25 (a) Analysis for 70R wheeled vehicle for symmetric condition and (b) Maximum deflection under 70R wheeled vehicle for symmetric condition

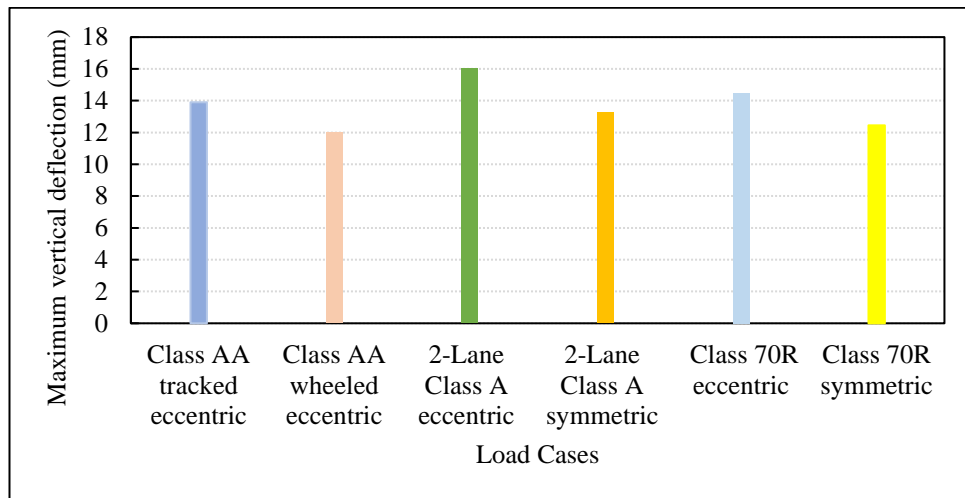


Fig. 4.26 Maximum deflections under various load cases

Table 4.3 Vehicle position for maximum deflection for different load cases

Load Cases	Velocity, V (mm/sec)	Time, t (sec)	Position from the reference point, Zp, (mm)	Eccentricity of load from the reference point, (mm)	Maximum Vertical deflection (mm)
Class AA tracked vehicle eccentric loading condition	28200	0.50	14100	1200	-13.90
Class AA wheeled vehicle eccentric loading condition	28200	0.57	16074	1200	-11.99
2-Lane Class A wheeled vehicle eccentric loading condition	28200	0.18	5076	150	-16.02
2-Lane Class A wheeled vehicle symmetric loading condition	28200	0.25	7075	1325	-13.26
70R wheeled vehicle eccentric loading condition	28200	0.42	11844	1200	-14.47
70R wheeled vehicle symmetric loading condition	28200	0.35	9870	2830	-12.45

4.7 CONCLUDING REMARK

A numerical investigation of the deflection behaviour in a reinforced concrete bridge subjected to various Indian Road Congress (IRC) moving load scenarios was done. From different types of load cases have been considered in this study namely (a) Class AA tracked vehicle for eccentric condition, (b) Class AA wheeled vehicle for eccentric condition, (c) 2-lane Class A vehicle for eccentric condition, (d) 2-lane Class A vehicle for symmetric condition, (e) 70R wheeled load for eccentric condition and (f) 70R wheeled load for symmetric condition, 2-lane Class A vehicle for eccentric condition was found to be critical case with maximum deflection of -16.02mm. This chapter builds up the understanding of the nuances of the static load test where different loading conditions are to be modelled for a particular bridge and find deflection and moment. The next chapter proposes a detailed methodology to perform dynamic load test while using the experimental parameters determined from the static load test for the same bridge and numerically modelling to determine the dynamic parameter.

CHAPTER 5

PROPOSED METHODOLOGY FOR DYNAMIC LOAD TEST

5.1 GENERAL

This chapter provides a comprehensive study to supplement the static load test with the dynamic load test by relating the static load test parameter with the dynamic load test parameter. The same type of bridge is used in this chapter that has already been introduced in detailed and used for study in chapter 4. The static load test data for the same span of bridge is introduced in this chapter based on the CSIR-CRRI report. As mentioned in previous chapter, the bridge type is a prestressed concrete bridge and is located in Mirzapur, India. A photograph, showing the bridge, taken during the static load test performed by CSIR-CRRI is shown in Fig. 5.1.



Fig. 5.1 Showing the bridge on which the static load test was performed
(Source: CRRI Report, 2019)

5.2 STATIC LOAD TEST

The load testing is done mainly to assess the flexural capacity of the bridge superstructure at working load in the elastic range, through measuring the deflections of the superstructure.

5.2.1 Loading Scheme for Static Load Test

The bridges in India are normally designed for a particular class of loading as specified in IRC-6:2017 which represents hypothetical vehicles. Loaded Trucks were planned to be placed over spans to produce the same maximum Bending Moment of the outer girder as could have been produced due to live load on the carriageway. It is worth noting that the usage of the commercial vehicle is recommended in para-6 of IRC Special Publication No. 37. The loading scheme, prepared by the CSIR-CRRI, for the load testing of the span P3-P4 is as shown in Fig. 5.2.

In CSIR-CRRI report, modelling of the bridge was done in the software RM Bridge V11. The support condition was considered as the simply supported condition. The grade of concrete was taken as M30 based on the NDT conducted. Different load cases as per IRC-6:2017 were run; theoretical maximum bending moment and deflection in one span girder were analyzed in RM Bridge which is shown in Table 5.5. Then a load scheme was determined for the commercial vehicle corresponding to the IRC load case giving maximum bending moment and maximum deflection. Table 5.5 shows the theoretical maximum bending moment of 4232 KNm and the theoretical maximum deflection of -16.9032 mm was produced under 70R-Wheeled One Lane eccentric loading condition. The live load mentioned in the IRC:6-2017 is hard to make available during the experimental static load test. Therefore, an equivalent commercial vehicle load corresponding to designed IRC loading is necessary to be simulated. The details of the commercial vehicle weighing 42T and 62T used in the experimental load testing are shown in Table 5.1. Truck Loading of 42T+62T giving a theoretical maximum bending moment of 4285 KNm and a theoretical maximum deflection of -17.2806 mm as in Table 5.5 was finalized as the equivalent loading corresponding to design IRC loading.

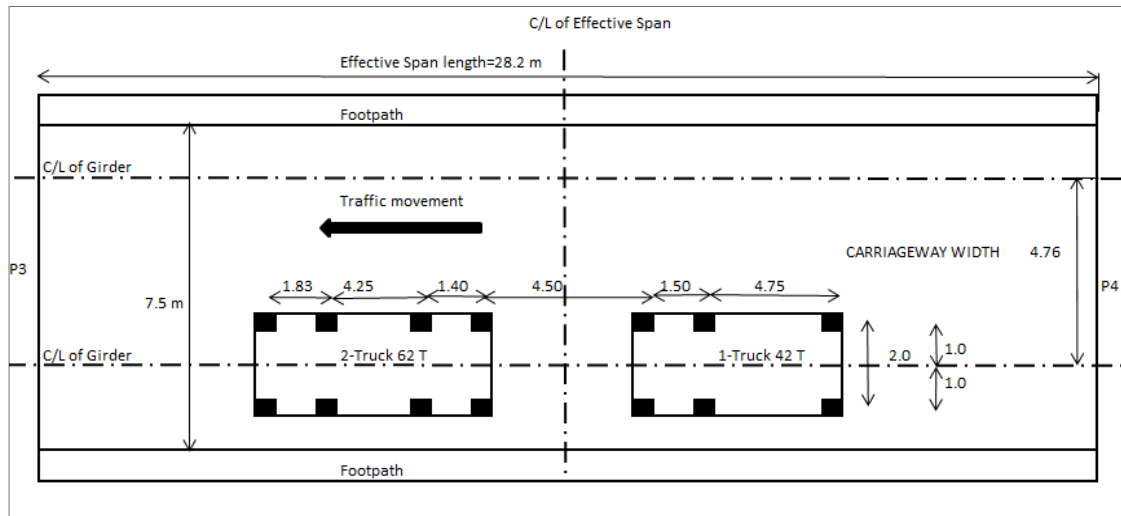


Fig. 5.2 Load Testing Scheme for span P3-P4 (Source: CRRI Report, 2019)

Table 5.1 Weight of Loaded Trucks for Load Testing of Span P3-P4
(Source: CRRI Report, 2019)

Vehicle No.	Type of Truck Three /four Axles	Load on			Total Weight of loaded Truck (kg)
		Front one Axle (Kg)	Front two Axle (Kg)	Rear two Axle (Kg)	
1.	Three	10500	NA	31500	42000
2.	Four	NA	18500	43500	62000
The total weight of all the above trucks				1040000 kg Say 104 ton	

5.2.2 Experimental Static Load Test

Deflections of each span were measured at locations accessible out of three locations along the span length i.e., both the quarter spans and mid-span (i.e. $\frac{1}{4} L$, $\frac{1}{2} L$ and $\frac{3}{4} L$) of the longitudinal girders. CRRI suspension wire method for deflection measurement was installed at these locations and deflections were measured. A hydraulic lift was used to fix steel wires for the installation of dial gauges for the measurement of the deflection of the superstructure. Besides measuring the vertical deflection of the span, the longitudinal and transverse displacement of the bearings was also monitored.

Before conducting the load testing of any bridge, it is mandatory to observe the behaviour (sagging/hogging) of the superstructure due to the variations in the ambient temperature. Due to site constraints, the bridge was not possible to close for 72 hours as per IRC:SP:51 guidelines for load testing. Hence, all the load tests were performed at night, noting the temperature for the temperature correction. The locations of loaded truck placement were marked on the deck of the span.

Firstly, the initial readings of all the installed dial gauges at no load on the span were recorded. The entire span was checked for the presence of any distress such as cracks etc. before placement of loaded trucks over the span. The loaded trucks were then placed over the bridge deck in two stages of loading and at the end of each incremental loading stage, the readings of dial gauges as well as ambient temperatures were recorded. The entire span was again inspected for the presence of any distress such as cracks before the start of the next incremental loading.

5.2.3 Discussion of Results

The test results of load testing of span P3-P4 are given in Table 5.2. Table 5.2 shows the initial reading R1 was taken at a temperature of 32.5°C. The final deflection after 3 hours of loading R3 at the mid-span of upstream girder was -5.35mm and that of the downstream girder was -23.06mm (theoretical deflection -17.28mm), at 29.55°C.

The residual deflection after 30 minutes of unloading R5 at the mid-span of the upstream girder was -0.5mm and that of the downstream girder was 0.04mm. The percentage recovery for the upstream girder was 90.7% and that for the downstream girder was 100.2%. The general acceptance criteria for load tests are, (i) harmony between measured and calculated deflections, and (ii) Recovery percentage on the removal of the applied load. The placement of vehicular load had produced an equivalent maximum bending moment at the mid-span inclusive of the impact factor. It can be seen from Table 5.2, that the magnitudes of deflection at the mid-span ($L/2$) of the span of Girder G1 due to equivalent vehicular loading after 3 hours was -23.06mm. The deflection values were higher than the corresponding theoretical value of 17.28mm. It is worth noting that the magnitude of the observed deflections of the tested P3-P4 is higher than ($L/1500$) of the span i.e., 18.8mm ($28200/1500$) mm

Table 5.2 Deflection Data during load test of Span P3-P4
(Source: CRRI Report, 2019)

Loading Stage	Average Temp(°C)	Mid-Span Girder u/s (G2)	Mid-Span Girder d/s (G1)
Dial Gauge No.		D-2	D-1
Initial Reading - R1	32.5	0	0
Final Deflection after 3 hours of loading R3	29.55	-5.35	-23.06/17.28
Residual Deflection after 30 minutes of unloading - R5	31.1	-0.5	0.04
Parentage recovery $[(R3-R1) * 100 / (R5-R1)]$		90.7%	100.2%

specified by IRC Special Publication-37 and less than $(L/1000)$ of span i.e. 28.2 mm $(28200/1000)$ specified by IRC-6:2017.

The superstructure's % recovery following the removal of the test load is the most crucial requirement in an acceptance test. Table 5.2 displays the instantaneous percentage recovery of the deflection at the midpoint of the tested span, P3-P4. Table 5.2 shows that for the mid-span of both girders, the average percent recovery of deflection upon removal of the test load is greater than 90%. The minimal percentage recovery of deflection after 24 hours following the removal of the test load is 85%, according to IRC: SP:51-2015, and this is the acceptance criterion for prestressed concrete structures when the vehicle live load is removed. Given that P3–P4's percentage recovery exceeds the predetermined 85 percent threshold, the tested span is considered to be responding elastically. During the stress testing in the span, Pier P3, and Pier P4, no new flexural cracks appeared, nor did any of the preexisting ones spread.

5.3 NUMERICAL MODELLING OF THE BRIDGE IN MIDAS CIVIL

As in the CRRI report, the numerical parameters to be studied for the load testing of the structure are bending moment and deflection. These parameters depend

on the mass of the structure, the modulus of elasticity of concrete, and the moment of inertia of the section. Also, The modulus of elasticity (MOE) of concrete is a variable that plays an important role in the dynamic analysis of a bridge model (Islam et al., 2015). Therefore, the tendon and its prestressing have been ignored during the numerical modelling. In this chapter, the bridge data mentioned in Table 4.1 and Table 4.2 of the previous chapter were modelled in the MIDAS CIVIL 2024 V 1.1, unlike the previous chapter where ABAQUS software had been used. This is due to the reason that in ABAQUS direct value of bending moments can not be extracted from the results of the software: therefore, it was decided to use MIDAS CIVIL 2024 V 1.1. Therefore, the validation of the numerical has been carried out again to ensure the correctness of the results. The 3D view of the bridge in the MIDAS CIVIL is shown in Fig. 5.3. The support condition of the bridge has been considered as the simply supported condition. Fig. 5.4 shows the material chosen was of grade M30, which was as per the Indian Standard and the type of material was isotropic, as mentioned in the case study. Table 5.3 shows the left girder section properties namely: Cross-Sectional Area (A), Effective Shear Area (A_{sy}), Effective Shear Area (A_{sz}), Torsional Resistance (I_{xx}), Area Moment of Inertia (I_{yy}), Area Moment of Inertia (I_{zz}) and geometry of sections. As both the left and right girders are symmetrical, the right girder also has the same properties as the left girder.

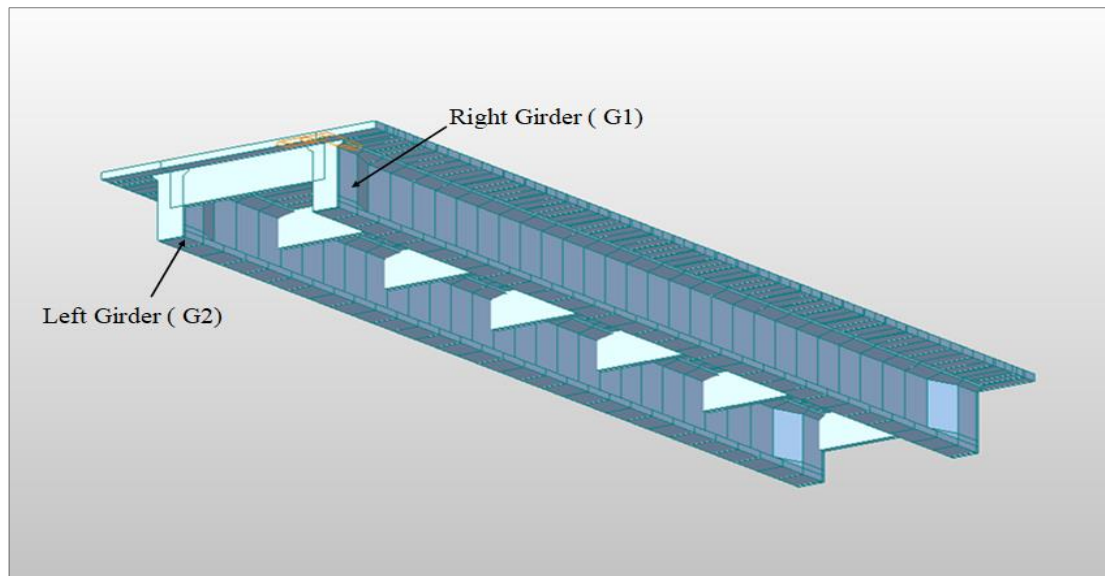


Fig. 5.3 3D view of Bridge in Midas Civil 2024 V1.1

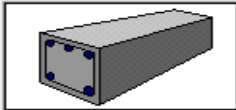
Material Data

General

Material ID: 2 Name: M30 girder

Elasticity Data

Type of Design: Concrete



Type of Material: ☒ Isotropic ☐ Orthotropic

Steel

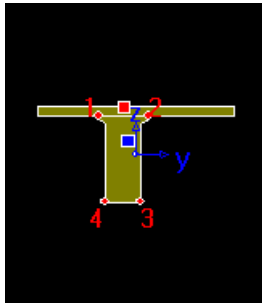
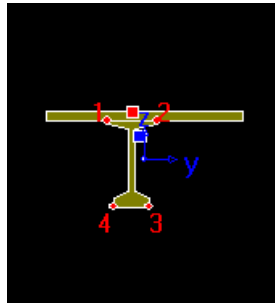
Standard: DB:

Concrete

Standard: IS(RC) Code: DB: M30

Fig. 5.4 Material properties chosen in Midas Civil 2024 V1.1

Table 5.3 Section Properties of left end girder (G2)

Properties	End-Section	Mid- Section
Cross-Sectional Area (A)	$2.3095 \times 10^6 \text{ mm}^2$	$1.3981 \times 10^6 \text{ mm}^2$
Effective Shear Area (Asy)	$7.9559 \times 10^5 \text{ mm}^2$	$7.2876 \times 10^5 \text{ mm}^2$
Effective Shear Area (Asz)	$1.2242 \times 10^6 \text{ mm}^2$	$2.7551 \times 10^5 \text{ mm}^2$
Torsional Resistance (Ixx)	$2.2852 \times 10^{11} \text{ mm}^4$	$2.3418 \times 10^{10} \text{ mm}^4$
Area Moment of Inertia (Iyy)	$9.7536 \times 10^{11} \text{ mm}^4$	$6.5072 \times 10^{11} \text{ mm}^4$
Area Moment of Inertia (Izz)	$1.3740 \times 10^{12} \text{ mm}^4$	$1.3011 \times 10^{12} \text{ mm}^4$
Geometry		

The moving load paths for the IRC loading and Commercial vehicle loadings were defined as per IRC:6-2017. The moving load path for all the moving load cases mentioned in Table 5.3 was done concerning the middle of the right girder, which is shown by the red line in Fig. 5.5. Fig. 5.5 shows the moving load path for the 70R eccentric loading condition. The eccentricity values taken for defining the moving load path for various loading conditions have been calculated as per IRC:6-2017 considering a cross barrier width of 0.5m and are shown in Table 5.4.

Table 5.4 Eccentricity values calculated to define the moving load path concerning the reference line

Load Cases	Eccentricity values (m)
Class A Wheeled 2-Lane Eccentric loading	-3.455, 0.045
Class A Wheeled 2-Lane Symmetric loading	-0.63, -4.13
70R-Wheeled 1-Lane Eccentric loading	-1.25
70R-Wheeled 1-Lane Symmetric loading	-2.38
Class AA-Wheeled Eccentric loading	-1.105
Class AA-Tracked Eccentric loading	-1.305
Truck Loading-Stage-1	0
Truck Loading-Stage-2	0

5.3.1 Validation of The Model

Fig. 5.6 to Fig.5.23 provides the deflected shape of the bridge in 3D with maximum values of the deflection and the bending moment diagram of the girders with maximum values of bending moments for different IRC loading cases including self-weight. The results were confirmed with those available in the CRRRI report determined using RM Bridge software. The results of maximum bending moment and maximum deflections under various load cases in both software namely RM Bridge and MIDAS CIVIL are almost similar with minimum error and are tabulated in Table 5.5. Table 5.5 shows the results for the maximum bending moment and maximum deflection of the bridge for load cases namely self-weight, Class A wheeled 2-lane eccentric

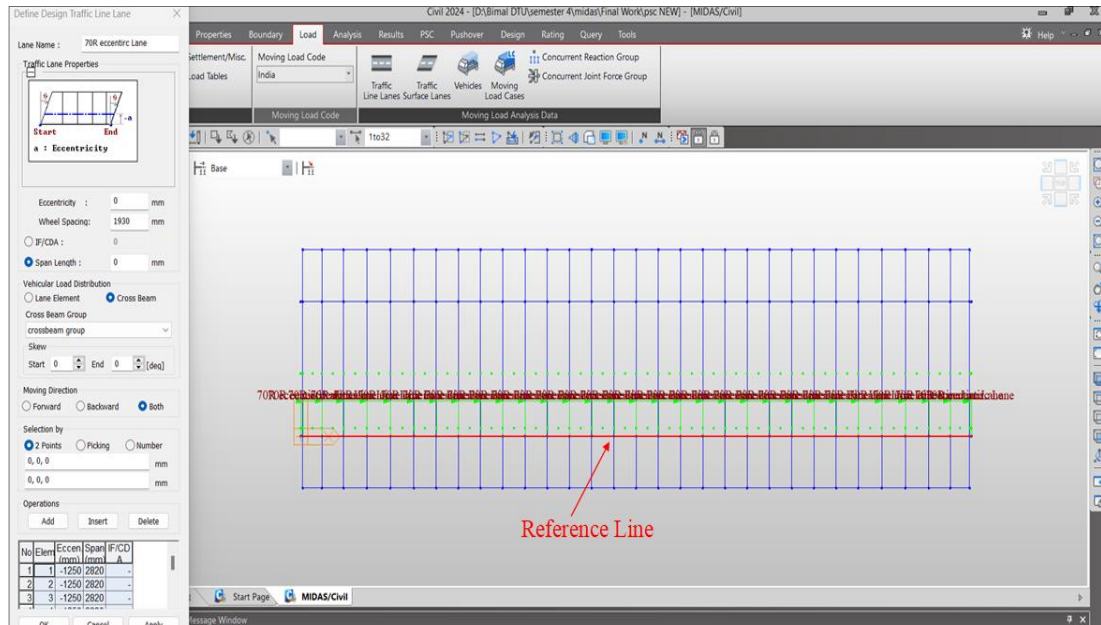


Fig. 5.5 Moving load path for the 70R eccentric loading condition

loading, Class A wheeled 2-lane symmetric loading, 70R 1-lane eccentric loading, 70R 1-lane symmetric loading, Class AA wheeled eccentric loading, Class AA tracked eccentric loading, Stage-1 loading (42T) and Stage-2 loading (42T+62T). It has been observed from Table 5.5 that the design IRC load case for this bridge span P3-P4 is 70R 1-lane eccentric loading because it is the case in which there is a maximum bending moment value and the maximum deflection value in the bridge. From Table 5.5, the maximum bending moment and maximum deflection under this load case obtained from the RM Bridge and MIDAS CIVIL were 4232 KNm and 3903.1 KNm respectively and the maximum deflection obtained from the same were 16.90mm and -17.872mm respectively. Since the IRC moving vehicles are hypothetical vehicles and are not available, hence commercial vehicles equivalent to the design IRC loading should be arranged for the load testing at the site. The results for the commercial vehicle load case (42T+62T) equivalent to this design IRC 70R 1-lane eccentric load case obtained from the RM Bridge and MIDAS CIVIL were 4285 KNm and 4494.8 KNm respectively and the maximum deflection obtained from the same were -17.28 mm and -20.733 mm respectively. Fig. 5.24 shows the load scheme for 42T+62T loading (i.e. for maximum bending moment) in MIDAS CIVIL, which is the same as the load scheme determined by the CRRI as shown in Fig.5.2.

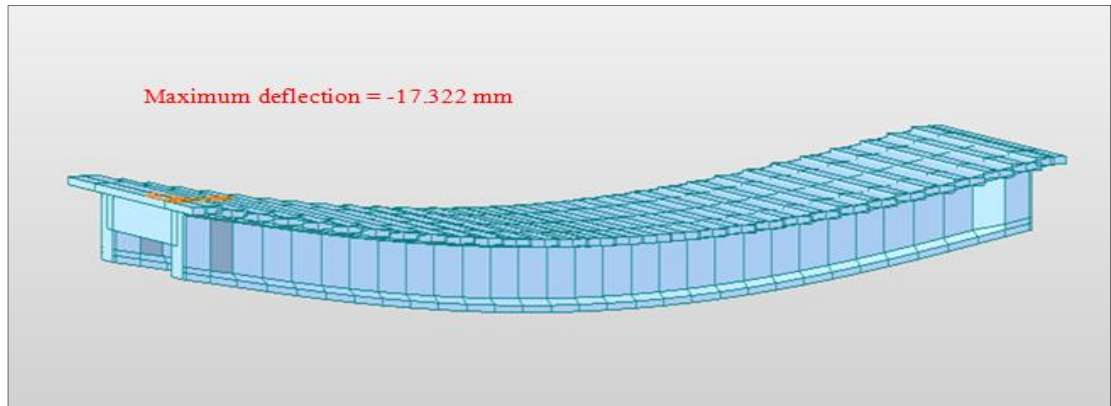


Fig. 5.6 Deflected shape of the bridge in 3D under self-weight

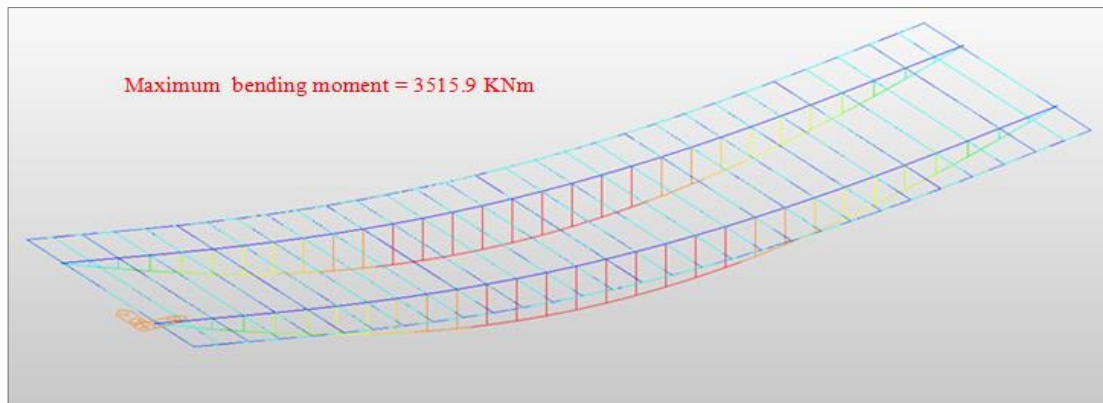


Fig. 5.7 Bending moment diagram of girders under self-weight

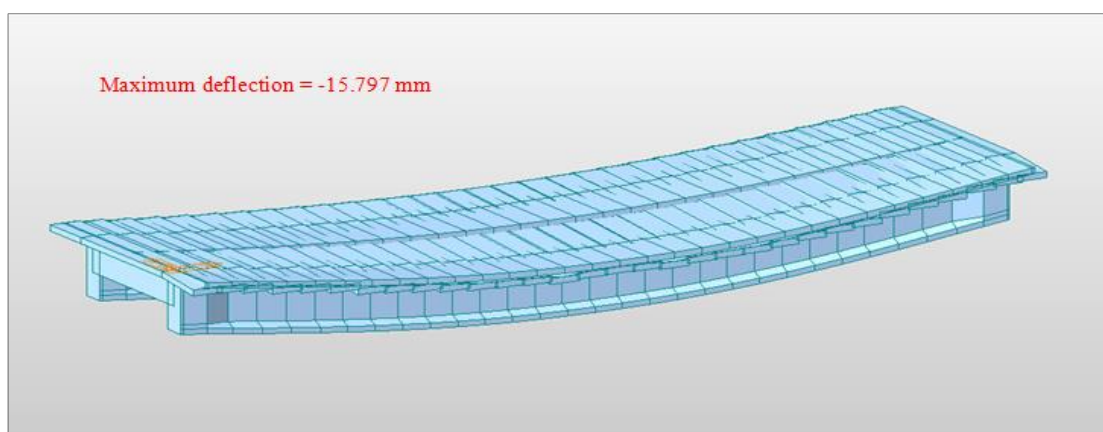


Fig. 5.8 Deflected shape of the bridge in 3D under Class A wheeled 2-lane eccentric loading

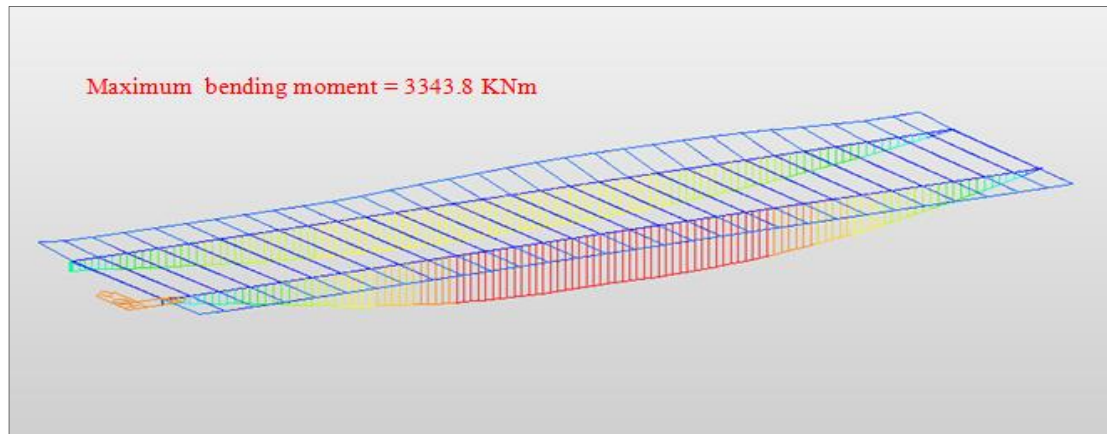


Fig. 5.9 Bending moment diagram of girders under Class A wheeled 2-lane eccentric loading

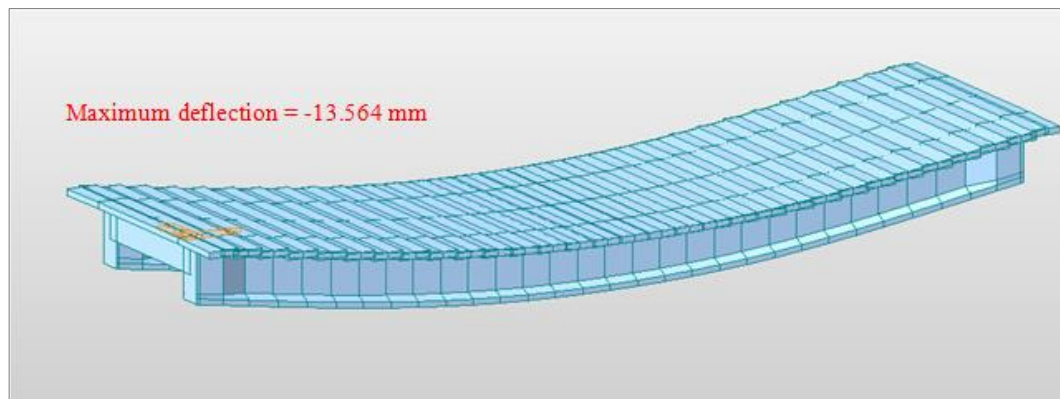


Fig. 5.10 Deflected shape of the bridge in 3D under Class A wheeled 2-lane symmetric loading

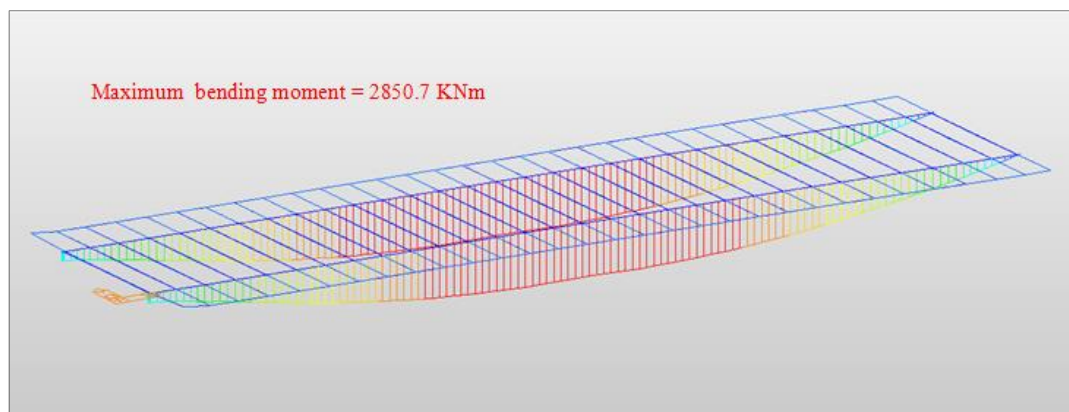


Fig. 5.11 Bending moment diagram of girders under Class A wheeled 2-lane symmetric loading

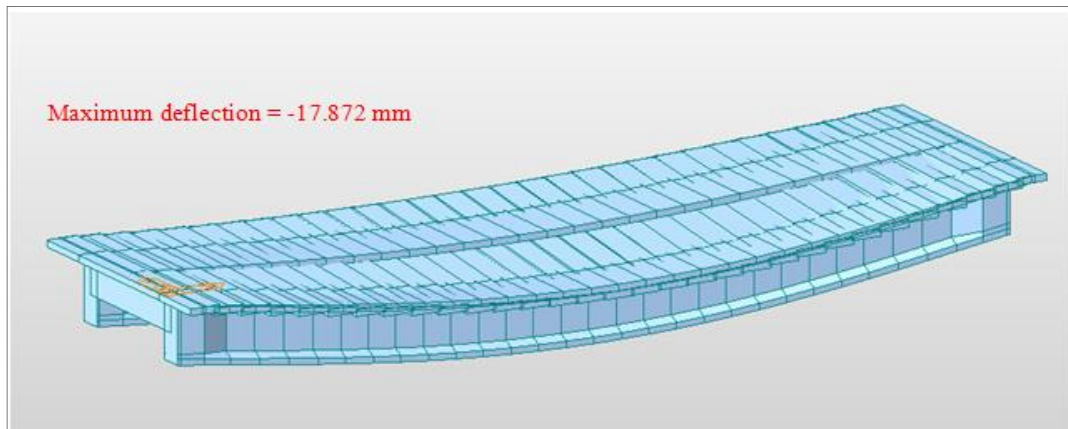


Fig. 5.12 Deflected shape of the bridge in 3D under 70R 1-lane eccentric loading

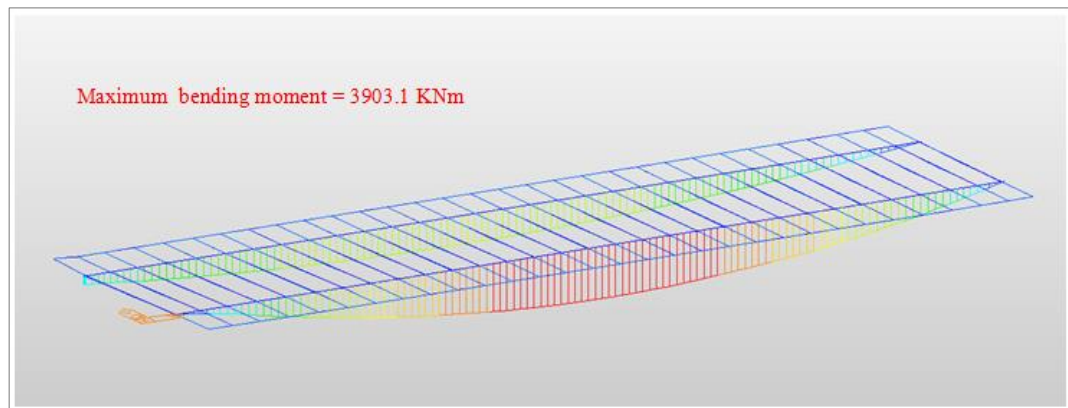


Fig. 5.13 Bending moment diagram of girders under 70R 1-lane eccentric loading

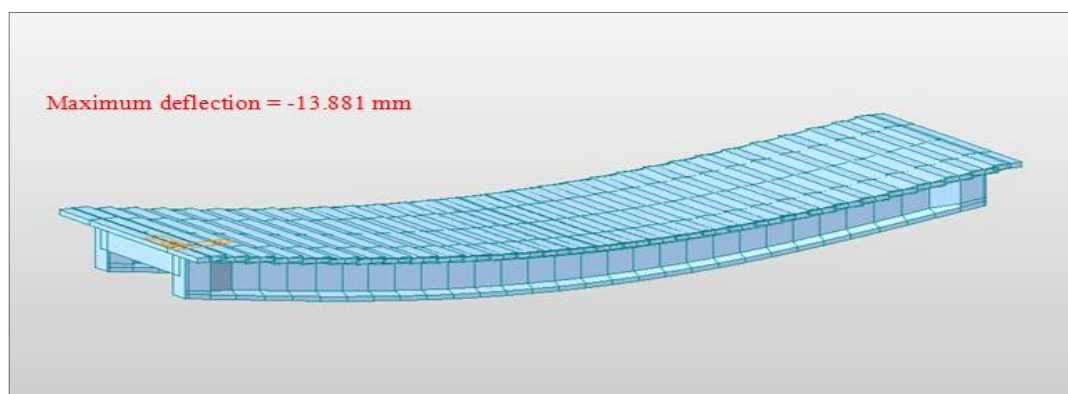


Fig. 5.14 Deflected shape of the bridge in 3D under 70R 1-lane symmetric loading

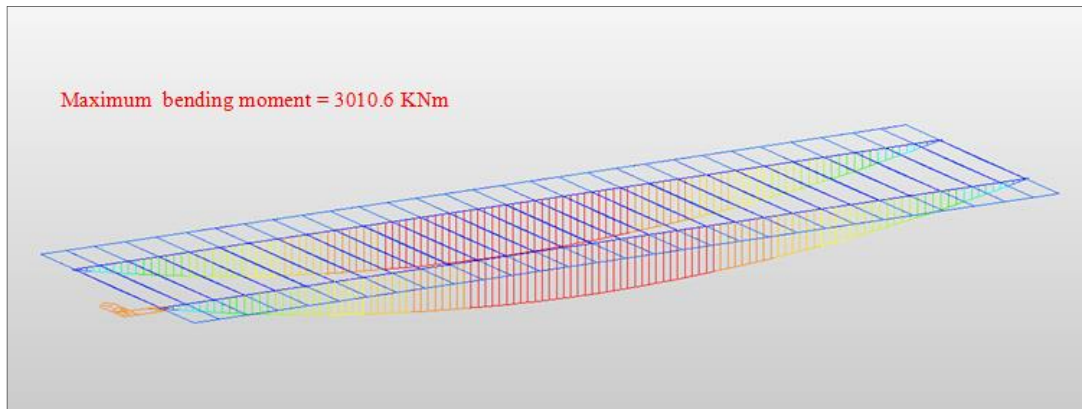


Fig. 5.15 Bending moment diagram of girders under 70R 1-lane symmetric loading

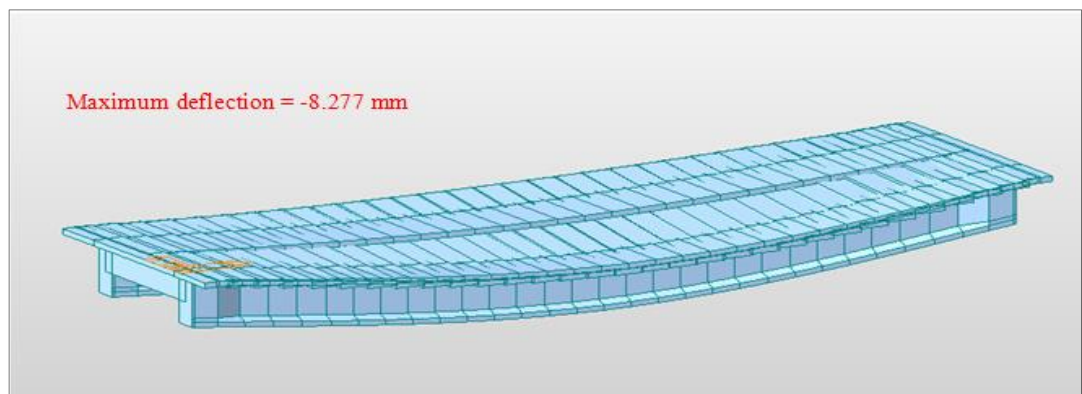


Fig. 5.16 Deflected shape of the bridge in 3D under Class AA wheeled eccentric loading

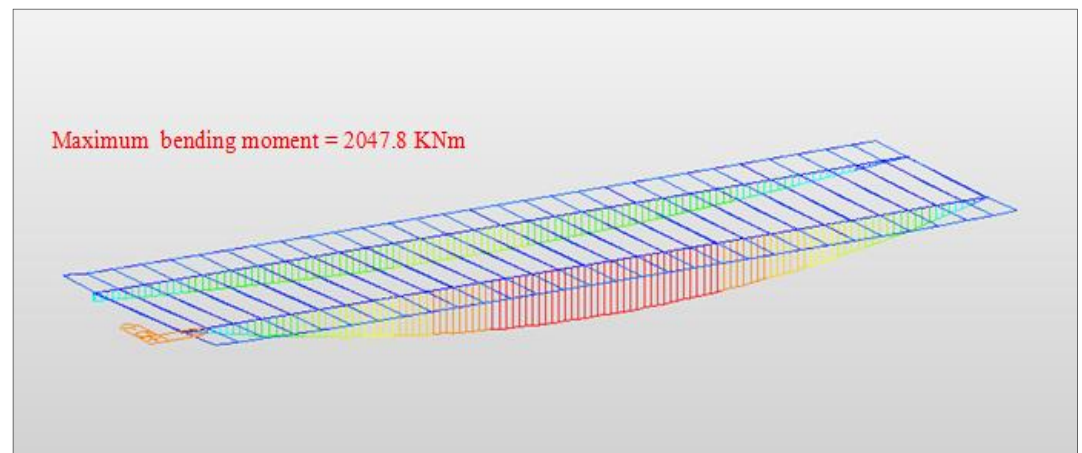


Fig. 5.17 Bending moment diagram of girders under Class AA wheeled eccentric loading

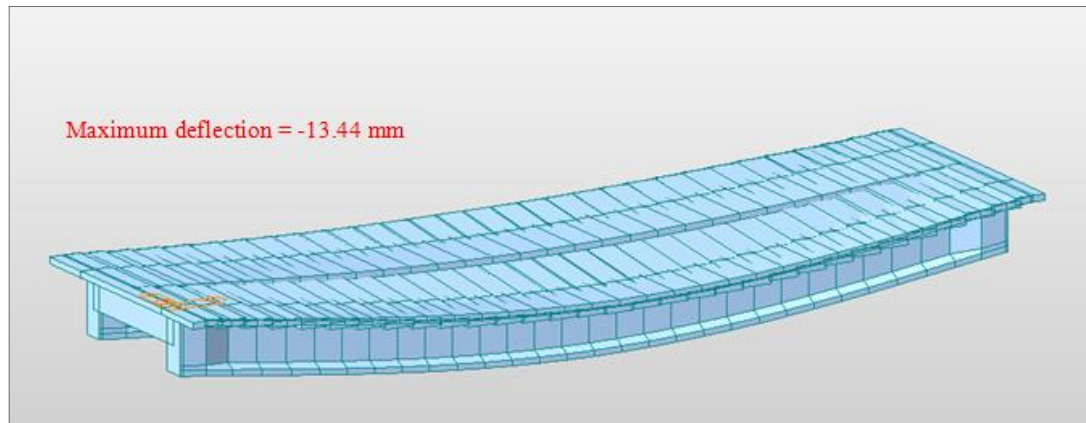


Fig. 5.18 Deflected shape of the bridge in 3D under Class AA tracked eccentric loading

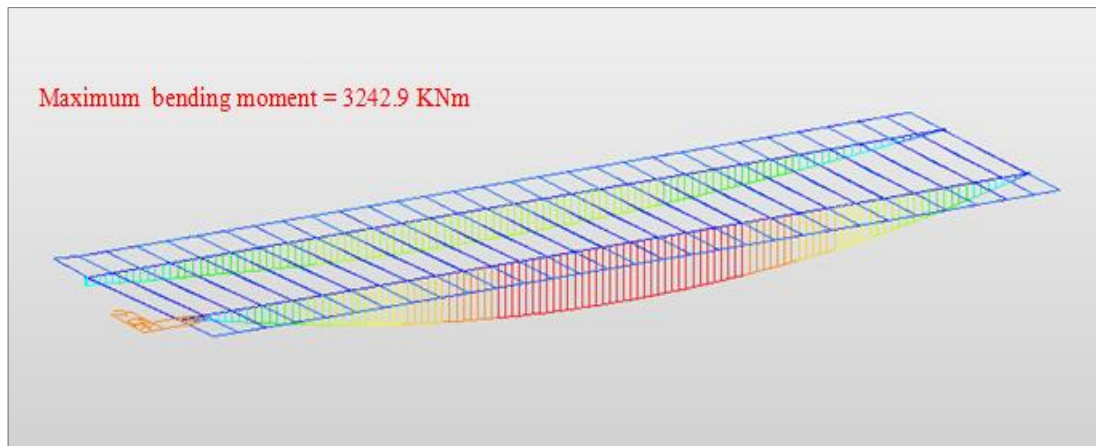


Fig. 5.19 Bending moment diagram of girders under Class AA wheeled eccentric loading

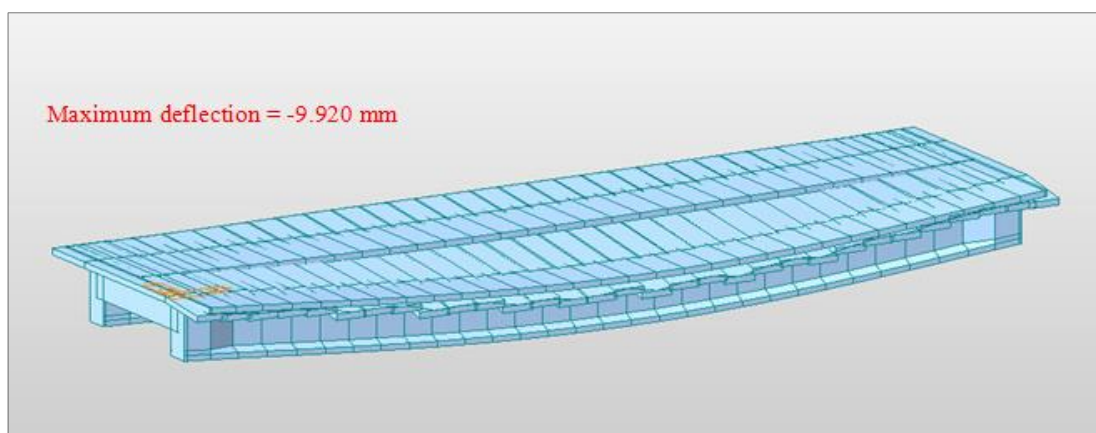


Fig. 5.20 Deflected shape of the bridge in 3D under Stage -1 (42T) loading

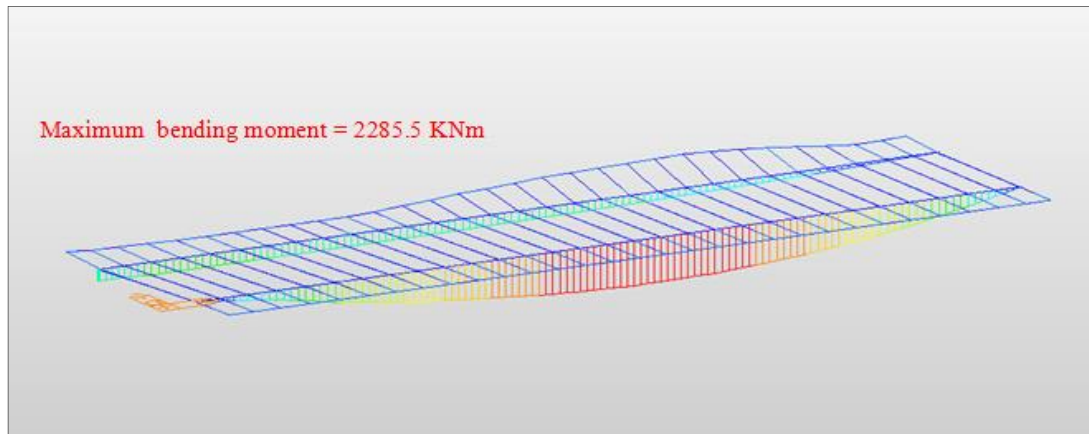


Fig. 5.21 Bending moment diagram of girders under Stage -1 (42T) loading

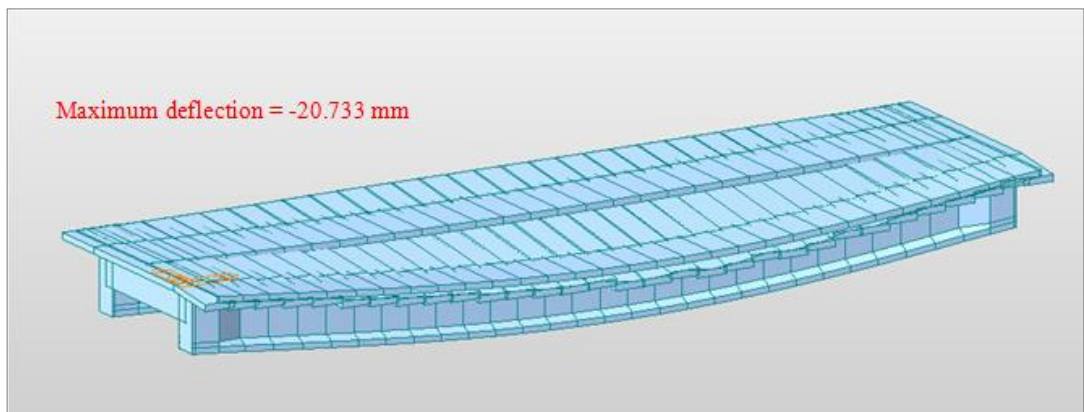


Fig. 5.22 Deflected shape of the bridge in 3D under Stage -2 (42T+62T) loading

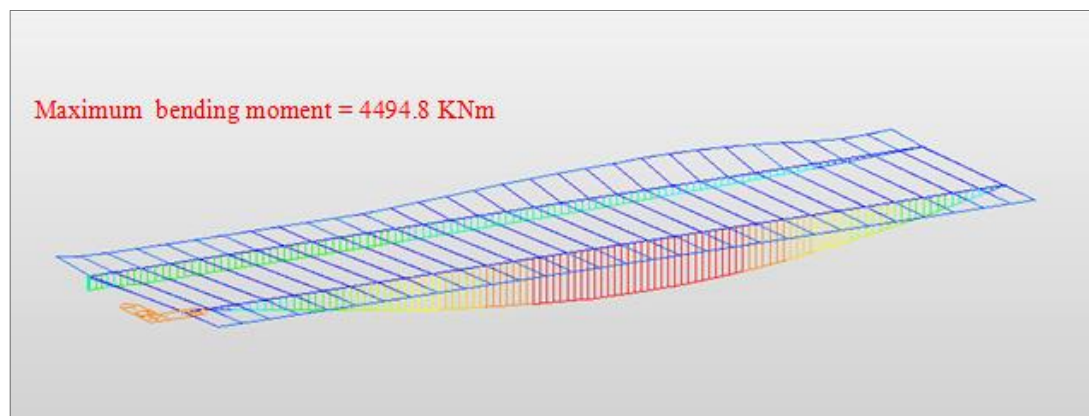


Fig. 5.23 Bending moment diagram of girders under Stage -2 (42T+62T) loading

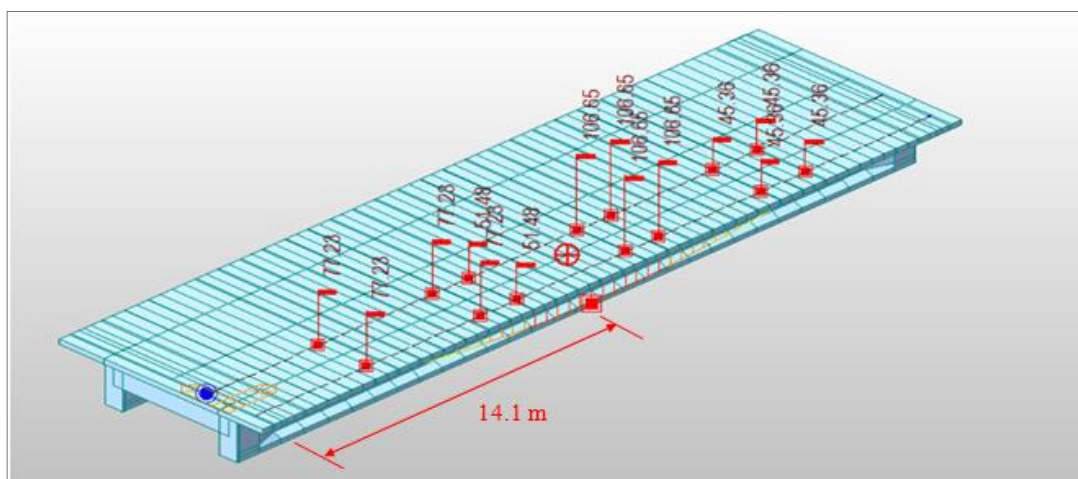


Fig. 5.24 Load Scheme for 42T+62T loading in MIDAS CIVIL

Table 5.5 Maximum Bending moment and Maximum deflection in RM bridge and MIDAS CIVIL under various load cases considered

Load Cases	All load cases with IRC load cases	RM Bridge		MIDAS CIVIL	
		B.M (KNm)	Deflection (mm)	B.M (KNm)	Deflection (mm)
Case 1	Self Weight	3778.1	-16.35	3515.9	-17.322
Case 2	Class A wheeled 2-lane eccentric loading	3444	-14.28	3343.8	-15.797
Case 3	Class A wheeled 2-lane symmetric loading	2867	-11.64	2850.7	-13.564
Case 4	70R 1-lane eccentric loading	4232	-16.90	3903.1	-17.872
Case 5	70R 1-lane symmetric loading	3000	-12.11	3010.6	-13.881
Case 6	Class AA wheeled eccentric loading	1128	-3.97	2047.8	-8.277
Case 7	Class AA tracked eccentric loading	3577	-12.91	3242.9	-13.44
Case 8	Stage-1 loading (42T)	1839	-6.511	2285.5	-9.920
Case 9	Stage-2 loading (42T+62T)	4285	-17.28	4494.8	-20.733

5.4 DYNAMIC LOAD TEST

For the Dynamic Load Test, natural frequency and mode shapes are the most important parameters for a structure. In bridge vibration analysis, several modes of vibration can be significant, depending on the bridge's design, environmental conditions, and loading scenarios. However, one of the most critical modes of vibration for bridges is typically the first mode of vibration, also known as the fundamental mode. The mode shape, in the first mode of vibration of the bridge span P3-P4, in the MIDAS CIVIL 2024 v 1.1, is shown in Fig. 5.25. The time-period to this mode of vibration is 0.2412 seconds and the natural frequency corresponding to this time-period is 4.145 Hz.

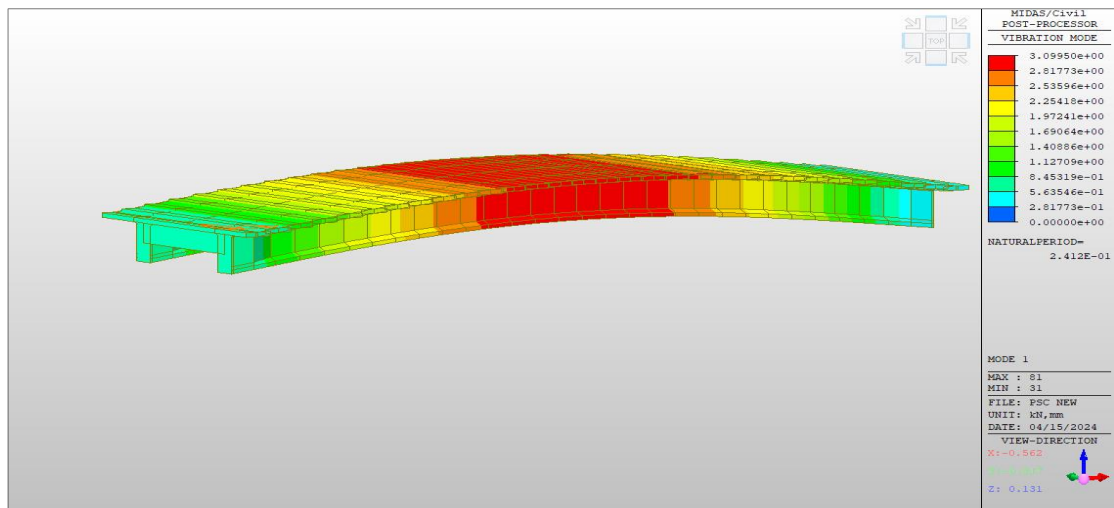


Fig. 5.25 Mode shape of the bridge span P3-P4 in 1st mode of vibration

5.4.1 Proposed Methodology for Determining Load Carrying Capacity of Bridge Using Static and Dynamic Parameters

The bridge span is numerically modelled in the software considering its all properties like above where span P3-P4 was modelled in the MIDAS CIVIL. Then IRC moving load is applied over the bridge and the maximum bending moment and displacement in the bridge corresponding to that moving load are found to validate with the design data as done in the above study. Also, the natural frequency corresponding to the first mode of vibration of the bridge span is found using the software as in the above study. The boundary conditions taken for the span are simply

supported conditions. Initially, maximum displacement (d_n) and natural frequency (f_n) are determined in the numerical model for IRC loading by considering that; (i) there is no change in boundary conditions (i.e. perfectly simply supported / no change in B), (ii) there is no material degradation (i.e. no change in E) and (iii) there is no cracks developed in along the span (i.e. no change in I). Also, we have experimental static load test data (i.e. deflection, d_e). When comparing the numerical simulation data with the experimental static load test data, we find some errors. This happens because the numerical model is represented at its ideal condition and the experimental load test is carried out over the bridge which is not in the ideal condition. The reason behind the bridge not being in its ideal condition (in its field condition) may be that the bridge is not constructed as desired or there is damage in the structural integrity of the bridge over the period.

Now, to match these two data, some tuning is required in the numerical model based on the above three conditions: (i) to (iii) and we get an updated model. Again, for this updated model, we find the updated natural frequency (f_n') and deflection (d_n') of the bridge. This study aims to make a comparative study of the parameters obtained from the experimental static load test (i.e. d_e) and experimental dynamic load test (i.e. f_e) to find the dynamic load carrying capacity of the bridge. Fig. 5.26 shows the two methodologies to determine the load carrying capacity of the bridge. Methodology 1 uses the numerical parameter (f_n') and experimental parameters (d_e) determined from static load testing and Methodology 2 uses the numerical parameter (d_n') and experimental parameter (f_e) determined from dynamic load testing. The formula to determine the dynamic load-carrying capacity of the bridge is given below (Islam et al., 2015).

$$\text{Dynamic Load Carrying Capacity (DLCC)} = K \times \Delta \quad (5.1)$$

Where, K = stiffness of the bridge and Δ = deflection value. The value of K can be calculated using the formula $K = (48 * EI_{\text{effective}}) / L^3$. Where, $EI_{\text{effective}}$ is the effective rigidity of the bridge and can be calculated using the formula $EI_{\text{effective}} = (4 * f^2 * L^3 * m_t) / \pi^2$. Where, f is the natural frequency of the bridge, L is the effective span and m_t is the total mass of the bridge. Using the formula for K in equation (5.1), a consolidated formula to calculate the dynamic load carrying capacity of the bridge can be written as,

$$\text{Dynamic Load Carrying Capacity (DLCC)} = \frac{192 * f^2 * m_t}{\pi^2} * \Delta \quad (5.2)$$

In this study, Methodology 1 is used due to the availability of experimental results for the static load test. It is proposed to use Methodology 2 in future to assess the dynamic load carrying capacity using the experimental dynamic parameter in terms of its natural frequency (f_e).

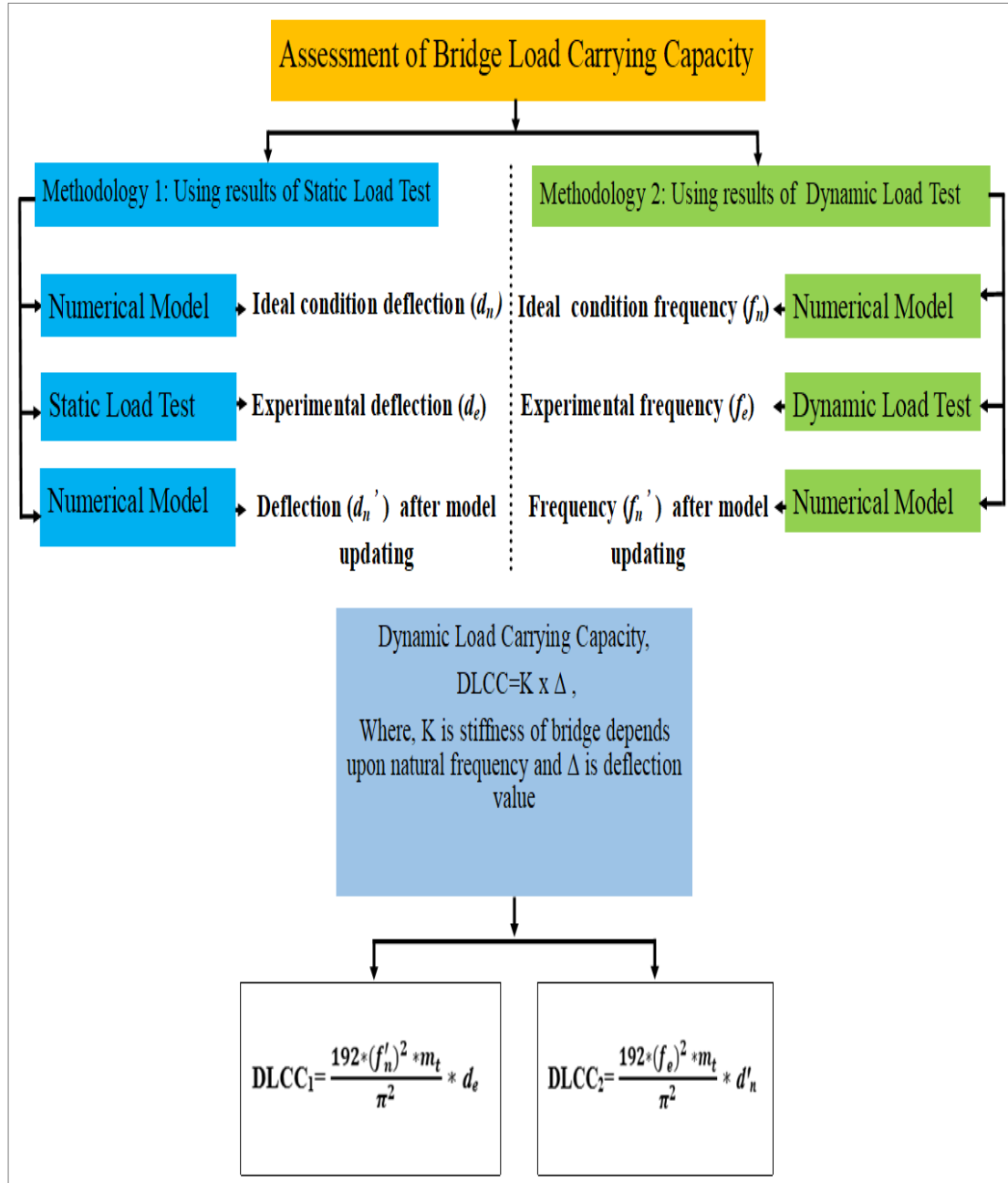


Fig. 5.26 Scheme for the comparative study of Static Load Test and Dynamic Load Test

5.4.2 Dynamic Load Carrying Capacity (DLCC) for the Bridge

As per the experimental load testing done by CSIR-CRRI, the Static Load Carrying Capacity (SLCC) of the bridge was found to be equivalent to 70R wheeled load including impact factor as per IRC:6-2017. The experimental maximum deflection value (d_e) from the static load test was -23.06mm. The natural frequency (f_1) of the bridge, from numerical modelling, in the ideal condition was 4.145 Hz. The Dynamic Load Carrying Capacity (DLCC) of the bridge, using the experimental deflection value (d_e) and the natural frequency (f_n) from the numerical model is calculated in Table 5.6. From Table 5.6 it has been observed that the dynamic load carrying capacity (DLCC₁) of the bridge before model updating was 170.49 tons which was not equal to the static load carrying capacity (SLCC) of 113.15 tons (i.e equivalent to 70R wheeled load including impact factor as per IRC:6-2017). Since, dynamic load carrying capacity (DLCC₁) was not same as static load carrying capacity (SLCC), therefore model updating was required.

Table 5.6 Calculation for the dynamic load carrying capacity (DLCC₁) of the bridge before model updating

Parameters	Calculated Values
Static Load Carrying Capacity (SLCC)	113.15 tons
Experimental deflection (d_e)	0.02306 m
Total Volume of R.C.C (V)	91.86132 m ³
Density of R.C.C taken by MIDAS (D)	2407 kg/m ³
Total mass of the bridge ($m_t = V \cdot D$)	22.1110 tons s ² /m
Frequency (f_n)	4.145 Hz
Dynamic Load Carrying Capacity (DLCC ₁) using the equation (5.2)	170.49 tons

5.4.3 Numerical Model Updating

In the above calculation, the dynamic load-carrying capacity of the bridge has not been matched with the static load-carrying capacity of the bridge. Now, to match the dynamic load-carrying capacity of the bridge with the static load-carrying capacity the parametric study has been performed to get the desired value of natural frequency (f_n') in the numerical model. For this, we can play with three parameters i.e. material property (E), boundary condition (B) and moment of inertial (I) that affect the structural properties of the bridge.

In this study, boundary conditions has been considered as simply supported and 'E' & 'I' were varied. 'I' was varied from 100% to 60% of the ideal condition. Here 60% 'I' represents 40% reduction in the ideal value of 'I' due to any reason including cracks, etc. 'E' was varied from M20 to M60 where M20 represents the grade of concrete for which modulus of elasticity (E) can be calculated using the formula $E=5000\sqrt{f_{ck}}$ N/mm², where $f_{ck}=20$ for M20 grade of concrete.

Table 5.7 lists the values of frequencies for 'I' varying from 60% to 100% with 5% intervals and E changing from M20 to M60. The same is plotted in Fig.5.27 for better clarity. From Table 5.7 and Fig.5.27, it has been observed that the target frequency (f_n') was closer to that corresponding to 'I' 65% and M30. Further, from the minute study, the target frequency (f_n') of value 3.376 Hz of the updated model was achieved corresponding to 'I' 65.1% and M30. Using this updated frequency, the dynamic load carrying capacity (DLCC₁) of the bridge after model updating was again calculated like in Table 5.6 and was observed as,

$$\text{Dynamic Load Carrying Capacity (DLCC}_1\text{)} = 113.05 \text{ tons}$$

Hence, Dynamic Load Carrying Capacity (DLCC₁) is now similar to Static Load Carrying Capacity (SLCC). Therefore it can be concluded that the flexural load carrying capacity of the bridge determined using dynamic parameter is 4232 KNm that is similar to the flexural load carrying capacity of 4232 KNm determined experimentally.

Table 5.7 Frequency of the bridge for varying E & I
Target $f=3.376$ Hz

E, Iyy and frequency										
		E1	E2	E3	E4	E5	E6	E7	E8	E9
		M20	M25	M30	M35	M40	M45	M50	M55	M60
Iyy1	60%	2.9334	3.1017	3.2457	3.3738	3.4880	3.5920	3.6873	3.7764	3.8580
Iyy2	65%	3.0497	3.2237	3.3738	3.5063	3.6245	3.7327	3.8329	3.9246	4.0112
Iyy3	70%	3.4965	3.3411	3.4965	3.6337	3.7566	3.8685	3.9714	4.0667	4.1563
Iyy4	75%	3.2669	3.4542	3.6140	3.7566	3.8835	3.9984	4.1051	4.2034	4.2955
Iyy5	80%	3.3693	3.5625	3.7272	3.8745	4.0048	4.1237	4.2337	4.3365	4.4307
Iyy6	85%	3.4686	3.6670	3.8373	3.9872	4.1220	4.2463	4.3592	4.4623	4.5600
Iyy7	90%	3.5638	3.7679	3.9432	4.0984	4.2355	4.3630	4.4783	4.5851	4.6860
Iyy8	95%	3.6563	3.8655	4.0453	4.2034	4.3459	4.4763	4.5956	4.7059	4.8077
Iyy9	100%	3.7467	3.9620	4.1459	4.3085	4.4543	4.5851	4.7081	4.8216	4.9261

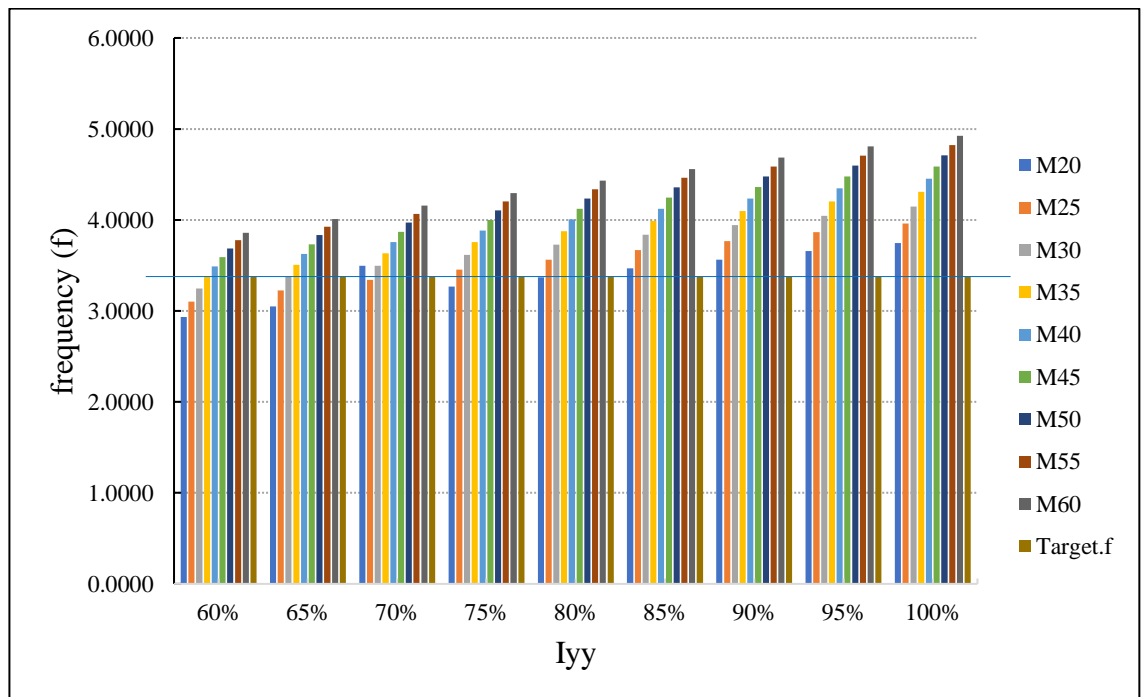


Fig. 5.27 Graph Showing frequency (f_n) for varying I&E

5.5 CONCLUSION

The available data in CSIR-CRRI report is used to develop the comprehensive numerical model. With the help of the numerical model and the experimental static load testing data, the static parameter and the dynamic parameter of the bridge are used for the calculation of the Dynamic Load Carrying Capacity (DLCC) of the bridge. Initially, when the deflection value (d_e) of 23.06 mm, measured experimentally during the static load test and frequency value (f_n) of 4.145 Hz, obtained from numerical modelling, are used to calculate the Dynamic Load Carrying Capacity (DLCC₁) of the bridge and is found as 170.49 tons, which is found to be not similar to the Static Load Carrying Capacity (SLLC) of equivalent 70R loading including impact factor as per IRC:6-2017 (i.e 113.15 tons). Then parametric study for the frequency of the bridge is done based on E, I and B and an updated numerical model which resembles the current condition of the bridge is generated. For the frequency (f_n') value 3.376 Hz of the updated model, the Dynamic Load Carrying Capacity (DLCC₁) of the bridge is found similar to the Static Load Carrying Capacity (SLLC) of the bridge. Moreover, it can be concluded that the flexural load carrying capacity of the bridge determined using dynamic parameter is 4232 KNm that is similar to the flexural load carrying capacity of 4232 KNm determined experimentally.

CHAPTER 6

CONCLUSION AND FUTURE WORK

6.1 GENERAL

The primary objective of the work is to explore the feasibility of using the Dynamic Load Test (DLT) as an alternative to the conventional Static Load Test (SLT) for evaluating the load carrying capacity of bridges. For this, a comprehensive numerical model is developed utilizing advanced structural analysis techniques to simulate the response of bridge structures under both static and dynamic loading conditions, enabling the quantitative evaluation of their performance, using the existing available literature data for the static load test to determine the dynamic parameters of the bridge. The final objective is to analyze the obtained data from the numerical simulations for establishing a methodology for determining the load carrying capacity using the dynamic parameter of the bridge. Fig. 6.1 illustrates the summary of the layout of the thesis.

6.2 CONCLUSION

The conclusions of the work covering all the research objectives are summarized below ;

- A numerical study for the finite element analysis of concrete bridge under IRC class- AA tracked moving load shows that parameters namely, total deformation, maximum equivalent stress and maximum equivalent strain decrease with the increasing eccentricity of the moving load path from the kerb. The percentage decrease in maximum total deformation from the load path at 1200mm position to the load path at 2300mm position (symmetric loading case) from the kerb is 13.76%, the percentage decrease in equivalent stress from the load path at 1200mm position to load path at 2300mm position (symmetric loading case) from the kerb is 9.48% and the percentage decrease in equivalent strain from the load path at 1200mm position to load path at 2300mm position (symmetric loading case) from the kerb is 9.48%. Moreover, it is seen that among all load paths, the maximum total deformation of 8.06mm, maximum equivalent stress of 51.63 MPa and

maximum equivalent strain of 0.00163 are obtained for the load path at 1200mm from the kerb.

- A numerical investigation of the deflection behaviour in a concrete bridge subjected to various Indian Road Congress (IRC) moving load scenarios shows that the maximum deflection produced for a 2-lane Class A wheeled vehicle with eccentric loading conditions is -16.02mm. Hence, among all load case scenarios

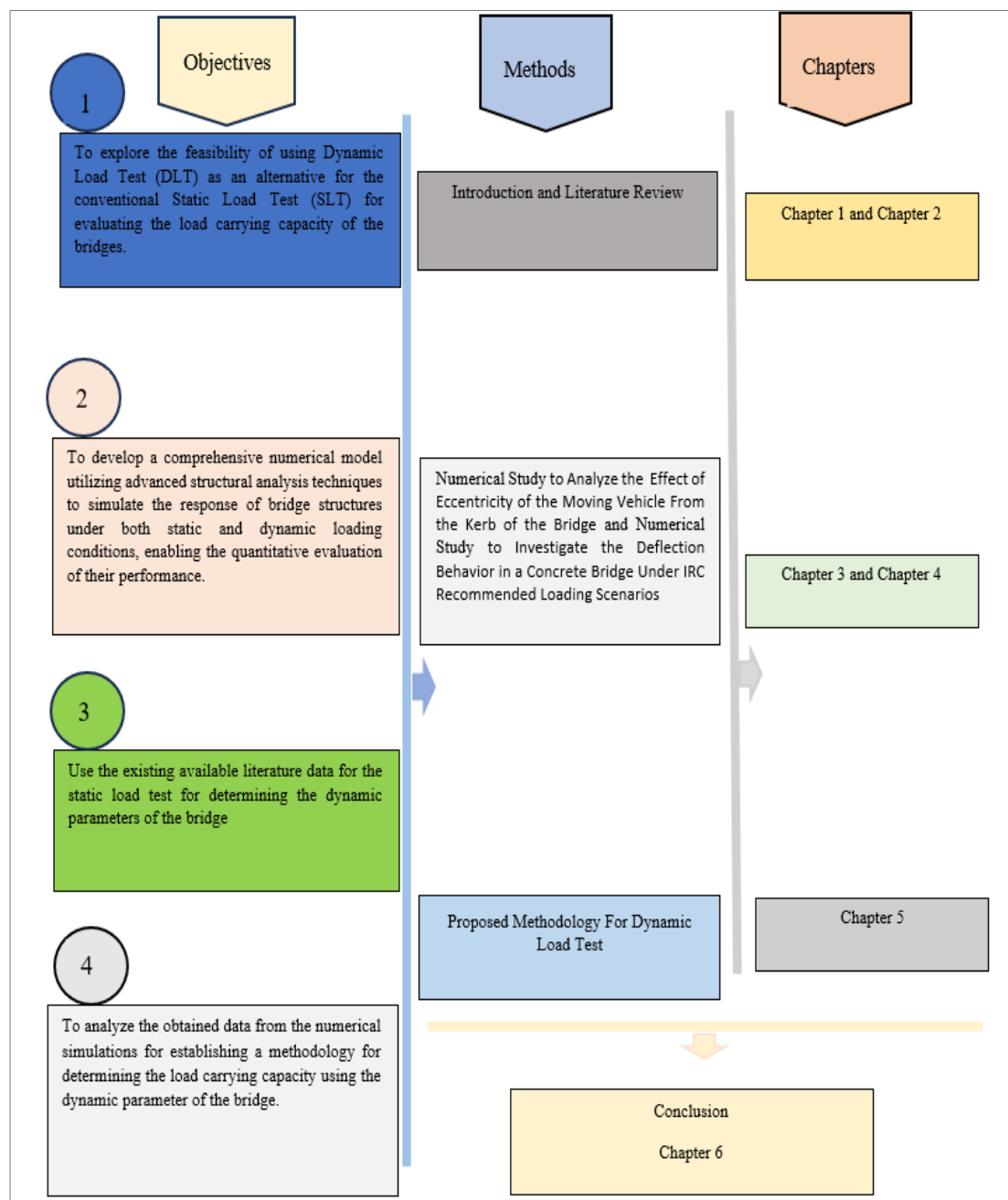


Fig. 6.1 Summary of Layout of the thesis

taken for the study namely, (a) Class AA tracked vehicle for eccentric condition, (b) Class AA wheeled vehicle for eccentric condition, (c) 2-lane Class A vehicle for eccentric condition, (d) 2-lane Class A vehicle for symmetric condition, (e) 70R wheeled load for eccentric condition and (f) 70R wheeled load for symmetric condition, 2-lane Class A wheeled vehicle with eccentric loading conditions is found the critical load case for this study.

- The dynamic load carrying capacity ($DLCC_1$) is calculated using a deflection value (d_e) of 23.06 mm from the experimental load testing and frequency value (f_n) of 4.145 Hz from the numerical model and found as 170.49 tons, which is not similar to the static load carrying capacity (SLCC) equivalent to the 70R wheeled vehicle including the impact factor (113.15 tons corresponding to bending moment of 4232 KNm) as reported by the CRRI. This is because the numerical model is not in onsite condition but in ideal condition. With the period of time and usage, the structural integrity of the bridge changes as parameters namely, material property (E), boundary condition (B) and moment of inertia (I) affecting the structural properties of the bridge changes. Then, to tune the numerical model with the onsite condition of the bridge, a parametric study is carried out based on the parameters: material property (E), boundary condition (B) and moment of inertia (I) and an updated model which resembles with the bridge onsite condition is generated. The target frequency (f_n') of 3.376 Hz is observed for the updated numerical model with modulus of elasticity (E) of M30, moment of inertia (I) of 65.1% and boundary condition as simply supported. Then, the dynamic load carrying capacity ($DLCC_1$) is again calculated using a deflection value (d_e) of 23.06 mm and frequency value (f_n') of 3.376 Hz and found as 113.05 tons, which is now similar to the static load carrying capacity (SLCC) equivalent to the 70R wheeled vehicle including the impact factor (113.15 tons) as reported by the CRRI. Therefore, it can be concluded that the flexural load carrying capacity of the bridge determined using dynamic parameter is 4232 KNm which is similar to the flexural load carrying capacity of 4232 KNm determined experimentally.

6.3 FUTURE WORK

Here in this work, dynamic load carrying capacity of the bridge (DLCC₁) is calculated based on the numerical parameter (f_n') and experimental parameter (d_e) determined from static load testing (Methodology 1). The parametric studies have been carried out on material property (E) and moment of inertia (I) considering boundary condition (B) as simply supported. In future, following work may be extended in the following ways:

- i) Dynamic Load Carrying Capacity (DLCC₂) of the bridge shall be calculated using deflection value (d_n') from the numerical model and experimental parameter (f_e) determined from dynamic load testing (Methodology 2). The parametric study concerning E, B and I will be carried out in the numerical model in the same way as done in this work.
- ii) It shall be shown that both DLCC₁ and DLCC₂, achieved for the numerical model having E value for M30, boundary conditions (B) as simply supported and Keeping I value as 65.1% of that in an ideal condition, are giving similar values for the load carrying capacity of the bridge.
- iii) The dynamic load carrying capacity (DLCC) for different types of boundary conditions other than simply supported shall be calculated as per Table 6.1.

Table 6.1 Different Formulae to calculate DLCC for different boundary conditions (Islam et al., 2015)

Boundary conditions	Formulae to calculate DLCC
Simply Supported	$\frac{192*f^2*m_t}{\pi^2} * \Delta$
Fixed-Hinged	$\frac{4800*\pi^2*f^2*m_t}{2611} * \Delta$
Fixed-Fixed	$\frac{192*\pi^2*f^2*m_t}{126} * \Delta$

- iv) Change in boundary conditions (B) has been neglected in this study, the same may be explored in the future.

REFERENCES

1. Abedin, M., y Basalo, F.J.D.C., Kiani, N., Mehrabi, A.B. and Nanni, A., 2022. Bridge load testing and damage evaluation using model updating method. *Engineering structures*, 252, p.113648.
2. Baisthakur, S. and Chakraborty, A., 2021. Experimental verification for load rating of steel truss bridge using an improved Hamiltonian Monte Carlo-based Bayesian model updating. *Journal of Civil Structural Health Monitoring*, 11(4), pp.1093-1112.
3. Benčat J and Kohár R (2018) Bridges Subjected to Dynamic Loading. Bridge Engineering. InTech. Available at: <http://dx.doi.org/10.5772/intechopen.73193>.
4. Caglayan, B.O., Ozakgul, K. and Tezer, O., 2012. Assessment of a concrete arch bridge using static and dynamic load tests. *Structural Engineering and Mechanics*, 41(1), pp.83-94.
5. Chen, W.F. and Duan, L., 2014. Substructure design. *Bridge Engineering Handbook*, 2nd edn. CRC Press, Taylor & Francis Group.
6. Cook, W., 2014. *Bridge failure rates, consequences, and predictive trends*. Utah State University.
7. CRRI Report, 2019. Assessment and Rehabilitation Scheme for Shashti Bridge across Ganger River, Mirzapur (CNP-2419).
8. De Angelis, A. and Pecce, M.R., 2023. Model assessment of a bridge by load and dynamic tests. *Engineering Structures*, 275, p.115282.
9. Dissanayake, R. and Bandara, C.S., 2016. Retrofitting of damaged bridges—the sustainable solution. *International journal of urban sciences*, 20(sup1), pp.50-59.
10. Garg, R.K., Chandra, S. and Kumar, A., 2022. Analysis of bridge failures in India from 1977 to 2017. *Structure and Infrastructure Engineering*, 18(3), pp.295-312.
11. Gatti, M., 2019. Structural health monitoring of an operational bridge: A case study. *Engineering Structures*, 195, pp.200-209.
12. Gupta, N., Kaushal, A.K. and Ranjan, R., 2023. Parametric study on reinforced concrete T-beam girder bridges. *Materials Today: Proceedings*.
13. Indian Road Congress, 2010. IRC: SP:037-2010, *Guidelines for Evaluation of Load Carrying Capacity of Bridges (First Revision)*. New Delhi: Indian Road Congress.
14. Indian Road Congress, 2015. IRC: SP:51-2015, *Guidelines for Load Testing of Bridges (First Revision)*. New Delhi: Indian Road Congress.

15. Indian Road Congress, 2017. IRC:6-2017, *Standard Specifications and Code of Practice for Road Bridges, Section-II Load and Combinations (Seventh Revision)*. New Delhi: Indian Road Congress.
16. Islam, A.A., Jaroo, A.S. and Li, F., 2015. Bridge load rating using dynamic response. *Journal of Performance of Constructed Facilities*, 29(4), p.04014120.
17. Ko, S.W. and Kim, J.K., 2023. A Framework for Evaluating the Load-Carrying Capacity of Bridges without Design Document Using an AI Technique. *Applied Sciences*, 13(3), p.1283.
18. Laura, M., Francesco, C. and Antonio, F., 2020. Static and dynamic testing of highway bridges: A best practice example. *Journal of Civil Structural Health Monitoring*, 10(1), pp.43-56.
19. Lin, W. and Yoda, T., 2017. *Bridge engineering: classifications, design loading, and analysis methods*. Butterworth-Heinemann.
20. Liu, H., He, X., Jiao, Y. and Wang, X., 2019. Reliability assessment of deflection limit state of a simply supported bridge using vibration data and dynamic bayesian network inference. *Sensors*, 19(4), p.837.
21. Lu, P., Li, D. and Chen, Y., 2023. Prediction of the static load test results of bridges based on the dynamic load test and the Kriging model. *Artificial Intelligence Review*, 56(8), pp.7613-7632.
22. Magalhães, F., Cunha, Á. and Caetano, E., 2008. Dynamic monitoring of a long-span arch bridge. *Engineering Structures*, 30(11), pp.3034-3044.
23. Omar, T. and Nehdi, M.L., 2018. Condition assessment of reinforced concrete bridges: Current practice and research challenges. *Infrastructures*, 3(3), p.36.
24. Padgett, J.E., Dennemann, K. and Ghosh, J., 2010. Risk-based seismic life-cycle cost-benefit (LCC-B) analysis for bridge retrofit assessment. *Structural safety*, 32(3), pp.165-173.
25. Raju, N.K., 2010. *Design of Bridges*. Oxford 6 and IBH Publishing Co. Pvt. Ltd.
26. Ryan, T.W., Lloyd, C.E., Pichura, M.S., Tarasovich, D.M. and Fitzgerald, S., 2023. *Bridge Inspector's Reference Manual (BIRM)(2022 NBIS)* (No. FHWA-NHI-23-024). National Highway Institute (US).
27. Samali, B., Li, J., Crews, K.I. and Al-Dawod, M., 2007. Load rating of impaired bridges using a dynamic method. *Electronic Journal of Structural Engineering*.
28. Sasidharan, N. and Johny, B., 2015. Finite element analysis and parametric study of curved concrete box girder using Abaqus software. *International Journal of Research in Engineering and Technology*, 4(10), pp.425-429.

29. Shaikh, M.F. and Nallasivam, K., 2022. Static analysis of box-girder bridge under the influence of Indian railway vehicle loading using ANSYS finite element model. *Advances in bridge engineering*, 3(1), p.25.
30. Song, H.W., You, D.W., Byun, K.J. and Maekawa, K., 2002. Finite element failure analysis of reinforced concrete T-girder bridges. *Engineering Structures*, 24(2), pp.151-162.
31. Sun, Z., Siringoringo, D.M. and Fujino, Y., 2021. Load-carrying capacity evaluation of girder bridge using moving vehicle. *Engineering Structures*, 229, p.111645.
32. Wang, N.B., Shen, W., Guo, C. and Wan, H.P., 2022. Moving load test-based rapid bridge capacity evaluation through actual influence line. *Engineering Structures*, 252, p.113630.
33. Zhang, X.D., Wang, J.Z. and Guo, J.F., 2012. Inspection and Evaluation of Load-Bearing Capacity of Single Tower Composite Girder Cable-Stayed Bridge. *Advanced Materials Research*, 538, pp.1785-1788.
34. Zhou, Y., Prader, J., Weidner, J., Dubbs, N., Moon, F. and Aktan, A.E., 2012. Structural identification of a deteriorated reinforced concrete bridge. *Journal of Bridge Engineering*, 17(5), pp.774-787.

APPENDIX A

DLOAD SUBROUTINE CODE FOR IRC CLASS AA WHEELED VEHICLE

```

1      subroutine DLOAD(F,KSTEP,KINC,TIME,NOEL,NPT,LAYER,KSPT,
2      &                COORDS, JLTYP, SNAME)
3      C
4      include 'ABA_PARAM.INC'
5      C
6      dimension TIME(2), COORDS(3) CHARACTER*80 SNAME
7
8      X=COORDS(1) Y=COORDS(2) Z=COORDS(3)
9
10     X1=1200!for eccentric load minimum distance from edge
11     X2=1501!minimum distance 1200+ 300( tyre width )+1( +1 is taken to maintain 300mm
12     with as we are doing >x1 and <x2): FIST TYRE ALONG WIDTH LOCATED
13
14     X3=1800!1500+300
15     X4=2101!1800+300+1:SECONTYRE
16     ALONG WIDTH LOCATED
17     X5=2800!2100+700
18     X6=3101!2800+300+1:THIRD TYRE
19     ALONG WIDTH LOCATED: d
20     X7=3400!3100+300
21     X8=4001!3400+300+1: FOURTH TYRE
22     ALONG WIDTH LOACTED
23     a=150
24     !b=300
25     LA=1050
26     P1=0.83
27     P2=1.39
28     Velocity = 28200
29     Displac
30     ment = Velocity*TIME(2)
31
32
33
34
35
36
37
38
39
40
41
42
43
44
45

```

```

28      if ( X.le.X2.and. X.ge.X1) then
29
30          ! in longitudinal direction
31          if ( Z.ge.displacement+a .and. z.le.displacement) then
32              F=0.83
33          else if(z.le.displacement+a+LA1 .and. z.ge.displacement+LA1) then
34
35              F=0.83
36          else
37
38              F=0.0
39          end if
40
41      else if ( X.ge.X3.and.X.le.X4) then
42          ! in longitudinal direction
43          if ( Z.ge.displacement+a .and. z.le.displacement) then
44              F=1.39
45          else if (z.le.displacement+a+LA1 .and. z.ge.displacement+LA1) then
46
47              F=1.39
48          else

```

```

46             F=0.0
47         end if
48     else if ( X.ge.X5.and.X.le.X6) then
49         ! in longitudinal direction
50         if ( Z.ge.displacement+a .and. z.le.displacement) then
51             F=1.39
52         else if (z.le.displacement+a+LA1 .and. z.ge.displacement+LA1) then
53             F=1.39
54         else
55             F=0.0
56         end if
57     else if ( X.ge.X7.and.X.le.X8) then
58         ! in longitudinal direction
59         if ( Z.ge.displacement+a .and. z.le.displacement) then
60             F=0.83
61         else if (z.le.displacement+a+LA1 .and. z.ge.displacement+LA1) then
62             F=0.83
63         else
64             F=0.0
65         end if
66     else
67         F=0.0
68     end if
69     F=0.0
70
71 end if
72
73 RETRUN
74 END

```

PUBLICATIONS

(1) Raid conference:

[1] Sharma, B., Kaur, N., Kumar, P., and Pal, S. (2024), “Numerical Investigation of the Deflection Behavior in a Reinforced Concrete Bridge Subjected to Various Indian Road Congress Moving Load Scenarios” 1st International Conference on Recent Advances in Infrastructure Development (RAID-2024), Department of Civil Engineering, NIT Calicut, 12th -13th February 2024.



(2) CECT conference:

[2] Sharma, B., Pal, S., Kaur, N., and Kumar, P. (2024), “Finite Element Analysis of Concrete Bridge Under Moving Load Across and Along the Span” International Conference on Civil, Environment and Construction Technology: Ecological Resilient & Sustainable Development Goals Integration-Research Agenda (CECT-2024), Department of Civil Engineering, Graphic Era (Deemed to be) University, Dehradun, 17th - 18th May 2024.



PLAGIARISM REPORT

CURRICULUM VITAE

CURRICULUM VITAE

BIMAL SHARMA

bimals935@gmail.com

ADDRESS:

- **Country:** Nepal, **Province:** Sudurpaschchim, **Zone:** Mahakali, **District:** Kanchanpur, **Municipality:** Dodhara Chandani 07, **Zip code:** 10400.

EDUCATION:

Class	Passing Year	Institution	Marks	Rank
M.Tech.(Structural Engineering)	2024	Delhi Technological University, Delhi	8.89/10	1 st (till 3 rd sem)
B.E. (Civil Engineering)	2020	Far-Western University, Nepal	3.89/4	2 nd (in faculty)
HSEB (Class XII)	2016	Radiant HSS, Nepal	71.4%	-
SLC (Class X)	2014	Laxmi Ma vi, Nepal	69.13%	1 st (in class)

TRANING / INTERNSHIP:

- “**Construction Operation Project**” from a broad institute “**Civil Guruji**”.
- Attended **motivational talk** on **being** an **entrepreneur** (10th November 2022).
- Attended **seismic academy** annual **conference** (31st August 2023).

ACADEMIC PROJECTS:

- **B.E. Final Year Project** on “**Seismic analysis and design of multi-storied commercial building**”(Multi Storied building was modelled in SAP and analysis was done as per IS standards).
- **Seminar** on “**Advantages and challenges of modular construction of buildings**”, in M. Tech 1st semester, under Dr. Shilpa Pal.
- **M.Tech Final Year Project** on “**Assessment of Bridge Load-Carrying Capacity Under Static and Dynamic Load Testing**” under Dr. Shilpa Pal, Associate professor, Delhi Technological University, Delhi-110042 and Dr. Naveet Kaur, Senior Scientist, CSIR-CRRI, New Delhi-110025.

ACADEMIC ACHIEVEMENTS AND AWARDS:

- *Awarded ICCR scholarship* from Embassy of India *to pursue M. Tech in Delhi Technological University.*
- *Awarded a merit-based scholarship* to *study B.E (Civil Engineering).*
- Secured *2nd position* in Civil Engineering department *in University.*
- Ranked *1st position* in Class *in 10th.*

POSITION OF RESPONSIBILITY:

- *Trainee Engineer* at “*Ripple Training and Consulting Services*”, Kathmandu, Nepal. My responsibility there was to prepare structural drawings of buildings, analysis of buildings using ETABS (using IS-codes and NBC), estimation, etc.

SOFTWARE SKILLS:

- AutoCAD
- STAAD PRO
- MS OFFICE
- ETABS
- SAP
- MIDAS
- ANSYS
- ABAQUS